Annals of Computer Science and Information Systems
Volume 46

Proceedings of the International Conference on Engineering, Technology and Applied Science Innovations

October 1–3, 2025. Grand Elis Hotel, Amaliada, Greece

Gerasimos Pylarinos, Christos P. Antonopoulos,
George Syrrokostas, Panteleimon Apostolopoulos,
Stratos David (eds.)

PTI

Annals of Computer Science and Information Systems, Volume 46

Proceedings of the International Conference on Engineering, Technology and Applied Science Innovations

Gerasimos Pylarinos, Christos P. Antonopoulos, George Syrrokostas, Panteleimon Apostolopoulos, Stratos David (eds.)

POLSKIE TOWARZYSTWO INFORMATYCZNE
POLISH INFORMATION PROCESSING SOCIETY

2025, Warszawa, Polskie Towarzystwo Informatyczne

Annals of Computer Science and Information Systems, Volume 46
Proceedings of the International Conference on Engineering, Technology and Applied Science Innovations

ISBN 978-83-973291-5-7

ISSN 2300-5963
DOI 10.15439/978-83-973291-5-7

Ul. Solec 38/103
00-394 Warsaw
Poland

Contact: secretariat@fedcsis.org
http://annals-csis.org/

Cover photo:
Łukasz Kotyński,
Elbląg, Poland

Also in this series:

Volume 45: Communication Papers of the 20th Conference on Computer Science and Intelligence Systems (FedCSIS), **ISBN 978-83-973291-9-5**

Volume 44: Position Papers of the 20th Conference on Computer Science and Intelligence Systems (FedCSIS), **ISBN 978-83-973291-8-8**

Volume 43: Proceedings of the 20th Conference on Computer Science and Intelligence Systems (FedCSIS), **ISBN WEB: 978-83-973291-6-4, ISBN ART 978-83-973291-7-1**

Volume 42: Proceedings of the Ninth International Conference on Research in Intelligent Computing in Engineering **ISBN 978-83-973291-5-7**

Volume 41: Communication Papers of the 19th Conference on Computer Science and Intelligence Systems (FedCSIS), **ISBN WEB: 978-83-973291-0-2, ISBN USB: 978-83-973291-1-9**

Volume 40: Position Papers of the 19th Conference on Computer Science and Intelligence Systems (FedCSIS), **ISBN WEB: 978-83-969601-9-1, ISBN USB: 978-83-969601-0-8**

Volume 39: Proceedings of the 19th Conference on Computer Science and Intelligence Systems (FedCSIS), **ISBN WEB: 978-83-969601-6-0, ISBN USB: 978-83-969601-7-7, ISBN ART 978-83-969601-8-4**

Volume 38: Proceedings of the Eighth International Conference on Research in Intelligent Computing in Engineering, **ISBN WEB: 978-83-969601-5-3**

Volume 37: Communication Papers of the 18th Conference on Computer Science and Intelligence Systems, **ISBN WEB: 978-83-969601-3-9, ISBN USB: 978-83-969601-4-6**

Volume 36: Position Papers of the 18th Conference on Computer Science and Intelligence Systems, **ISBN WEB: 978-83-969601-1-5, ISBN USB: 978-83-969601-2-2**

Volume 35: Proceedings of the 18th Conference on Computer Science and Intelligence Systems, **ISBN WEB 978-83-967447-8-4, ISBN USB 978-83-967447-9-1, ISBN ART 978-83-969601-0-8**

Volume 34: Proceedings of the Third International Conference on Research in Management and Technovation **ISBN 978-83-965897-8-1**

Volume 33: Proceedings of the Seventh International Conference on Research in Intelligent and Computing in Engineering, **ISBN WEB: 978-83-965897-6-7, ISBN USB: 978-83-965897-7-4**

THE International Conference on Engineering, Technology and Applied Science Innovations (ICETASI) is a premier gathering of professionals and academics dedicated to advancing knowledge and fostering innovation. The scope of the conference is to provide an academic-meets-industry forum on recent developments and innovations, while giving a local aspect on the recent advancements and major issues concerning the region.

All presented works were reviewed by members of the scientific committee (all academic scholars or industry-occupied Ph.D holders) and volunteer reviewers with at least an M.Sc. degree in relevant fields.

Selected full conference papers will be published by the International Journal Annals of Computer Science and Information Systems (ACSIS).

During the conference, new engineering trends were explored, focusing on the environmental, social, and individual impact of modern society and technology, and ways to mitigate arising issues related to water and waste management, overtourism, artificial intelligence, education, laws and regulations, new materials, green technology, and quality of life.

ICETASI 2025 was the first academic conference organized by EOS Association, a non-profit organization established in Northwest Ileia, Greece, and we hope that many more will follow. It was held on October 1-3, 2025 at the Grand Elis Hotel, Amaliada, Greece. The principal objectives of EOS Association are the promotion of culture, education, and science through the organization of various actions and events.

Proceeding's Editors – ICETASI 2025:

Gerasimos Pylarinos,
Christos P. Antonopoulos,
George Syrrokostas,
Panteleimon Apostolopoulos,
Stratos David

ICETASI SPONSORS

EOS Cultural Association

Ionian University

Region of Western Greece

Engineering, Technology &
Applied Science Research

OAKPINE

Clinic To Cloud

Turbomed

Annals of Computer Science and Information Systems, Volume 46

International Conference on Engineering, Technology and Applied Science Innovations

October 1–3, 2025. Amaliada, Greece

TABLE OF CONTENTS

Proceedings of the International Conference on Engineering, Technology and Applied Science Innovations pp. 1–7
DOI: 10.15439/2025I23
ISSN 2300-5963 ACSIS, Vol. 46

University Dropout: The Case Study of the Petroleum-Gas University of Ploiesti

Irina Dumitrescu
Philology Department
Petroleum-Gas University of Ploiesti
Ploiesti, Romania
irina.dumitrescu@upg-ploiesti.ro

Alexandru Savulescu
Automatics, Computers and Electronics Department
Petroleum-Gas University of Ploiesti
Ploiesti, Romania
asavulescu@upg-ploiesti.ro

Andrei Dumitrescu
Mechanical Engineering Department
Petroleum-Gas University of Ploiesti
Ploiesti, Romania
andrei_d@upg-ploiesti.ro

Dragos Gabriel Zisopol
Mechanical Engineering Department
Petroleum-Gas University of Ploiesti
Ploiesti, Romania
zisopold@upg-ploiesti.ro
(corresponding author)

***Abstract*—University dropout is at present the greatest scourge of the Romanian academic education. The main goal of this paper consists in the identification of the principal factors leading to dropout and consequently of the most efficient modalities of prevention and control of this phenomenon within the Petroleum-Gas University of Ploiesti (PGUP). To that purpose, an interdisciplinary study regarding the difficulties encountered by the students in their adaptation to the PGUP environment has been performed. The results of this study, based on a questionnaire distributed to the subjects in risk situation, are summarized and commented in the present paper. A predictive model developed by the authors trying to assess the future evolution of university dropout for the PGUP engineering faculties is also included in the paper.**

***Index Terms*—university dropout, equality of opportunities, career development, continuous learning, Markov process.**

I. Introduction

THE issue of university dropout has an important part in the worldwide preoccupations aiming at the social dimensions of education. These include even since the years `80 politics for increasing the participation and the degree of graduation in higher education, using edifying concepts such as: *"dropout"*, *"non-persistence"*, *"academic performance / academic success versus failure"*, *"retreat"*, *"disengagement"* [1-12].

From a public policy perspective, data regarding the participation in higher education are periodically collected by OECD using the *"completion of studies rate"* and the Eurydice structural indicators for monitoring education systems, which are also linked to the participation policies of the European Commission [13, 14]. The definition of the indicator concentrates on the percentage of students completing the high education program they have begun.

In Romania, the absence of such preoccupation is felt, University dropout being at present the greatest scourge of the Romanian education [15-20]. It perpetuates the shaky mentality of some young people who, lacking efficient means of control, do not succeed in wisely managing their choices. Permanent and continuous learning, the inoculation of the need for education involve learning activities warranting both fundamental academic knowledge and skills, and autonomous thinking abilities. Romanian education experiences today a huge provocation: the adaptation to the new requests of the labour market, simultaneously with the awareness of the utility of higher education.

That is why the achievement of a study regarding the students adaptation to the academic environment appears to be imperiously necessary in order to identify the factors causing dropout. Mostly, such concept is regarded as the renunciation at a wright. A responsible person, with a pragmatic attitude, is less predisposed to abandon. Instead, a reduced *"locus of control"* of a person who does not experiment the freedom of choice, triggers almost instantaneously the dropout idea.

The school dropout represents not only a willingly renunciation at the wright to education, but also at an evolution of the individual system of thinking. Superior education facilitates the adaptation of the future professional to the requirements of the labour market by directly involving the students in the selection of their formative trajectory. The transition high school – university is demanding: new exigencies, a different manner of teaching and learning, the need for independent study. The student's expectances, often unrealistic, the lacunar emotional preparation, the confrontation with new personal and social experiences generate an adaptation effort intensely felt.

The adaptation process is neither easy nor fast, involving several *stages* [21]: *accommodation* (dominated by fears), *adaptation* (attracting benevolence), *participation* (based on psycho-social maturation and acceptance by the others), and also the *integration,* corresponding to the group dependence. That is why the link between the level of adaptation of the students and their academic performance becomes essential.

II. Research Design, Participants and Methodology

The investigation ground used to identify the main factors stimulating or inhibiting the university dropout is one of the most important academic institutions from Romania, that is the Petroleum-Gas University of Ploiesti (PGUP). Table I indicates a summary of the dropout rate for the five faculties of PGUP in the last four academic years (data collected by the authors from PGUP statistics).

The present study supplements the beneficial consequences of the supportive policy already initiated at PGUP level. Focused on the multifaceted approach of the factors mentioned above, our research cumulates inter-disciplinary aspects. The behavioural model foreshadowed from the first semester of the first year of study leads to an outcome marked by the dropout. The analysis takes into account both the human behaviour attracted by rewards and the individual elements guaranteeing the unpredictability of the human nature.

TABLE I. PGUP Faculties DropOut Rates

Faculty	Academic Year				
	2019 -2020	***2020 -2021***	***2021 -2022***	***2022 -2023***	***2023 -2024***
Letters and Sciences	8.83 %	9.71 %	8.26 %	11 %	20.43 %
Economic Sciences	7.83 %	9.75 %	10.75 %	7.8 %	9.85 %
Mechanical and Electrical Engineering	11.1 %	16.08 %	12 %	11.68 %	6.56 %
Petroleum and Gas Engineering	6.97 %	14.23 %	14.83 %	12.23 %	5.13 %
Petroleum and Petrochemical Technology	15.37 %	11.6 %	15 %	10.6 %	9.9 %

For such reason, an interpretative approach of this investigation was selected, the "reality" being built by the interpretation of some perceptions and attitudes of the students regarding the manner in which the level of education affects their own values system. Obtaining a university diploma cannot be achieved without investing time for education inside and outside school. However, the academic performance does not constitute a viable choice for all in the context in which the meritocratic principles based on academic education do not necessarily attract the desired status and financial rewards.

The information has been collected in May-June 2024 using the direct research method – gathering data directly from the respondent students. The used investigation instrument has been the questionnaire. The same questions have also been distributed on-line, using Google Forms. Answers have been obtained from a number of 66 students (from the 1st and 2nd years) in risk situation (at least three remaining exams from the 1st year).

Even if the number of students being in such situation is much greater, 512 in the whole university, the lack of desire for cooperation can be partially justified by means of the psychological concept of "*acquired indifference/inability*". Due to the repeated exposure to negative events, such as difficulties in assimilating school information, accumulation of failed exams, generating a less favourable image at the level of the study group, a person considers himself deprived of control means and gives up the attempt to improve his behaviour.

The structuring of the proposed questionnaire was based on addressing target-zones, such as: frequency of absenteeism and the main factors inhibiting the appetence for study, the general system of needs and interests correlated with the specificity of the perspective of each respondent, proposals/strategies of remediation of the subjects in risk situation in order to improve their attitude towards school / education results. In its componence, there are seven questions, beginning with questions with closed answer fixing the statistical characteristics of the basic behaviour of the respondent. The questions with open answer follow aiming at highlighting the factors generating the university dropout. The subsequent open questions point out the compatibility between the needs and expectations of the student and PGUP managerial policy.

The major objectives of the present study are the configuration of strategic lines attenuating the discrepancy between the present situation and a desirable one, with beneficial changes of attitude from the part of the students towards the act of education, but also the outlining of typological profile of the PGUP student in risk situation. The basic premise is that, during the transition to adult age, the young people identify them with their projects, many times unrealistically ambitious. Such distance between aspirations and the capacity to satisfy them can induce a state of social alienation, promoting university dropout.

III. Analysis Results and Disscusions

Within our study, looking at the distribution according to faculties of the respondents (Figure 1), a high percentage of those from the three engineering faculties (IME, IPG and TPP) was observed (39 students, that is 59.1%), fact correlated with an increased difficulty of the studies, especially in the situation of a major inconsistency between their option and the previous high school training. In addition, the duration of bachelor degree studies in this case is 4 years, increasing the time needed to be invested in education. Therefore, even if *"the investment in knowledge brings the best interest"*, according to Benjamin Franklin, the *"blank cheque"* payed is considered less and less prolific

for a person wishing to rapidly enjoy financial results due to the lack of material support from his family.

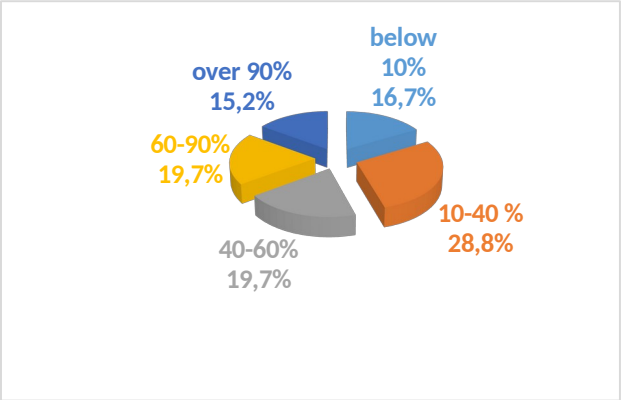

Fig. 1. Distribution according to the faculties of the respondents in risk situation: IME – Mechanical and Electrical Engineering; IPG – Petroleum and Gas Engineering; TPP – Petroleum and Petrochemical Technology; SE – Economic Sciences; LS – Letters and Sciences.

Analysing the distribution according to the year of study of the respondents, we observed that the students from the 1st year are the dominant category (62.9%), proving the preoccupation of equilibrating the balance effort (invested time, positive attitude, implication in the learning process) – effect (favourable results). In case of lack of equilibrium, the student will consider that the academic integration imposes him to reach high standards, clearly superior to his capability. The *"socially prescribed perfectionism"* diminishes the feeling of personal self-efficiency supplemented by the social comparison and by advertising in mass media of the profile *"man of success"*. The students from the 2nd year (37.1%) thus consider that the only option is to retire from the academic environment. We therefore consider that the validation of the effort and not of the relative results, the accent on highlighting the competences and not the requirement to mechanically assimilate the information, the symbolic rewards based on encouragements and appreciations constitute beneficial means in order to support these students.

The distribution of the answers regarding the periodicity of attendance at the teaching hours (Figure 2) show that the students understand the importance of participating at these hours (54.6%). Their precarious results require support from the didactical staff for a better tuning between their knowledge from high school and the curriculum of the university. There are also students (28.8%) that do not succeed in efficiently managing the transition towards the university environment, either due to the commitment to a job, or due to the underestimation of the difficulties of the academic requirements. A tailored counselling could constitute a sustainable remedy in such situation. Not lastly, 16.7% of the respondents are not keeping in touch with school, favouring the conditions for dropout. There is a clear tiebreaker between the students from the 1st year and the ones from the 2nd year. In the first situation, a high percentage (52.4%) involving themselves physically in the learning process, while in the second case, 75% from the students loose the connection with school thus generating favourable circumstances for dropout.

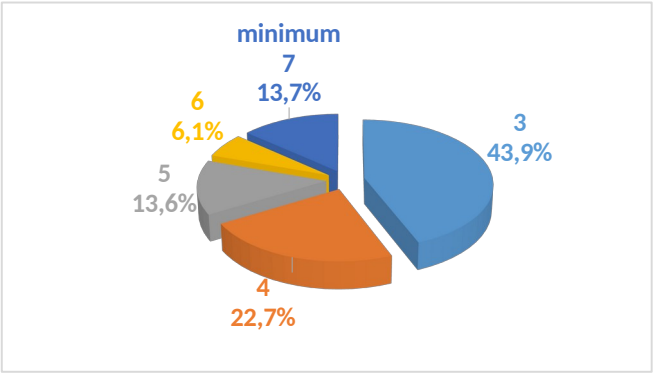

Fig. 2. Distribution of the periodicity of attendance at the teaching hours by the respondents.

We consider that the methods of stimulating the efforts of those who have difficulties of adaptation should be implemented as earlier as possible (after the 1st semester of the 1st year) by means of a proactive attitude of the teaching staff who, keeping their formative coherence, will prepare the students for a mature anchoring in the professional life. It is needed to rethink the modalities of assimilating information, by identifying the eventual errors (mechanical learning, lack of connection between theory and practice).

The next question targets the number of failed exams accumulated which, in the conditions of transgressing a reasonable limit (3-4 remaining exams), place the students in the risk area. When the real possibility of rehabilitation decreases, that tend to cease any action and to consider the university dropout normal. Figure 3 attest the fact that a percentage of 66.6% (43.9% with 3 failed exams and 22.7% with 4 remaining exams) from the respondents have real chances to fix their school results, requiring the corroboration of the self-management of their own learning style with the implication and support of the teaching staff. The motivational stimuli are partially of extrinsic nature, aiming at obtaining short (favourable results) and long (getting the university diploma) term benefits, but, at the same time, aversion reactions develop towards the possible unpleasant consequences (expulsion, dropout). Intrinsic motivations also appear such as: shaping a social finality of work, fulfilling the achievement desired [22].

In the second situation – 13.7% of students with at least 7 failed exams, we encounter an attitude of non-involvement / rejection of the influence of this pro-training campaign. The repeated negative school results generate psychic discomfort cancelled by substituting school performances with various achievements (choosing a job). The wrong impression of easily accessing well payed jobs with limited studies and especially the cult of the "models" of public persons in whose success learning did not count, leads to less wise choices.

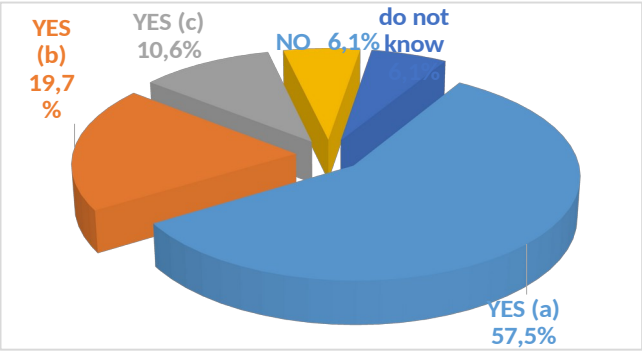

Fig. 3. Distribution of the students according to the declared number of the remaining exams.

The answers to the question aiming at the degree of importance of high education for personal development (Figure 4) attests almost unanimously (87.8%) the awareness by the students of the importance of continuing their studies. A percentage of 57.5% (from the total number of respondents) reclaim the need for self-achievement by giving answers convergent towards the basic idea: career/personal development. If the personal vision is not preceded by planning and efficient time management, such need remains only an unachievable aspiration. The incompatibility between the study program selected and the vocational characteristics will lead to the lack of interest for the chosen domain and to unrealistic expectations regarding the occupational profile.

Another category of respondents (19.7%) considers getting a university diploma a warranty for later obtaining sensibly greater incomes that in the case of a limited education. The answer attests either a pro-meritocratic attitude or a possible emblem of the provenience from disadvantaged environments. A minor category of students (10.6%) do not justify their position, fact correlated with an uncertain vision of the future or with the fact that their enrolment in the university was not a volunteer action. 6.1% of the respondents, even if enrolled in a faculty, deny the importance of studies for increasing the quality of life (Figure 4), and other 6.1% are undecided.

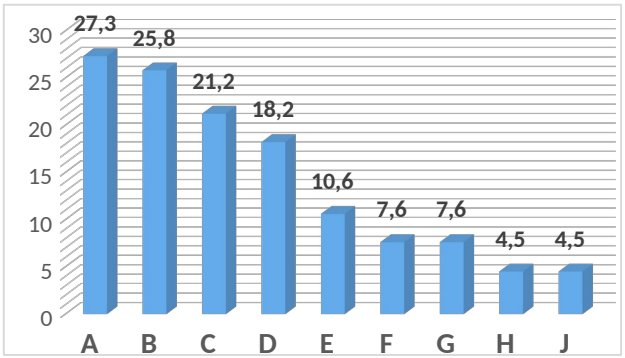

Fig. 4. Importance of the university studies for the personal / professional development and the distribution of the arguments (needs, interests, aspirations) sustaining such importance: **a** – personal / career development;
b – better paid job; **c** – no arguments.

The next question is focused on detecting the main reasons for dropout of the students (Figure 5). Some motives are cumulated at the individual level, leading to the sensibly hindered management of some obstacles of various types. Lack of time (27.3%), financial problems (25.8%), accumulated stress (21.2%) and the feeling of lack of efficiency, as well as the eventuality of a job carried out in parallel with the educational act (18.2%), represent aspects often mentioned.

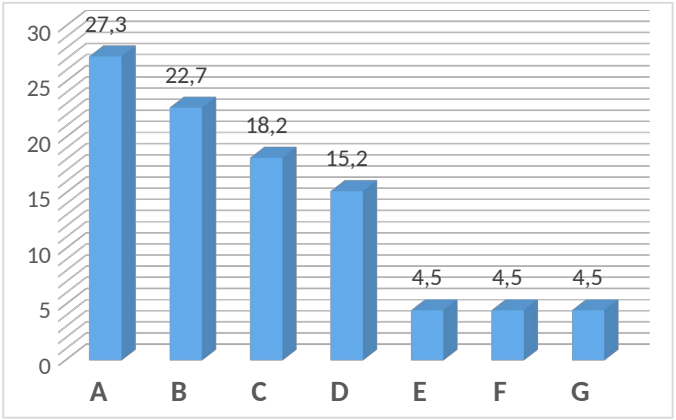

Fig. 5. Distribution of the motives favouring the university dropout: A – lack of time; B –financial problems; C –stress accumulation; D – a parallel job; E – lack of interest / uselessness of continuing the academic studies; F – inadequate choice of the study program; G – negative attitude of the professors / inadequate teaching methods; H – motives connected to the family; J – other motives.

The pressure/lack of time (27.3%) is developing in a context in which the respondents often expect to decide themselves their schedule, to have neither deadlines nor restrictions or confinements. The great number of teaching hours and their uneven scheduling contributes to the diminishment of the selection possibilities. The further dependence on their parents is not usually a valid option for young people who want to be more and more autonomous. However, their option (getting a job) makes difficult the fulfilment of the requirements of the student life, even if at a minimum level.

The financial problems invoked (25.8%) can block the full completion of the educational trajectory. Most of the young people well integrated in the university environment have often delegated to their parents the responsibility regarding the costs related to their personal life. The ones coming from disadvantaged environments (families with increased risk of poverty / social exclusion) do not have such opportunity, and the means of support for social cases are insufficient (the social scholarship strictly covers the accommodation and meals costs). That is why such persons are concomitantly searching for a place on the labour market. The autonomous commitment to education in the absence of a guide, the self-management of the resources, if lacking the parental protection, is inefficient.

Excessive stress constitutes another reason generating dropout (21.2% - Figure 5). The lack of a sufficient number

of credits (40) for advancing to the next year increases the feeling of inefficiency of their efforts. In the context of a random choice of the study program, of a vocational incompatibility causing disinterest, of an option under family pressure, of a precarious previous training, all corroborated with a great volume of information, deadlines, inefficient time management, the inoculation of a high level of stress is perpetuated.

The option for a job (even part-time) (18.2%) becomes a problem hard to manage for young people just passed by the age of adolescence. The pressure put on their shoulders by the employers by requiring years of experience goes against the universities rigours, prioritising a high frequency at the teaching hours and an active implication in projects. Having a parallel job while assuming the role of student presupposes, beyond the immediate benefits (financial support and autonomy, combining theory with practice, an early responsibility, etc.), additional time, effort and especially a lot of stress. Therefore, the student with a job resets his system of needs and interests and puts his studies in a secondary plane.

The lack of interest (10.6%) together with the inadequate selection of the study program (7.6%) are motives less invoked. Continuing the studies is a subjective option in a flawed context in which the correlation between the income and the level of studies is not always visible. Lesser percentages (4.5%) refer to the less adequate/empathic behaviour of the professors and to various family motives. We mention the fact that, due to the accumulation of more than one motive at the individual level, the sum of the invoked percentages is greater than 100%.

Summarising the listed motives, we can easily conclude that when the daily survival is at stake, many young people dropout the university studies (25.3% from the whole university even from the 1st year). It is not just a voluntary choice, but also a consequence of the provocations with which the society tests them. The students coming from disadvantaged environments are the most vulnerable ones. Time management favouring the job and the social life development, the interest for the interaction with the others facilitate a mentality favourable to sacrifice the academic projects, the students seeing in the offering fields (retail, call centre, tourism, etc.) gates to build their career and to gain experience.

Many times, young people do not understand that the option of enrolling in a faculty is in the first place a great opportunity offered to him by facilitating his professional achievement. The mature anchoring to this reality presupposes a permanent updating of their speciality knowledge and acquiring new one. However, when the student reaches the situation in which he does not find himself in the selected study program, he resents the inadequacy/non-adherence to the academic environment.

In addition, the fear of maladaptation to the academic requirements is correlated in some situation with the lack of flexibility of the teaching staff. The relationship with the student must be nuanced and democratic, combining the exigence with the opening towards his needs and opinions. If the professor has an excessively reticent attitude towards the inadequate performance of the student, combined with a great number of absences, this can be easily converted in hostility. At the same time, the indifference of the professor threatens the integration need of the student in the academic environment.

The responding students understand the necessity to adopt individual measures, which can help them overcome the critical moment. Figure 6 illustrates different modalities to approach such problem, a better time management representing one of the most frequent opinions (27.3%).

$$T = \begin{pmatrix} 1.21 & 0.015 & 0.116 \\ 0.001 & 1.14 & 0.116 \\ 0.104 & 0.132 & 1.168 \end{pmatrix}$$

Fig. 6. Distribution of the student's proposals for the remediation of the risk situation: A – much greater frequency at the teaching hours; B – increased learning effort; C – increased motivation; D – they do not have proposals; E – no answer; F – giving up their job; G – another answer.

A majority percentage of respondents (50% - Figure 6, A and B) understand that the self-management of the academic educational process needs a revaluation, as they still have the required determination for self-motivation. In favourable conditions (support from the professors, cooperation and help from their colleagues), they will rehabilitate themselves, converting failure in success. There are also students (19.7% - Figure 6, D and E) for which the probability of improving their results is severely diminished due to absenteeism and passivity.

We select some of the most interesting modalities of improving the personal efficiency: high frequency (27.3%), motivation and determination (18.2%), changes in the learning methods (22.7%), increase of the level of self-discipline (1.5% – only one respondent), improving the communication with the professors (1.5%). Particularly, we point out the intention of some students (4.5%) to give up their job, aware of the fact that they are not able to establish a correct equilibrium between work and faculty. In only one case there is a complaint regarding a least supportive treatment carried out by some professors, complaint followed by the intention to continue the master degree within another university.

IV. Predictive Model Using Markov Chains

In the followings, a predictive model developed by the authors, using Markov chains / processes [23], is briefly presented and applied to assess the future evolution of university dropout for the PGUP engineering faculties (IME, IPG and TPP – see Figure 1) using data summarised in Table I.

The predictive model comprises the calculation steps below:

- The transformation of absolute data from Table I in relative data, shown in Table II.
- Calculation of the transition matrixes from each year to the next (using the methodology detailed in [23]).
- Adding the transition matrixes, M_{Tk}, the total transition matrix, T, is obtained:

$$T = \sum_{k=1}^{n} M_{T_k} \quad (1)$$

- By dividing each element of a line with the total of that line in the T matrix, the total probability transition matrix, P_T, results.
- The predicted structure for the next year, $year^T_{n+1}$, is obtained using the equation below:

$$year^T_{n+1} = P_T \, year^T_n \quad (2)$$

TABLE II. Relative Data for Markov Model

Academic Year	**PGUP Faculty** (relative values)			Total
	IME	***IPG***	***TPP***	
2019-2020	0.332	0.208	0.46	1.0
2020-2021	0.384	0.340	0.277	1.0
20121-2022	0.287	0.355	0.359	1.0
2022-2023	0.338	0.354	0.307	1.0
2023-2024	0.304	0.238	0.459	1.0

The total transition matrix T, the probability transition matrix P_T and the predicted structure for $year^T_{VI}$ (academic year 2024-2025) calculated for the data in Table II are the followings:

$$T = \begin{pmatrix} 1.21 & 0.015 & 0.116 \\ 0.001 & 1.14 & 0.116 \\ 0.104 & 0.132 & 1.168 \end{pmatrix}$$

$$P_T = \begin{pmatrix} 0.9203 & 0.0112 & 0.0865 \\ 0.0008 & 0.9069 & 0.0923 \\ 0.0741 & 0.094 & 0.8319 \end{pmatrix}$$

$$year^T_{VI} = \begin{pmatrix} 0.3165 \\ 0.2581 \\ 0.4263 \end{pmatrix}$$

Based on the results above, the following values have been assessed for the dropout rates of the three engineering faculties in the academic year 2024-2025: 6.7% for IME, 5.35% for IPG and 9.55% for TPP.

V. Conclusions

On the background of quasi-permanent social changes and of the relativity of laws and regulations in education, school remains more and more often at the mercy of dropout. We are confronting today the disparition of the certitude that only by working an individual can gain an honourable place in society. The academic studies lose their relevance if their graduation is not correlated with a job/status adequate to the training. The decline of apparently stable occupations and the unprecedented development of AI creates major uncertainties when planning the professional future. The mirage of specializations well quoted on the labour market attract without discernment students that, once in the 1st year, confront great difficulties in adapting to academic requirements. The incompatibility with the vocational profile supplements the feeling of lack of adaptation and thus facilitates dropout.

Even if school infrastructure and the norms of adhesion to the collectivity have been updated, the gap between generations creates asperities at the level of reciprocal adaptation professor-student. The academic requirements remain too high for the young people with a precarious training. Communication blockages occur and the Romanian school, even if interested to identify the problems distracting young people from study, obtains minimum results, facilitating dropout.

Our study aimed at outlining a detailed diagnosis of the dropout situation at the PGUP level, marking some strategic actions for its remediation. The behavioural analysis of the individual has demonstrated the link between the area of origin, the family antecedents, the degree of support (including financial) from the parents and his attitude towards education. Therefore, the dropout issue is based on a complex and interactive causality.

We consider that the commitment of the teaching staff in sustaining education by supporting the students with problems of adaptation/understanding, his proactive attitude, the continuous feedback could all be translated at the level of the students who will be aware of the importance of education. Therefore, even if the needs of the student requires in some situations the assumption of multiple roles (student, employee, supporter of the family etc.), it is important for him not to choose subjectively between them, but to prioritise them.

References

[1] G. S. Androulakis, D. A. Georgiou, P. Kiprianos, and G. Stamelos, "Examining the sequence of factors affecting student's tendency to drop out: a case study in Greece". International Journal of Education, 12(4), 2020, pp. 107-131.

[2] R. Q. Apumayta, J. C. Cayllahua, A. C. Pari, V. I. Choque, J. C. C. Valverde, and D. H. Ataypoma, "University Dropout: A Systematic Review of the Main Determinant Factors (2020-2024) ". F1000Research, 13, 2024, 942.

[3] B. M. Kehm, M. D. Larsen, and H. B. Sommersel, "Student dropout from universities in Europe: A review of empirical literature". The Hungarian Educational Research Journal, 9(2), 2019, 147–164. [Online]. Available: https://doi.org/10.1556/063.9.2019.1.18

[4] A. Llauró, D. Fonseca, S. Romero, M. Aláez, J. T. Lucas, and M.M. Felipe, "Identification and comparison of the main variables affecting early university dropout rates according to knowledge area and institution". Heliyon, 2023, 9(6).

[5] Nurmalitasari, Z. Awang Long, and M. Faizuddin Mohd Noor, "Factors influencing dropout students in higher education". Education Research International, 2023(1), 7704142.

[6] A. M. Ortiz, and V. Sriraman, "Exploring Faculty Insights into Why Undergraduate College Students Leave STEM Fields of Study-A Three-Part Organizational Self-Study". *American Journal of Engineering Education*, 6(1), 2015, pp. 43-60.

[7] G. Packham, P. Jones, C. Miller, and T. Brychan, "E-learning and retention: Key factors influencing student withdrawal". Education+ Training 46, no. 6/7, 2004, pp. 335-342.

[8] A. Tayebi, J. Gómez, and C. Delgado, "Analysis on the Lack of Motivation and Dropout in Engineering Students in Spain". IEEE Access, Vol. 9, pp. 66253-66265, 2021. DOI: 10.1109/ACCESS.2021.3076751.

[9] L. I. Valencia Quecano, A. Guzmán Rincón, and S. Barragán Moreno, "Dropout in postgraduate programs: a underexplored phenomenon – a scoping review". Cogent Education, 11(1), 2024 [Online]. Available: https://doi.org/10.1080/2331186X.2024.2326705

[10] S. Wild, Steffen, L.S. Heuling, "Student dropout and retention: An event history analysis among students in cooperative higher education". International Journal of Educational Research, 2020, 104: 101687.

[11] J. R. Casanova, A. Cervero, J. C. Núñez, L. S. Almeida, and A. Bernardo, Factors that determine the persistence and dropout of university students, 2018.

[12] J. N. M. Otero, N. R. Rabelo, H. B. Alonso, and E. R. C. Morales, "La formación doctoral: estudio comparativo entre Europa y América". Universidad y Sociedad, 13(4), 2021, pp. 170–182.

[13] * * * Organisation for Economic Co-operation and Development (OECD), *Education at a glance 2019. OECD indicators*. OECD Publishing, Paris, 2019 [Online]. Available: https://doi.org/10.1787/f8d7880d-en

[14] VA. Miñano, Review "Panorama de la Educación. Indicadores de la OCDE 2022. Informe Español". Supervisión 21. Jan. 30, 2023 ; 67(67).

[15] D.A. Coteț, M. Păunescu, M.C. Haj, Abandonul în învățământul superior românesc. Definire, măsurare, interpretare, UEFISCDI Publishing House, 2022 [Online]. Available: https://editura.uefiscdi.ro/6-abandonul-in-invatamantul-superior-romanesc-definire-masurare-interpretare

[16] C. Stăiculescu, E.R. Richiteanu Nastase, "University dropout. Causes and solution". Mental Health: Global Challenges Journal, 1(1), 2018, 71-75.

[17] * * * Hotărâre pentru organizarea și finanțarea Programului Național de Reducere a Abandonului Universitar (PNRAU) [Online]. Available: https://www.edu.ro/sites/default/files/PHG_PNRAU.pdf

[18] * * * Comunicat de presa nr. 155/20 iunie 2023, Institutul National de Statistica, Romania [Online]. Available: https://insse.ro/cms/sites/default/files/com_presa/com_pdf/sistemul_educational_2023_r.pdf

[19] * * * Raport privind starea invatamantului superior din Romania 2022-2023, Ministerul Educatiei, Bucuresti, December 2023 [Online]. Available: https://www.edu.ro/sites/default/files/_fi%C8%99iere/Minister/2023/Transparenta/Rapoarte_sistem/Raport-Starea-invatamantului-superior-2022-2023. pdf

[20] * * * Strategie de diminuare a riscului de abandon al studenților Universități Babeș-Bolyai [Online]. Available: https://senat.ubbcluj.ro/wp-content/uploads/2018/07/Strategie-abandon-academic-UBB-2018.pdf

[21] E. Puzur, "Specificul adaptării psihosociale la studenții anului I de studiu universitar", Conferinta Stiintifica Internationala *Evaluarea in sistemul educational: Deziderate actuale* [Online]. Available: https://ibn.idsi.md/sites/default/files/imag_file/446-452.pdf

[22] Irina Dumitrescu, Perspectivă optimist-tragica asupra motivatiei muncii in Romania. Editura Universitatii Petrol-Gaze din Ploiesti, 2013.

[23] D.G. Zisopol, A. Dumitrescu, Ecotehnologie – Studii de caz. Editura Universitatii Petrol-Gaze din Ploiesti, 2020, pp. 89-98.

Proceedings of the International Conference on Engineering, Technology and Applied Science Innovations pp. 9–14
DOI: 10.15439/2025I12
ISSN 2300-5963 ACSIS, Vol. 46

An Adaptive System Architecture for Creating Visual Stories for Children on the Autism Spectrum

Evanthia Faliagka
Electrical & Computer Engineering Department
University of Peloponnese
Patras, Greece
e.faliagka@esdalab.ece.uop.gr

Theodoros Skandamis
Electrical & Computer Engineering Department
University of Peloponnese
Patras, Greece
th.skandamis@esdalab.ece.uop.gr

Vicky Maratou
AVN Innovative Technology Solutions LTD
Patras, Greece
vicky.maratou@avntechgroup.com

Christos P. Antonopoulos
Electrical & Computer Engineering Department
University of Peloponnese
Patras, Greece
ch.antonop@uop.gr

Nikolaos Voros
Electrical & Computer Engineering Department
University of Peloponnese
Patras, Greece
voros@uop.gr

***Abstract*—Children with ASD need personalized therapy in order to overcome social and emotional difficulties that they experience in their daily routine. They have hugely varied, heterogeneous needs, and should therefore be well served by services truly tailored to an individual, with all of his/her personal needs and preferences. As they learn better visually, visual stories are often a valuable tool for their education and their everyday life. In this paper we propose a tool that enables parents make their own visual stories using artificial intelligence in order to be personalized to every child's needs.**

***Index Terms*—autism, visual stories, AI tool.**

I. Introduction

THE diagnoses of children with ASD are constantly increasing. Autism is a spectrum, which means it affects each child differently in terms of cognitive abilities, behavior, sensory processing, and social interaction [1]. Despite these variations the vast majority of children with ASD struggles with social cues, sensory sensitivities, or emotional regulation [2]. Except the social challenges that children with ASD have to face, they have also difficulties coping with changes [3]. If they have to interrupt their routine they may respond with repetitive behaviors, tantrums, or even aggression. A right preparation for the unpredictable situations such as a delay or a queue is crucial.

It has been found that children diagnosed with autism tend to learn better visually [4]. According to Temple Grandin, people with ASD translate spoken and written language into colorful movies. When someone addresses them, his words are automatically translated into images [5]. The method of visual stories largely reflects this particular way of thinking and consequently the way of learning. These stories present information visually in a clear and reassuring manner and this makes their environment more predictable and as a result more affordable. Visual stories are brief stories with images and short texts that describe social situations and how to respond and behave to the specific situations. This is really helpful when live sessions are not enough or not possible for various reasons, e.g. due to the pandemic or because the child is in isolated areas where there is no speech therapist.

Most technological applications focus on improving learning disabilities and have not concerned improving social skills [6], [7], [8]. In this paper a software application is presented with a strong focus on visual stories, helping children with ASD address social dysfunction. This application will help parents and therapists build custom visual stories. The application will integrate a set of functionalities assisted by appropriate recommendation mechanisms in order to address in the best way each child's special needs and will be accessible from everyone and everywhere.

The scope of the paper is to present and evaluate the architecture of a software application that will support parents and therapists to use and create visual stories that will improve their children's social skills and their everyday life. The impact of this solution is multifaceted as it will allow people to have access to multiple visual stories remotely without restrictions. Moreover, therapists will be supported by a powerful tool that will facilitate the creation of visual stories. This support will increase the capacity of therapists and medical experts, since the need for physical presence will be decreased significantly. On the technological point of view, the proposed platform incorporates technologies in a state-of-the-art, scalable architecture that manages to efficiently handle heterogeneous data in terms of data type (images, structured data) and data volume.

The rest of the paper is structured as follows: In Section 2 the proposed architecture is presented. In section 3 the basic components are shown and section 4 concludes this work.

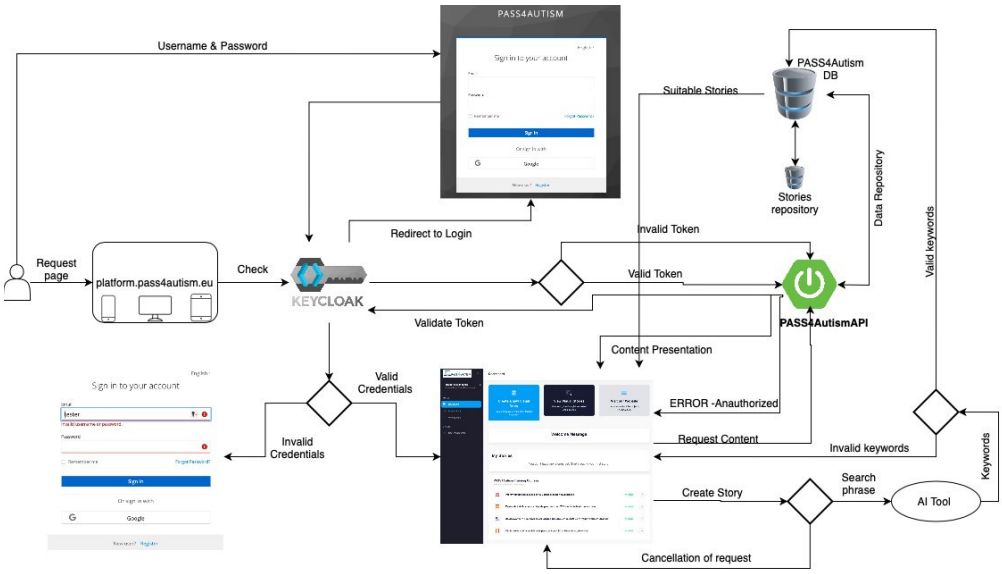

Figure 1. System Architecture

II. Architecture

The two main entities of the proposed application are: the cloud computing infrastructure and the graphical interfaces (Figure 1). The cloud computing infrastructure comprises of the stories component, the AI ranking and the stories repository and the graphical interfaces are the ones that are required to offer the user all the functionality and intelligence of the system.

The AI Tool is based on keyword matching algorithm to provide the most suitable story/environment according to the user's input. The user selects the story that is most relevant with the searching keywords according to the rankings provided by the AI Ranking module. Then, the story can be personalized based on the gender or the name of the child. The stories created are stored in the Stories repository as files as well as the images of the visual stories separately. The repository also includes all files of the educational module.

III. Basic Components

A. Cloud Infrastructure

An architectural style that can effectively address the above requirements of modern applications is micro-services [9]. Micro-services are small autonomous services that are developed independently, with a single and well-defined purpose. Their independent development capability has the advantage of continuous implementation and delivery of new versions of each application. They can be scaled up or down independently of other microservices and developed with tools that best suit their needs. In addition, because of their size, they are easier to maintain and more fault-tolerant, as the failure of one service does not affect the whole system, which could happen in a monolithic.

The infrastructure shown in Figure 2 is based on Docker technology [10] and follows the microservices architecture.

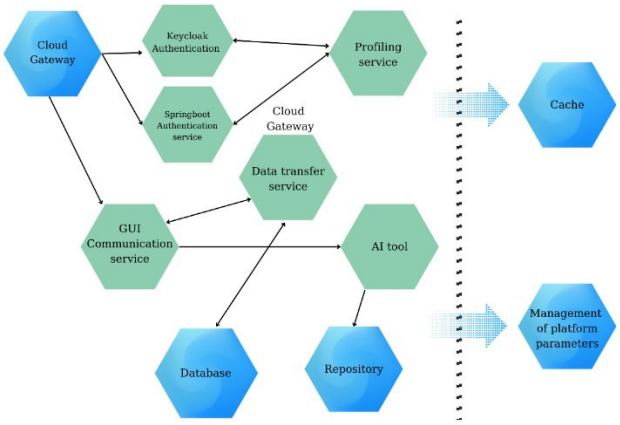

Figure 2. Microservices that are implemented

B. Database schema

The data of the stories and the users are stored in a relational database that was implemented in the open-source PostgreSQL solution [11]. There are 2 groups of users (parents, therapists) and for each entity a table is created as shown in Figure 3.

Each story is saved in the stories table, with a unique code, the images used and the corresponding texts. It also has the id of the user who created it, the keywords that characterize it and whether it is public or not. All the information needed for each user's feedback is stored in the table with the homonymous title.

A user can have multiple stories. Also, each user (parent or therapist) is provided by the application with a unique "token" through which they can enter and implement all the actions he/she wants. At the same time with the information stored in the "token" table and the time until the key is expired and needs to be refreshed, we can also have a record of how active the users are.

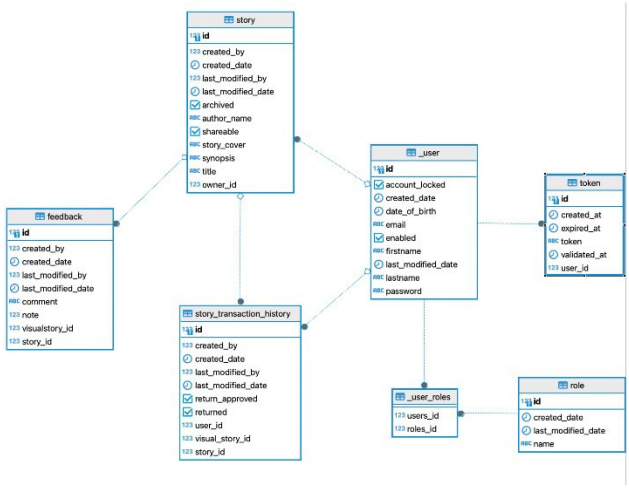

Figure 3. Database schema

The multimedia needed or resulting from the stories will be stored in the file repository that will be implemented and there will be tables that will associate the stories with the paths of the corresponding files.

C. *Authentication Service*

A primary concern for any web-based program is application security. Reliability and confidence are maintained only when user data is protected. Our application security procedures need to be strengthened as cyberattacks become more complex and common. One important step in this direction is the integration of Double Authentication (2FA) with Oauth [12].

Open Authorization (OAuth) is an open protocol that protects application authorization without requiring user credentials to be disclosed. This implies that without disclosing their passwords, users can grant access to particular data or features of an application. Tokens with a limited lifespan and particular access rights are used in place of passwords.

A security measure called double authentication (2FA) requires the user to provide two distinct forms of identity. This usually involves both something the person has (like a mobile phone or a unique token) and something they know (like a password). Even if the password is compromised, it will be far more difficult to access accounts with this additional degree of security.

OAuth and 2FA must be included to keep the application safe from online threats. The risk of eavesdropping is greatly reduced when user passwords are transmitted over OAuth instead of being stored. In addition, even if someone gets to get the password, 2FA adds an extra layer of security that makes it very difficult to access accounts illegally. Using these technologies also makes it easier to abide by laws requiring stringent data protection procedures. For instance, laws like the General Data Protection Regulation (GDPR) [13] mandate the adoption of sophisticated security mechanisms to safeguard consumers' personal information. By using the OAuth and 2FA protocols, our business can comply with these requirements and lower the risk of penalties and other legal repercussions.

Furthermore, improving the application's security boosts user confidence. Customers are more inclined to select and stick with a service that demonstrates its concern for data protection. In addition to safeguarding data, additional security improves our organization's reputation as a reliable, responsible corporation that makes investments to protect its clients.

We will utilize OAuth 2.0, the most recent version of the protocol that provides enhanced security and flexibility, to incorporate OAuth into our application. To authorize users, we will collaborate with reliable identity suppliers like Facebook, Google, and other reliable sources. By doing this, we will be able to take use of these providers' current security architecture and give our users a seamless, safe experience.

We will give several verification options to integrate 2FA in order to maximize flexibility and user-friendliness. Users will have the option of confirming through e-mail or verification apps like Google Authenticator. We'll make sure the verification procedure is simple to use and accessible while maintaining the highest level of security.

D. *Profiling Service*

User authentication and authorization services are supported by Keycloak [14]. Keycloak is an open source software product that enables simple connection to identity and access management aimed at modern applications and services. As of March 2018, this WildFly community project is managed by Red Hat and used as the upstream project for the RH-SSO product.

The proposed platform, through Keycloak, supports 3 three distinct user roles, each with specific permissions, reflecting the desired level of interaction with the platform’s content. The simple user can browse stories, create their own private stories, visible only through their personal profile, plus can delete them at will. The second user type is the “Therapist”, a verified professional accredited by the project’s partners. Therapists are granted extended rights: they can access all user-submitted stories, evaluate them using a 0–5 star rating system, and decide which stories are appropriate for public display. Lastly, the “Administrator” possesses all the aforementioned capabilities, along with the authority to remove stories or suspend user accounts that violate the platform’s usage policies.

E. *Repository*

The repository for all the images and training material will be implemented using the platform Minio [15]. MinIO is an efficient open-source distributed object storage server that offers the ability to store and manage large volumes of data and it is suitable for storing unstructured data such as photos, videos, logs, backups and containers. It is characterized by high performance, scalability and security, while supporting advanced functions such as load balancing and data replication. Integrating MinIO into an application can significantly improve the efficiency and reliability of data storage, while ensuring ease of infrastructure deployment and management. The architectural choice of microservices

through the distributed operation of multiple docker containers within a Kubernetes cluster gives many conveniences as has become clear so far. But at the same time, it also introduces many challenges such as that of managing the files that the platform must share. These files concern images that make up the visual stories. This challenge was addressed by adopting MinIO [3] as the technology to store and share the files necessary for the execution of the intervention plans.

The basic interface to the MinIO service is given in Figure 4, where the 3 endpoints are shown. The image illustrates the available RESTful API endpoints of the "File Handler" subsystem, which manages file storage and retrieval using the MinIO service. The POST /minio/fileHandler endpoint enables users to upload files to the storage system. The GET /minio/file-url endpoint returns a URL for secure and temporary access to a specific file, allowing users to download it without further authentication procedures. Finally, the GET /minio/all-files endpoint provides access to the full list of stored files, facilitating comprehensive oversight and management of the stored content.

Figure 4. Interface to the MinIO service

F. AI Tool

The AI Tool is responsible for providing a list of the most suitable stories according to the user's inputs. In specific, the tool allows users to perform a keyword search and ranking, listing their required environment (e.g., super market) and context (e.g., large crowd) in a search bar. Ranking is a fundamental concept in information retrieval, where the goal is to sort items in a way that the most relevant results appear first in response to a user's query. By effectively ranking documents, we ensure that users receive the most pertinent information first, enhancing the overall user experience.

The AI tool performs a keyword search on existing stories and ranks them as per their relevance to the user keywords. To this end, AI-driven document search and ranking will be implemented. Modern AI-based document ranking algorithms based on the Transformer architecture have superseded previous approaches (e.g., TF-IDF, bag of words, word2vec, etc.). AI ranking models are able to consider language semantics and not just keyword matching to rank items based on relevance to a given query (i.e., they can establish when items and queries are semantically related). To this end, the AI Tool will leverage the Transformer architecture, to capture context from and the semantic meaning of queries and social stories in ranking tasks. For a given query, the AI Tool will compute a relevance score for all existing social stories (pointwise ranking approach). In specific, the AI tool pointwise ranking approach is descripted in Figure 5 and will be implemented as follows:

- A pre-trained Transformer model and tokenizer is loaded.
- A user query and the list of social stories (i.e., items) with their description is provided as input.
- The query-item pairs are tokenized.
- The tokenized pairs are given as an input to the model to get their ranking scores.
- The items are ranked based on their scores.

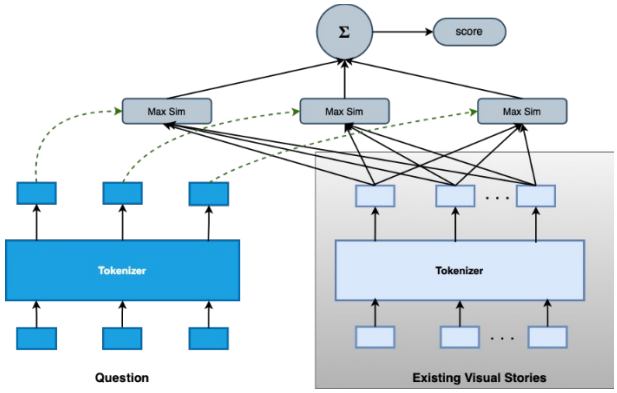

Figure 5. Ranking Process

G. Interfaces

The graphical interfaces are designed to provide end-users with the project's full range of services in a user-friendly, clear, and comprehensible manner. These interfaces aim to both therapists and parents. Through these, therapists and parents can create new visual stories aimed at addressing the specific challenges of parents of children with autism, while parents are encouraged to benefit from the use of technology and find the visual stories that interest them.

To achieve the goal of developing efficient reactive web interfaces, an important tool is the React library. React (also known as React.js or ReactJS) is a free and open-source JavaScript front-end library for building user interfaces and user interface components. It is maintained by Facebook and a community of individual developers and companies. React can be used as the foundation for developing web applications that are responsive to different screen sizes. The React code consists of building blocks called components. These components can be rendered to a specific element in the DOM using the React DOM library.

The View Stories page is one of the most critical pages of the platform and it is designed to provide users with a seamless and engaging experience for exploring all the visual stories created within the platform. This page serves as a comprehensive library, where users can view, filter, and navigate through a wide array of visual stories that have been crafted by others or themselves. The platform's intuitive design and

filtering capabilities ensure that users can easily find stories that meet their needs or interests.

Upon accessing the View Stories page, users are presented with a complete catalog of available visual stories. These stories may include those created by the user, as well as stories shared by the broader community, depending on their access level and privacy settings.

Story Display: Each visual story is displayed in a clean, organized layout, showing the story's title, a thumbnail image representing the story, and brief metadata such as language and target audience (age group or difficulty level). Users can click on any story to view it in full detail.

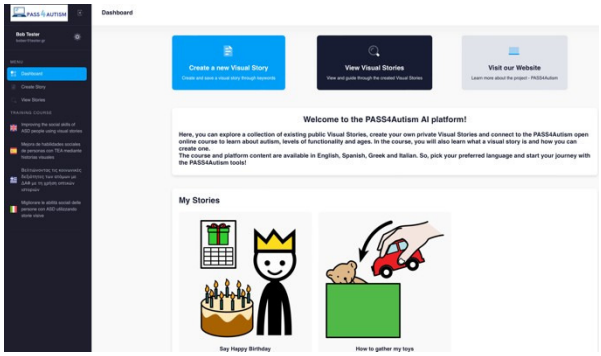

Figure 6. Main Dashboard

To ensure that users can quickly find the most relevant stories, the View Stories page includes robust filtering options. Users can refine their search results by using several key filters:

Language: This filter allows users to view stories in their preferred language. It's particularly helpful for those working in multilingual environments or for users who want to read stories in a specific language, such as English, Spanish, Greek, or Italian.

Levels: Users can also filter stories based on functionality levels. The three ASD levels of severity according to the DSM-5 were used in the filter to ensure users can find stories appropriate for different developmental or language stages. Specifically, the levels are: level 1 - "requiring support", level 2 - "requiring substantial support" and level 3-"requiring very substantial support".

Age: This filter helps users sort visual stories based on the age group they are targeting. Whether the user is searching for stories designed for young children, teenagers, this option ensures that the content they view is age-appropriate and developmentally suitable.

These filters provide a streamlined browsing experience, enabling users to quickly narrow down the available stories to those that align with their specific needs.

Once a user finds a visual story that interests them, they can click on it to view the story in full. The detailed view showcases the sequence of images and titles that make up the story. Users can navigate through the story page-by-page, gaining insight into how each visual and caption builds the narrative.

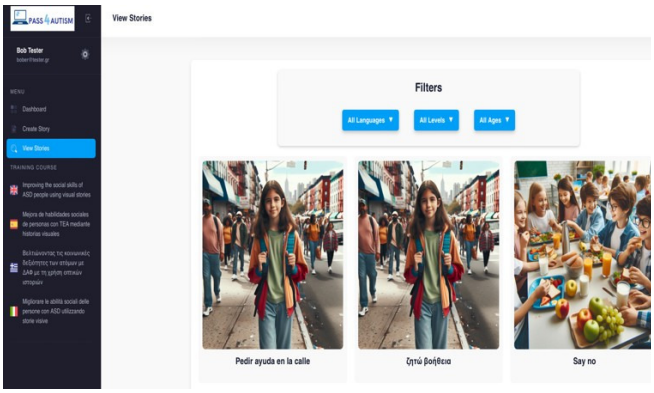

Figure 7. Search stories page

Additionally, users can benefit from the following options while viewing a story:

Story Overview: The detailed view provides an overview of the story, including the language, level, and target age group. This helps users immediately understand the context of the story and how it can be used effectively.

Story Preview: As users scroll through the pages of the visual story, they can gain a full preview of the content, making it easier to decide whether the story is suitable for their needs.

For users who want to explore similar stories, the platform offers story recommendations based on the current selection. If a user views a particular story related to social skills, for example, the platform may suggest other stories that also focus on social development for individuals with autism. This enhances the user's discovery experience and promotes engagement with additional content.

The View Stories page is not only a tool for browsing, but also a showcase of the collective work of the community. Users who have chosen to make their stories public contribute to a growing repository of resources that others can ben-

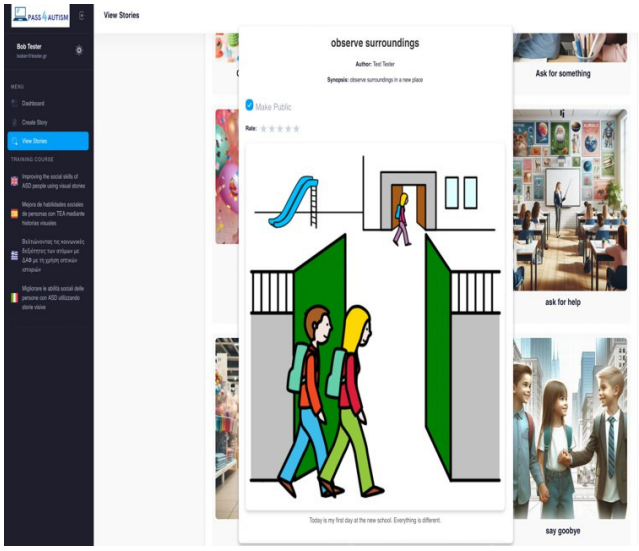

Figure 8. View story interface

efit from. These shared stories can be used for teaching, therapeutic interventions, or even personal use, helping to support the social and communication skills development of individuals with autism.

Acknowledgments

This work has been developed in the context of PASS4Autism project, funded by the European Union. Project Nr. 2023-1-ES01-KA220-ADU-000154910.

References

[1] Lord, C., Elsabbagh, M., Baird, G., & Veenstra-Vanderweele, J. (2018). Autism spectrum disorder. *The lancet*, *392*(10146), 508-520.

[2] Samson, A. C., Hardan, A. Y., Podell, R. W., Phillips, J. M., & Gross, J. J. (2015). Emotion regulation in children and adolescents with autism spectrum disorder. *Autism Research*, *8*(1), 9-18.

[3] Ibañez, L. V., Kobak, K., Swanson, A., Wallace, L., Warren, Z., & Stone, W. L. (2018). Enhancing interactions during daily routines: A randomized controlled trial of a web-based tutorial for parents of young children with ASD. *Autism Research*, *11*(4), 667-678.

[4] Grandin, G. (2006). Empire's workshop: Latin America, the United States, and the rise of the new imperialism. Metropolitan Books.

[5] Grandin, T. (1995). How people with autism think. In Learning and cognition in autism (pp. 137-156). Boston, MA: Springer US.

[6] Ayres, K. M., Mechling, L., & Sansosti, F. J. (2013). The use of mobile technologies to assist with life skills/independence of students with moderate/severe intellectual disability and/or autism spectrum disorders: Considerations for the future of school psychology. *Psychology in the Schools*, *50*(3), 259-271.

[7] Pontikas, C. M., Tsoukalas, E., & Serdari, A. (2022). A map of assistive technology educative instruments in neurodevelopmental disorders. *Disability and Rehabilitation: Assistive Technology*, *17*(7), 738-746.

[8] Klavina, A., Pérez-Fuster, P., Daems, J., Lyhne, C. N., Dervishi, E., Pajalic, Z., ... & Sousa, C. (2024). The use of assistive technology to promote practical skills in persons with autism spectrum disorder and intellectual disabilities: A systematic review. *Digital Health*, *10*, 20552076241281260.

[9] Oyeniran, O. C., Adewusi, A. O., Adeleke, A. G., Akwawa, L. A., & Azubuko, C. F. (2024). Microservices architecture in cloud-native applications: Design patterns and scalability. International Journal of Advanced Research and Interdisciplinary Scientific Endeavours, 1(2), 92-106.

[10] Muzumdar, P., Bhosale, A., Basyal, G. P., & Kurian, G. (2024). Navigating the Docker ecosystem: A comprehensive taxonomy and survey. arXiv preprint arXiv:2403.17940.

[11] Salunke, S. V., & Ouda, A. (2024). A Performance Benchmark for the PostgreSQL and MySQL Databases. Future Internet, 16(10), 382.

[12] Sutradhar, S., Karforma, S., Bose, R., Roy, S., Djebali, S., & Bhattacharyya, D. (2024). Enhancing identity and access management using hyperledger fabric and oauth 2.0: A block-chain-based approach for security and scalability for healthcare industry. Internet of Things and Cyber-Physical Systems, 4, 49-67.

[13] Voigt, P., & Von dem Bussche, A. (2017). The eu general data protection regulation (gdpr). A practical guide, 1st ed., Cham: Springer International Publishing, 10(3152676), 10-5555.

[14] Thorgersen, S., & Silva, P. I. (2021). Keycloak-identity and access management for modern applications: harness the power of Keycloak, OpenID Connect, and OAuth 2.0 protocols to secure applications. Packt Publishing Ltd.

[15] https://min.io/

Proceedings of the International Conference on Engineering, Technology and Applied Science Innovations pp. 15–20
DOI: 10.15439/2025I24
ISSN 2300-5963 ACSIS, Vol. 46

Study on the optimization of FDM parameters for the manufacture of flexural specimens from recycled ASA in the context of the transition to the circular economy

Iacob Dragos Valentin
Doctoral School, Mechanical Engineering Department
Petroleum-Gas University of Ploiesti
Ploiesti, Romania
dragoshicb@gmail.com

Zisopol Dragos Gabriel
Mechanical Engineering Department
Petroleum-Gas University of Ploiesti
Ploiesti, Romania
zisopold@upg-ploiesti.ro
(corresponding author)

Minescu Mihail
Mechanical Engineering Department
Petroleum-Gas University of Ploiesti
Ploiesti, Romania
mminescu@upg-ploiesti.ro

***Abstract*—This paper investigates how variable 3D printing parameters by fused deposition modeling (FDM) influence the mechanical properties of 3-point bending specimens made from recycled acrylonitrile styrene acrylate (rASA) filament. Using variable thermoplastic extrusion parameters [layer height Lh = (0.10, 0.15, 0.20) mm and fill percentage Ip = (50, 75, 100)%], 45 3-point bending specimens were additively fabricated from Everfil rASA filament on the QIDI Q1 Pro 3D printer. All fabricated specimens were subjected to 3-point bending tests on the Barrus White 20 kN universal testing machine. The analysis shows that both selected parameters (Lh and Ip) contribute to the changes in the maximum flexural stress (σf) of the rASA filament additive manufacturing specimens. Of the two, the filling percentage shows a significantly stronger effect, exceeding the influence of the layer height by 55.89%.**

***Index Terms*—FDM; flexural; experimental study; FDM parameters.**

I. Introduction

GIVEN climate change, the continuous increase in plastic production and the negative impact of plastic waste, the need to decrease the quantity of plastic waste and adopt a circular economy is becoming increasingly urgent. In this context, extensive action plans have been developed at the European Union level to ensure that all plastic packaging is fully recyclable by 2030, [1]. Given the extraordinary advantages offered by additive manufacturing technologies (low manufacturing costs, efficient use of materials. Consequently, the application of the circular economy concept in the domain of additive manufacturing through thermoplastic extrusion engenders novel opportunities for the management of plastic waste, [2-13]. In this context, there are studies that investigate the impact of using recycled plastics in the field of additive manufacturing technologies through plastic extrusion, [14-30], however, certain branches have been found that have not yet been exploited, and through the present study the authors address a topic that has not yet been researched. In the paper [31], the authors demonstrate the viability of using recycled polycarbonate (PC) and acrylonitrile butadiene styrene (ABS) materials as raw materials for the manufacture of parts by thermoplastic extrusion of plastic granules. In the paper [32] a comparative study was carried out between the performances of parts additively manufactured from virgin carbon fibers (vCF) and recycled carbon fibers (rCF), the research results show that the bending strengths of the samples additively manufactured from rCF are 12.73% higher than the bending strengths of the samples manufactured from vCF. The findings of the study demonstrate that the utilisation of recycled carbon fibres (rCF) in the domain of additive manufacturing technologies through plastic extrusion constitutes an efficient and sustainable solution for the management of waste from this material.

In the paper [33], the study on the influence of the filling pattern and the filling percentage on the mechanical properties of tensile and dynamic stresses of sandwich structures additively manufactured from recycled polyethylene terephthalate glycol (rPET) is presented. The conclusions of the study show that the smallest dimensional deviations from the CAD model were obtained for the parts manufactured using the Concentric filling pattern and the filling percentage of 25%. In terms of mechanical performance, the parts additively manufactured using the Concentric filling pattern and the filling percentage of 50%, obtained the best tensile characteristics (tensile strength, elongation at break), but also the best ratio between strength and mass of the part.

In this study, the authors propose a sustainable approach for the recovery of acrylonitrile styrene acrylate (ASA) waste in the framework of additive manufacturing technologies by extrusion of plastics. The proposed solution is highlighted by reducing ASA waste, increasing the life span of the material, and reducing production costs. In the study, a statistical analysis is performed on the influence of process parameters on 3-point bending strengths, and subsequently the optimization of process parameters is performed in order to maximize 3-point bending strengths. In order to predict the values of 3-point bending strengths depending on the

values of the thermoplastic extrusion parameters (L_h and I_p), the regression equation was generated.

II. Determination of the Influence of FDM Parameters on the 3-Point Bending Behavior of Specimens Manufactured Additive From Recycled ASA Filament

A. Additive manufacturing of 3-point bending specimens by thermoplastic extrusion of rASA filament

The basis of the additive manufacturing process is the digital model in STL format (Standard Triangle Language), which contains the dimensional information of the part in the form of surface approximations using a network of triangles. In this context, using the CAD software Solidworks 2022, the technical drawing of the specimen in 2D format was created (fig. 1, a), and subsequently based on it the 3D model of the specimen was generated (fig. 1, b), this being the basis for creating the digital model in STL format, (fig. 1, c), [34].

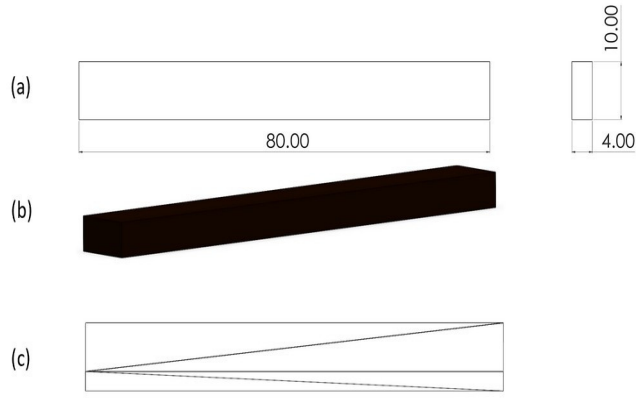

Fig. 1. 3 point bending sample: a) 2D model; b) 3D model; c) STL model.

The STL file of the 3-point bending sample was imported into the QIDI Slicer software. The thermoplastic extrusion parameters were setted were set in accordance with to the data in Table 1.

TABLE I. Parameters for Additive Manufacturing by Thermoplastic Extrusion of 3-Point Bending Specimens

Printing parameters	**QIDI Q1 Pro**
Material, Mat	rASA
Part orientation, P_o	X-Y
Extruder temperature, T_e	250 °C
Platform temperature, P_t	90 °C
Print speed, P_s	30 mm/s
Fill pattern, F_p	Grid
Layer height, L_h	0.10; 0.15; 0.20 mm
Fill percentage, I_p	50; 75; 100 %

Using the STL model corresponding to the 3-point bending specimen and the thermoplastic extrusion parameters from Table 1, 9 G-Code files (one file for each combination of parameters) were generated in the QIDI Slicer software, which contain the work instructions for the additive manufacturing of the 3-point bending specimens from rASA filament from the Everfil brand. Figure 2 shows the 3-point bending specimens in the QIDI Slicer software, [35].

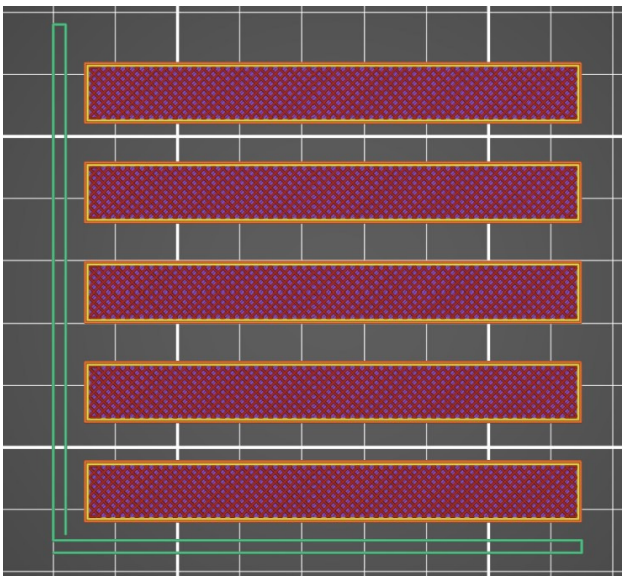

Fig. 2. 3-point bending specimens in QIDI Slicer.

The 9 G-Code files containing the work instructions for the additive manufacturing of 3-point bending specimens through thermoplastic extrusion of rASA filament were transferred to the QIDI Q1 Pro 3D printer. A total of where 45 specimens were manufactured for 3-point bending testing, (Fig. 3).

Fig. 3. 3-point bending specimens additively manufactured from rASA filament.

B. Evaluation of the influence of FDM parameters on the 3-point bending strengths of additively manufactured specimens from rASA filament

The 45 3-point bending samples samples, manufactured by means of additive manufacturing using thermoplastic extrusion of rASA filament, were tested for 3-point bending using the Barrus White 20 kN universal testing machine

(Fig. 4). The testing was conducted in accordance with the ISO 178:2019standard, with a speed of 5 mm/min, [36].

Fig. 4. 3-point bending test on the Barrus White 20 kN machine.

As demonstrated in Figure 5, the 45 specimens were subjected to the three-point bending test using the Barrus White 20 kN machine.

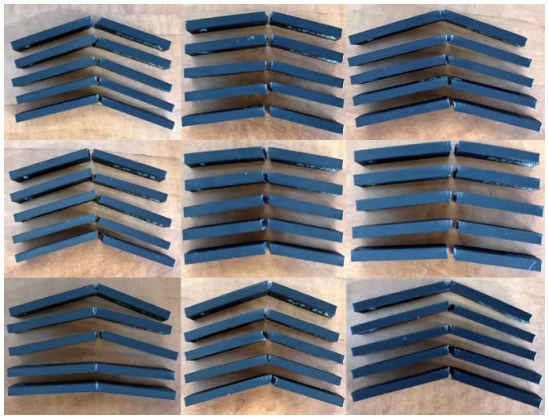

Fig. 5. Additively manufactured specimens on the QIDI Q1 Pro 3D printer, after performing the three-point bending test on the Barrus White 20 kN machine

Table 2 presents a summary of the 3-point bending strengths of the samples that were manufactured using additive manufacturing through thermoplastic extrusion of rASA filament.

Figure 6 graphically represents the average values of the 3-point bending strengths of the samples additively manufactured by thermoplastic extrusion of the rASA filament.

Figure 7 shows the graph expressing the influence of the variable parameters of thermoplastic extrusion (FDM) on the bending strengths of the additively manufactured samples from rASA filament. Analyzing the data in Table 2, it can be seen that the maximum value of the three-point flexural strength was obtained for sample 1 from the set manufactured with L_h = 0.20 mm and I_p = 100%. The lowest value of the flexural strength for the additively manufactured rASA filament specimens was obtained for sample 1 from the set produced with L_h = 0.10 mm and I_p = 50%.

TABLE II RESULTS OF 3-POINT BENDING TESTS OF SPECIMENS MANUFACTURED FROM RASA.

L_h, (mm)	I_p, (%)	FLEXURAL STRENGTH, σ_f					
		Sample number					
		1	2	3	4	5	Average
0.10	**50**	38.72	39.31	39.19	39.31	38.83	39.07
	75	44.01	45.07	44.72	44.48	44.48	44.55
	100	63.19	64.61	62.61	64.49	63.55	63.69
0.15	**50**	43.90	44.60	44.37	44.01	44.95	44.37
	75	44.01	45.07	44.72	44.48	44.48	44.55
	100	64.14	64.84	63.55	64.37	66.02	64.58
0.20	**50**	48.72	47.31	48.60	49.07	48.37	48.41
	75	59.90	60.37	59.90	59.55	59.90	59.92
	100	67.67	67.20	65.67	67.31	66.72	66.91

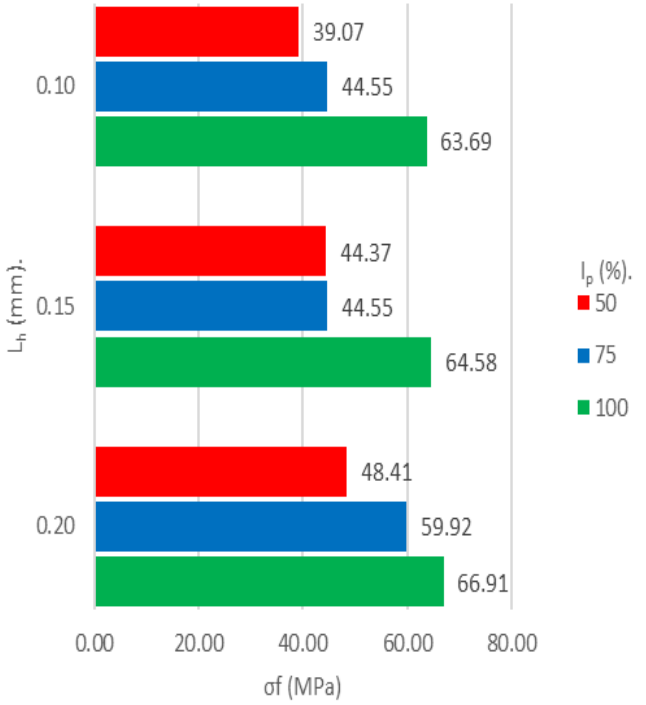

Fig. 6 Average flexural strength of rASA 3-point bending specimens.

The maximum average flexural strength, of 66.91 MPa, was obtained for the set of printed specimens with L_h = 0.20 mm and I_p = 100%. Increasing the filling percentage from 50% to 75% led to an improvement in the average flexural strength with values ranging from 0.42% to 23.77%. Increasing the filling level from 75% to 100% resulted in an additional increase in flexural strength ranging from 11.67% to 44.95%.

Minitab software was used to analyze the influence of FDM parameters (L_h and I_p) on the flexural behavior of specimens made on the QIDI Q1 Pro 3D printer by extruding rASA filament [37]. Figure 7 shows the diagram that highlights how these variable parameters of the thermoplastic extrusion process influence the flexural strength of additively manufactured rASA specimens.

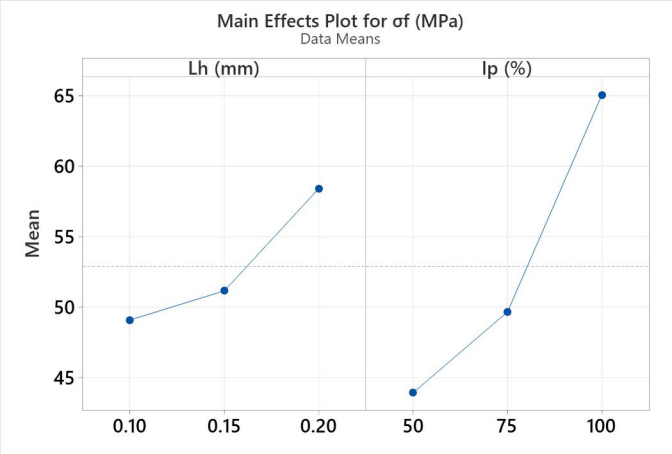

Fig 7. Influence of variable parameters of FDM on flexural strengts of samples made of rASA filament.

Analyzing the graph from figure 7, it can be seen tat the variable parameters of the 3D printing through thermoplastic extrusion L_h = (0.10, 0.15, 0.20) mm and I_p = (50, 75, 100)%, influence the flexural strength values of the specimens additively manufactured from rASA filament.

Figure 8 presents the Pareto chart, which illustrates how the variable parameters of thermoplastic extrusion (A = L_h and B = I_p) affect the flexural strength of the specimens obrained by additive manufacturing from rASA filament.

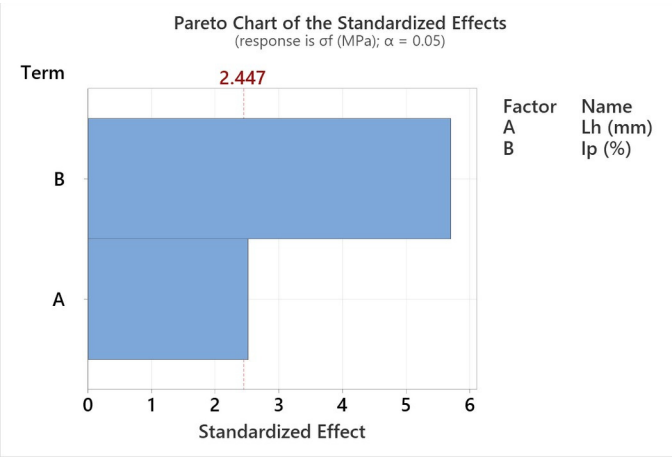

Fig. 8. Pareto chart regarding the influence of variable parameters of the FDM process (A = L_h and B = I) on the bending strength of specimens manufactured from rASA filament."

From the analysis of Figure 8, it appears that both variable parameters of thermoplastic extrusion influence the flexural strength of specimens additively manufactured from rASA filament, but the effect of the factor (B = I_p) is 55.89% greater than that of the factor (A = L_h).

Figure 9 presents the contour plot, which highlights how the variable parameters of the extrusion process (L_h and I_p) affect the values of the three-point flexural strength of specimens obtained by additive manufacturing from rASA filament.

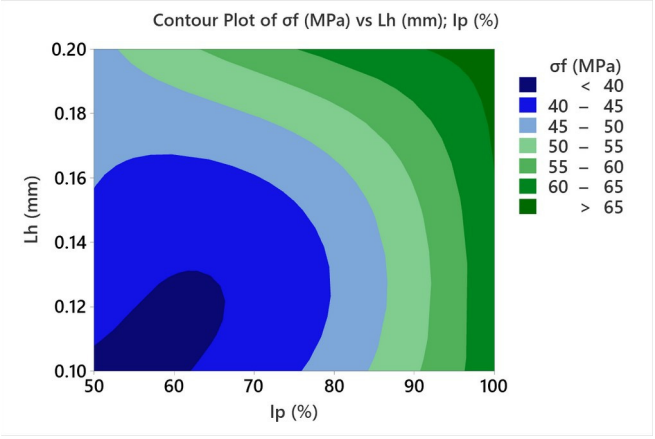

Fig. 9. Contour plot of the influence of variable FDM parameters (L_h and I_p) on the bending strengths of specimens manufactured from rASA filament.

Based on the contour diagram in Figure 9, it is observed that an increase in both the height of the layer (L_h) and the filling percentage (I_p) leads to higher values of three-point bending strength.

Using the statistical software Minitab, based on the variable parameters of the thermoplastic extrusion process (presented in Table 1) and the three-point flexural strength values for the additively manufactured samples of rASA filament (Table 2), optimization graphs of these parameters were generated, with the objective of obtaining maximum flexural strength values.

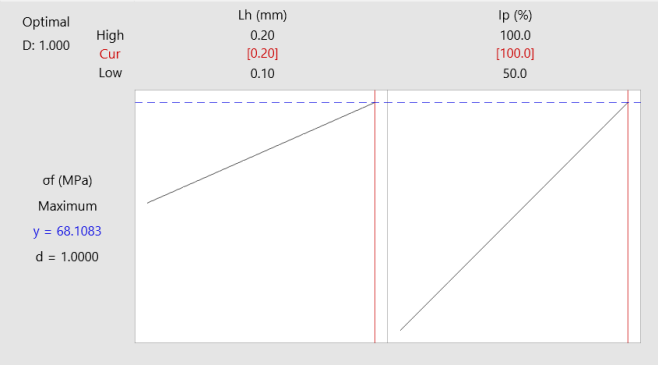

Fig. 10. Optimization graphs of variable thermoplastic extrusion parameters (L_h and I_p) for maximizing 3-point bending strengths.

According to the optimization graphs in Figure 10, it is concluded that the optimal thermoplastic extrusion (FDM) parameters for additive manufacturing of 3-point bending specimens from rASA are L_h = 0.20 mm and I_p = 100%.

In order to predict the 3-point bending strength depending on the values of the variable parameters of thermoplastic extrusion (L_h and I_p), using Minitab, the following regression equation was obtained:

$$\sigma f\ (MPa) = 7.26 + 93.1 \cdot L_h(mm) + 0.4222 \cdot I_p$$

III. Conclusions

This paper presents the results of research on the optimization of thermoplastic extrusion (FDM) parameters for the additive manufacturing of three-point bending test specimens from rASA filament, in the context of the transition to a circular economy. For the purpose of this study, 45 specimens were 3D printed on the QIDI Q1 Pro printer, using layer height values, L_h = (0.10, 0.15, 0.20) mm and filling percentages I_p = (50, 75, 100)%. Subsequently, all 45 specimens were tested for three-point bending on the Barrus White 20 kN universal testing machine, at a speed of 5 mm/min, according to the requirements of the ISO 178:2019 standard.

After performing the 45 experimental three-point bending tests on the Barrus White 20 kN machine, the following bending strength values were obtained:

- minimum average 3-point bending strength: 39.07 MPa;
- maximum average 3-point bending strength: 64.58 MPa;
- 3-point bending strength of the 45 specimens: 52.92 Mpa.

Using Minitab, the statistical influence of the influence of the variable parameters of thermoplastic extrusion (L_h and I_p) on the 3-point bending strengths of the specimens additively manufactured by thermoplastic extrusion of rASA filament was evaluated. The result of the analysis showed that both parameters have an influence on the 3-point bending strengths, but the influence of the I_p parameter is 55.89% greater than the influence of the L_h parameter.

Based on statistical analysis and the results obtained from three-point bending tests for additively manufactured rASA filament specimens, the optimization of the variable parameters of the thermoplastic extrusion process was carried out, with the aim of increasing the bending strength. The set of parameters identified as optimal is: L_h = 0.20 mm and I_p = 100%.

In order to predict the values of the bending resistance of the additively manufactured rASA filament specimens, depending on the values of the variable parameters, the regression equation 1 was generated.

Comparing the values of the 3-point bending strengths of specimens manufactured from rASA with L_h = (0.10, 0.15, 0.20) mm and I_p = 100% with those of specimens manufactured from virgin ASA using identical parameters, we conclude the following:

- for L_h = 0.10 mm, the 3-point bending strength of rASA is lower by 5.47%;
- for L_h = 0.15 mm, the 3-point bending strength of rASA is lower by 5.32%;
- for L_h = 0.20 mm, the 3-point bending strength of rASA is higher by 5.63%.

This study demonstrates that recycled materials can be a worthy alternative for additive manufacturing of parts with engineering applications.

By using optimal manufacturing parameters, material and equipment are efficiently utilized, superior mechanical characteristics are achieved, and the scrap rate is minimized.

The authors plan to extend the research to other types of materials as well as other types of mechanical tests.

References

[1] Available online: https://www.europarl.europa.eu/news/ro/press-room/20240419IPR20589/noi-norme-ue-pentru-a-reduce-refolosi-si-recicla-ambalajele (accesed on 14 February 2025).

[2] H. A. Colorado, E. I. G. Velásquez, and S. N. Monteiro, "Sustainability of additive manufacturing: the circular economy of materials and environmental perspectives," Journal of Materials Research and Technology, vol. 9, no. 4, pp. 8221–8234, Jul. 2020, https://doi.org/10.1016/j.jmrt.2020.04.062.

[3] M. Sauerwein, E. Doubrovski, R. Balkenende, and C. Bakker, "Exploring the potential of additive manufacturing for product design in a circular economy," Journal of Cleaner Production, vol. 226, pp. 1138–1149, Jul. 2019, https://doi.org/10.1016/j.jclepro.2019.04.108.

[4] F. A. Cruz Sanchez, H. Boudaoud, M. Camargo, and J. M. Pearce, "Plastic recycling in additive manufacturing: A systematic literature review and opportunities for the circular economy," Journal of Cleaner Production, vol. 264, p. 121602, Aug. 2020, https://doi.org/10.1016/j.jclepro.2020.121602.

[5] T. M. Tavares, G. M. D. Ganga, M. Godinho Filho, and V. P. Rodrigues, "The benefits and barriers of additive manufacturing for circular economy: A framework proposal," Sustainable Production and Consumption, vol. 37, pp. 369–388, May 2023, https://doi.org/10.1016/j.spc.2023.03.006.

[6] A. Cress, J. Huynh, E. Anderson, R. O'neill, Y. Schneider, and Ö. Keleş, "Effect of recycling on the mechanical behavior and structure of additively manufactured acrylonitrile butadiene styrene (ABS)," Journal of Cleaner Production, vol. 279, p. 123689, Aug. 2020, https://doi.org/10.1016/j.jclepro.2020.123689.

[7] J. Pakkanen, D. Manfredi, P. Minetola, and L. Iuliano, About the Use of Recycled or Biodegradable Filaments for Sustainability of 3D Printing. 2017, p. 785.

[8] A.-K. Behnert, O. Antons, and J. Arlinghaus, "Exploring the Challenges of Circular Economy Adoption: A Supply Chain Perspective," IFAC-PapersOnLine, vol. 58, no. 19, pp. 211–216, Jan. 2024, https://doi.org/10.1016/j.ifacol.2024.09.168.

[9] I. Ibrahim, A. Ashour, W. Zeiada, N. Salem, and M. Abdallah, "A Systematic Review on the Technical Performance and Sustainability of 3D Printing Filaments Using Recycled Plastic," Sustainability, vol. 16, p. 8247, Sep. 2024, https://doi.org/10.3390/su16188247.

[10] A. Oussai, B. Zoltan, and L. Kátai, "Development of 3D Printing Raw Materials from Plastic Waste. A Case Study on Recycled Polyethylene Terephthalate," Applied Sciences, vol. 11, p. 7338, Aug. 2021, https://doi.org/10.3390/app11167338.

[11] M. Jürgens and H.-J. Endres, "Environmental impacts of circular economy practices for plastic products in Europe: Learnings from life cycle assessment studies," Procedia CIRP, vol. 122, pp. 312–317, Jan. 2024, https://doi.org/10.1016/j.procir.2024.01.046.

[12] A. Mecheter, F. Tarlochan, and P. B. Pathare, "Exploring Recycled Polyethylene Terephthalate (PET) Based Cushioning Design to Reduce Bruise Damage in Pears," Applied Sciences, vol. 14, no. 13, p. 5936, Jan. 2024, https://doi.org/10.3390/app14135936.

[13] P. Q. K. Nguyen et al., "Influences of printing parameters on mechanical properties of recycled PET and PETG using fused granular fabrication technique," Polymer Testing, vol. 132, p. 108390, Mar. 2024, https://doi.org/10.1016/j.polymertesting.2024.108390.

[14] T. K. Meyer, N. G. Tanikella, M. J. Reich, and J. M. Pearce, "Potential of distributed recycling from hybrid manufacturing of 3-D printing and injection molding of stamp sand and acrylonitrile styrene acrylate waste composite," Sustainable Materials and Technologies, vol. 25, p. e00169, Sep. 2020, https://doi.org/10.1016/j.susmat.2020.e00169.

[15] W. Ma and J. L. Hao, "Enhancing a circular economy for construction and demolition waste management in China: A stakeholder engagement

and key strategy approach," Journal of Cleaner Production, vol. 450, p. 141763, Apr. 2024, https://doi.org/10.1016/j.jclepro.2024.141763.

[16] W. Ma, T. Liu, J. L. Hao, W. Wu, and X. Gu, "Towards a circular economy for construction and demolition waste management in China: Critical success factors," Sustainable Chemistry and Pharmacy, vol. 35, p. 101226, Oct. 2023, https://doi.org/10.1016/j.scp.2023.101226.

[17] J. Ahmed et al., "Mechanical properties evaluation of recycled high density polyethylene via additive manufacturing," vol. Vol. 2 No. 2, pp. 1–9, Dec. 2023, https://doi.org/10.5281/zenodo.10012303.

[18] N. K. Mansour et al., "Circular economy and 3D printing in the healthcare sector," Frontiers in Bioengineering and Biotechnology, vol. 13, Mar. 2025, https://doi.org/10.3389/fbioe.2025.1548550.

[19] A. Romani, S. Caba, R. Suriano, and M. Levi, "Recycling Glass and Carbon Fibers for Reusable Components in the Automotive Sector through Additive Manufacturing," Applied Sciences, vol. 13, no. 10, p. 5848, Jan. 2023, https://doi.org/10.3390/app13105848.

[20] L. E. Ruiz, A. C. Pinho, and D. N. Resende, "3D Printing as a Disruptive Technology for the Circular Economy of Plastic Components of End-of-Life Vehicles: A Systematic Review," Sustainability, vol. 14, no. 20, p. 13256, Jan. 2022, https://doi.org/10.3390/su142013256.

[21] J. Zhao, Y. Yang, M. H. Kobir, J. Faludi, and F. Zhao, "Driving additive manufacturing towards circular economy: State-of-the-art and future research directions," Journal of Manufacturing Processes, vol. 124, pp. 621–637, Aug. 2024, https://doi.org/10.1016/j.jmapro.2024.06.018.

[22] T. A. Alka, R. Raman, and M. Suresh, "Research trends in innovation ecosystem and circular economy," Discover Sustainability, vol. 5, Oct. 2024, https://doi.org/10.1007/s43621-024-00535-5.

[23] A. D. Dobrzańska-Danikiewicz, B. Siwczyk, A. Bączyk, and A. Romankiewicz, "Mechanical properties of recycled PLA and PETG printed by FDM/FFM method," Journal of Achievements in Materials and Manufacturing Engineering, vol. 119, pp. 49–59, Aug. 2023, https://doi.org/10.5604/01.3001.0053.9490.

[24] Der O., "Multi-Output Prediction and Optimization of CO2 Laser Cutting Quality in FFF-Printed ASA Thermoplastics Using Machine Learning Approaches," Polymers 2025, Polymers 2025, 17, 1910. https://doi.org/10.3390/polym17141910

[25] Ardeljan, D.D.; Frunzaverde, D.; Cojocaru, V.; Turiac, R.R.; Bacescu, N.; Ciubotariu, C.R.; Marginean, G. The Impact of Elevated Printing Speeds and Filament Color on the Dimensional Precision and Tensile Properties of FDM-Printed PLA Specimens. Polymers 2025, 17, 2090. https://doi.org/10.3390/polym17152090

[26] D. V. Iacob, D. G. Zisopol, M. Minescu, Study on the Optimization of FDM Parameters for the Manufacture of Three-Point Bending Specimens from PETG and Recycled PETG in the Context of the Transition to the Circular Economy. Polymers 2025, 17, 1645. https://doi.org/10.3390/polym17121645

[27] D. G. Zisopol, M. Minescu, D. V. Iacob, A Technical–Economic Study on Optimizing FDM Parameters to Manufacture Pieces Using Recycled PETG and ASA Materials in the Context of the Circular Economy Transition. Polymers 2025, 17, 122. https://doi.org/10.3390/polym17010122.

[28] D. G. Zisopol, M. Minescu, and D. V. Iacob, "A Study on the Optimization of FDM Parameters for the Manufacturing of Compression Specimens from recycled ASA in the Context of the Transition to the Circular Economy", Eng. Technol. Appl. Sci. Res., vol. 15, no. 1, pp. 19898–19902, Feb. 2025.

[29] A. S. Jaber, A. M. Saleh, and M. Q. Ibraheem, "A Study on the Influence of Enclosure Temperature Control on the Printing of ABS Filament in a Three-Dimension Printer", Eng. Technol. Appl. Sci. Res., vol. 15, no. 2, pp. 20681–20686, Apr. 2025.

[30] V.-L. Trinh, T.-D. Hoang, and Q.-T. Ngo, "The Influence of Processing Parameters on the Tensile Strength of 3D Printed Products", Eng. Technol. Appl. Sci. Res., vol. 15, no. 3, pp. 22663–22668, Jun. 2025.

[31] A. Romani, M. Levi, and J. Pearce, "Recycled polycarbonate and polycarbonate/acrylonitrile butadiene styrene feedstocks for circular economy product applications with fused granular fabrication-based additive manufacturing," Sustainable Materials and Technologies, vol. 38, p. e00730, Sep. 2023, https://doi.org/10.1016/j.susmat.2023.e00730.

[32] M. Ateeq, A. Akbar, and M. Shafique, "Advancing circular economy: Comparative analysis of recycled and virgin carbon fiber 3D printed composites on performance and eco-efficiency," Polymer, vol. 317, p. 127865, Jan. 2025, https://doi.org/10.1016/j.polymer.2024.127865.

[33] A. Al Rashid and M. Koç, "3D-Printed recycled polyethylene terephthalate (PET) sandwich structures – Influence of infill design and density on tensile, dynamic mechanical, and creep response," International Journal of Lightweight Materials and Manufacture, vol. 8, no. 4, pp. 442–452, Jul. 2025, https://doi.org/10.1016/j.ijlmm.2025.03.001.

[34] Available online: https://eu.qidi3d.com/pages/software-firmware (accessed on 4 January 2025).

[35] ISO 178:2019, Plastics — Determination of flexural properties.

[36] Available online: https://www.minitab.com/en-us/, (accessed on 7 March 2025).

Proceedings of the International Conference on Engineering, Technology and Applied Science Innovations pp. 21–27 DOI: 10.15439/2025I2025 ISSN 2300-5963 ACSIS, Vol. 46

Assessing the Accuracy of ERA5-Land in Heatwave Monitoring

Panagiotis Ioannidis
Laboratory of Atmospheric Physics, University of Patras, Patras, Greece
up1019394@ac.upatras.gr

Anna Mamara
Hellenic National Meteorological Service
Hellinikon, Athens, Greece
anna.mamara@hnms.gr

Athanassios A. Argiriou
Laboratory of Atmospheric Physics, University of Patras, Patras, Greece
athanarg@upatras.gr

***Abstract*—This study investigates the ability of reanalysis data to accurately identify heatwave events (HEs) in Greece from 1960 to 2022. High-resolution gridded reanalysis data from ERA5-Land, providing consistent land variables, namely maximum daily temperature over several decades, are utilized. In addition, HEs have been identified through high-quality homogenized meteorological data provided by the Hellenic National Meteorological Service (HNMS) from 1960 to 2022. The HEs are identified through a percentile-based threshold, calculated via a bootstrap resampling methodology to address artificial discontinuities in the reference period of 1961-1990. Furthermore, the HEs from both datasets are analyzed in terms of frequency, duration, and severity of events. Finally, the HEs calculated from the ERA5 dataset are assessed across five intensity classes derived from five percentile-based thresholds to evaluate their accuracy to capture these events. Expected results reveal the strengths and weaknesses of ERA5-Land data in capturing heatwave characteristics across different climate regions of Greece. This study will provide insights into the reliability of ERA5-Land as a tool for heatwave monitoring and risk assessment, informing the development of more effective heat-health action plans and climate adaptation strategies. The findings will be particularly relevant for regions with limited observational data, where ERA5-Land can serve as a valuable source of information.**

***Index Terms*—heatwave, Greece, severity, duration, frequency, reanalysis, climate.**

I. Introduction

GLOBALLY, heatwaves are expected to become more frequent and severe in the future [1, 2]. Subsequently, robust and accurate monitoring is required to mitigate socio-economic and environmental impacts [3, 4]. Europe has experienced numerous intense heatwaves in the 21st century which account for a substantial proportion of disaster-related fatalities and economic losses [3, 4]. Specifically, the Mediterranean basin has been identified as a hotspot for climate change impacts [5]. Projections indicate a significant increase in the number and intensity of heatwaves, particularly during summer months [6-8]. In Greece, utilizing various heatwave indices, HEs have increased in terms of both duration and frequency [8-10].

Reanalysis datasets, such as ERA5-Land, are often utilized to study HEs. Specifically, ERA5-Land provides high spatial (9 km) and temporal (hourly) resolution, integrating model data with observations to provide a robust set of data suitable for applications including the analysis of extreme temperature events [11]. Studies across Europe demonstrated the potential of this dataset for the analysis and monitoring of HEs [12, 13]. Researchers in [14] used ERA5-Land to investigate land-atmosphere interactions during HEs, reporting that dry soils reduce evaporation and increase surface heating, creating a positive feedback loop that intensifies the event. In [15] the same dataset is used to evaluate temperature extremes across the European continent. In Greece, the ERA5-Land dataset has been used to examine thermal bioclimatic conditions and assess heatwave intensity [9]. Furthermore, other reanalysis datasets have been employed to study compound events and atmospheric preconditions in Greece [16, 17]. This type of reanalysis data is particularly valuable for studying extreme events in data-sparse or mountainous regions with a small number of meteorological stations, assisting in filling observational gaps and providing a consistent view of land variables over several decades [18-22].

Taking into account the growing threat of HEs and the availability of reanalysis datasets, it is essential to conduct a thorough evaluation of ERA5-Land's ability to capture heatwave characteristics in Greece's complex climatology. Although reanalysis datasets provide valuable information for climate analysis, studies have highlighted the need to further evaluate their capacity to capture land-atmosphere interactions and extreme conditions such as heatwaves, especially in regions with sparse station distribution [12, 22]. In addition, the complex terrain of Greece poses challenges for reanalysis products to fully capture finer-scale atmospheric phenomena and small scale processes, leading to uncertainties in model-based products [23, 24]. This study aims to contribute to the development of robust monitoring systems by assessing ERA5-Land's accuracy for heatwave monitoring in Greece.

II. Methodology

Greece is located between 34º and 42º N in latitude and 19º to 28º E in longitude, with the Aegean Sea to the east, the Ionian Sea to the west, and the eastern Mediterranean Sea to the south. Daily Maximum Air Temperature (TX) timeseries for the period 1960-2022 from 26 HNMS weather

stations as illustrated in Figure 1 were used. The datasets underwent quality control and homogenization [25].

To investigate the suitability of ERA5-Land reanalysis data to monitor HEs, high-resolution gridded daily TX data were extracted for the period 1960-2022 from the Copernicus reanalysis dataset "ERA5-Land post-processed daily statistics from 1950 to present" [26]. The dataset's post-processed daily statistics are derived from the ERA5-Land global reanalysis, which provides land variables hourly at a 9-km spatial resolution and extends back to 1950.

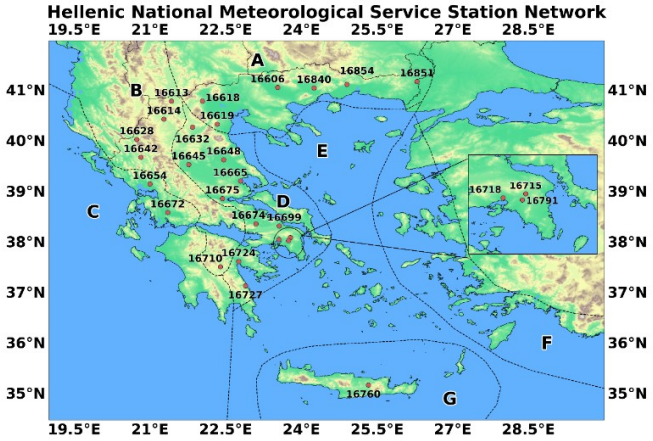

Fig. 1. HNMS weather station network and corresponding climate regions.

According to the World Meteorological Organization (WMO), there is no universally accepted definition of a heatwave, as its definition depends on the geographical and climatic context of the study area [27]. In general, the WMO defines a heatwave as a prolonged period of temperatures exceeding average values, often determined using a temperature-related threshold, lasting from two days to several months [28]. In this study, a heatwave day is defined as any day when the daily TX exceeds the climatological daily TX percentile-based threshold corresponding to the 95th percentile (TX95). A HE is defined as at least three consecutive heatwave days. The analysis is performed separately for each station and calendar day. Climatological TX percentile values were computed with respect to the 1961-1990 reference period. To mitigate inhomogeneity arising from artificial discontinuities at the edges of the reference period used for percentile calculations, the thresholds are determined using the bootstrap resampling procedure [29].

The Inverse Distance Weighting (IDW) spatial interpolation method is utilized to ensure a reliable comparison between weather station timeseries from HNMS and ERA5 data. The IDW is a technique that estimates variable values at unmeasured locations based on values from nearby measured locations [30]. Using this method, the two time series were compared using three climatological indices corresponding to Heatwave Frequency (HF), Heatwave Duration (HD), and Heatwave Severity (HS) of HEs and are represented by (1), (2), and (3), respectively.

$$HF = \sum_{i=1}^{n} D\left(HE_i\right) \tag{1}$$

$$HD = \frac{1}{m}\sum_{i=1}^{m} D\left(HE_i\right) \tag{2}$$

$$HS = \frac{1}{n}\sum_{i=1}^{n} \frac{1}{D\left(HE_i\right)} \sum_{j=sd_i}^{ed_i} TX_{ij} - TX_{p,j} \tag{3}$$

with HE_i the i-th HE, n the total number of identified HEs (i=1, 2, …, n), $D(HE_i)$ the duration in days of HE_i, m the number of days per period, TX_{ij} the daily maximum temperature of the j-th day of HE_i, and $TX_{p,j}$ the climatological percentile-based threshold of the daily maximum temperature for percentile p, (p: the 75th, 80th, 85th, 90th, or 95th percentile) for the j-th calendar day.

To assess the similarity between the measured and the reanalysis datasets during the different stages of the comparison, the two-sample Kolomogorov-Smirnov (KS) test was used. The KS test is a nonparametric statistical test used to determine whether two independent samples are drawn from the same underlying probability distribution [31]. It compares the empirical Cumulative Distribution Functions (CDFs) of the two samples to assess whether there is a statistically significant difference between them. This test does not require assumptions about the statistical distribution of the data, allowing for a robust comparison of the distributions of heatwave characteristics derived from both the weather station data and the ERA5 dataset. Finally, the occurrence of HEs within each time series from station measurements and ERA5 data was compared to determine the extent to which the latter dataset captures HNMS-derived Hes.

III. Results

The initial phase involved a comparative analysis between the spatially interpolated TX time series and their corresponding HNMS measurements. In Figure 2, a strong agreement between the ERA5-Land data and station measurements is observed as the distribution of the points closely aligned with the line of equality.

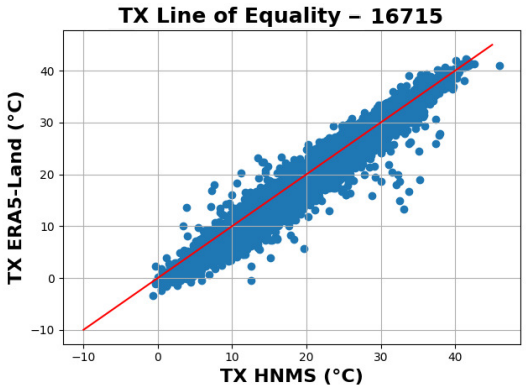

Fig. 2. Line of equality of the spatially interpolated, through IDW, ERA5-Land and HNMS weather station TX data for station 16715.

This alignment is further supported by Figure 3, which shows the CDFs of both datasets, displaying similar behavior. At high TX values, the reanalysis data exhibit stronger correlation than for lower TX values across all stations.

The small p-values across all stations, (Table I), indicate statistical significance for all cases. Furthermore, the KS statistic values ranging from 0.0560 to 0.2133 indicate a robust relationship between the interpolated values and observed measurements. At few stations stations (16619, 16628, 16654, 16675, 16727, 16840, and 16854) reanalysis TX values are underestimated, compared to measurements.

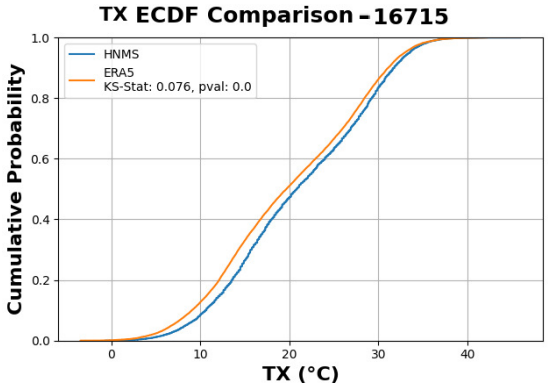

Fig. 3. CDF lines of the spatially interpolated ERA5-Land and HNMS weather station TX timeseries for station 16715.

TABLE I. KS TEST RESULTS BETWEEN ERA5 AND HNMS TX VALUES

Station Code	KS Statistic	p-value
16606	0.1449	0
16613	0.1521	0
16614	0.0971	0
16618	0.1063	0
16619	0.1985	0
16628	0.2492	0
16632	0.0560	0
16642	0.0993	0
16645	0.0881	0
16648	0.0623	0
16654	0.1890	0
16665	0.0631	0
16672	0.1432	0
16674	0.0944	0
16675	0.1714	0
16699	0.0601	0
16710	0.0862	0
16715	0.0763	0
16718	0.1328	0
16724	0.1581	0
16727	0.2133	0
16760	0.0548	0
16791	0.1159	0
16840	0.1769	0
16851	0.0884	0
16854	0.1936	0

TX95 thresholds were calculated for both measurements and the reanalysis data yielding two sets of TX95 values for each dataset per station: one for the reference period (1961–1990), referred to as the in-base period, and a second for the remaining years (1960 and 1991–2022), referred to as the out-of-base period. Figure 4 illustrates the comparison between the two datasets for station 16715. Most points from both periods lie below, but very close to, the line of equality, indicating a slight underestimation of TX95 station values by ERA5. This behavior is evident in most stations under study, except for stations 16632, 16648, 16665, 16674, 16699, 16715, 16718, 16724, 16760, and 16851, where values range between 15 °C and 25 °C.

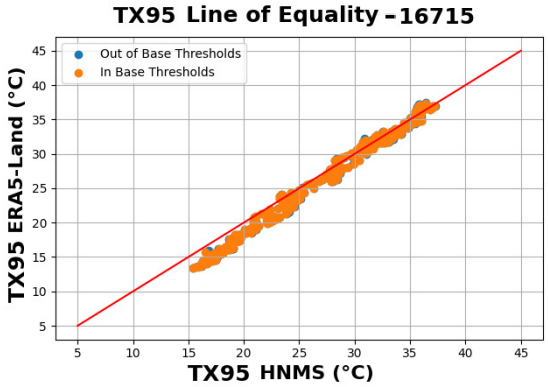

Fig. 4. Line of equality of the spatially interpolated, through IDW, ERA5-Land and HNMS weather station TX95 data for station 16715.

Figure 5 compares the CDFs of TX95 values for both in-base and out-of-base periods. The CDFs for ERA5 and HNMS closely follow one another in both periods, with only minor systematic deviations, mainly at lower values. The KS test indicates weak but statistically significant (p-value = 0.0) differences between the distributions across all stations. This suggests that while the datasets are not identical, they show a very high degree of similarity in representing the statistical distribution of TX95.

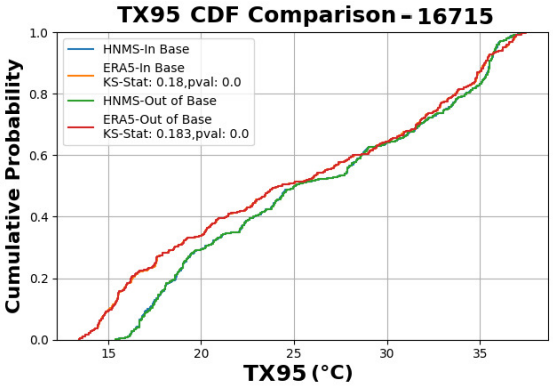

Fig. 5. CDF lines of the spatially interpolated, through IDW, ERA5-Land and HNMS weather station TX95 data for station 16715.

The summary of the KS test for all stations and both periods with respect to TX95 is shown in Table II. The KS statistic values range from 0.1530 to 0.3361 for the in-base years and from 0.1530 to 0.3388 for the out-of-base years, with all associated p-values very close to zero, indicating statistical significance. The maximum KS values (>0.3200) occur at stations 16619, 16628, and 16727, suggesting

stronger discrepancies between ERA5 and HNMS data. Conversely, the minimum KS value (0.1038) occurs at station 16648, where the agreement between datasets is strongest. Similarly, after the calculation of the climatological indices, the comparison is performed and the results are presented in Table III.

For the indices HF and HD, the KS statistics are generally high (HF: 0.2600–0.4448 and HD: 0.2317–0.4390), with consistently small p-values. This indicates systematic and statistically significant differences between ERA5 and HNMS index distributions. In particular, several stations (HF: 16675, 16715, 16718, 16724, 16727; HD: 16760) exhibit KS statistics above 0.4000, suggesting stronger discrepancies. In contrast, the HS index showed mixed results, with only 9 out of 26 stations presenting statistically significant differences. These include stations 16606, 16672, 16674, 16699, 16710, 16727, 16760, 16851, and 16854, with relatively low KS statistic values (0.1423–0.2401).

TABLE II. KS TEST RESULTS BETWEEN ERA5 AND HNMS TX95 VALUES

Station Code	KS Statistic In-Base Years	p-value In-Base Years	KS Statistic Out-of-Base Years	p-value Out-of-Base Years
16606	0.2814	0.0000	0.2814	0.0000
16613	0.2623	0.0000	0.2650	0.0000
16614	0.1995	0.0000	0.2022	0.0000
16618	0.1913	0.0000	0.1940	0.0000
16619	0.3224	0.0000	0.3197	0.0000
16628	0.3279	0.0000	0.3279	0.0000
16632	0.1749	0.0000	0.1831	0.0000
16642	0.2077	0.0000	0.2104	0.0000
16645	0.1749	0.0000	0.1776	0.0000
16648	0.1038	0.0386	0.1038	0.0386
16654	0.2869	0.0000	0.2814	0.0000
16665	0.1858	0.0000	0.1913	0.0000
16672	0.2623	0.0000	0.2623	0.0000
16674	0.2104	0.0000	0.2131	0.0000
16675	0.2787	0.0000	0.2787	0.0000
16699	0.1776	0.0000	0.1803	0.0000
16710	0.1749	0.0000	0.1803	0.0000
16715	0.1803	0.0000	0.1831	0.0000
16718	0.2486	0.0000	0.2459	0.0000
16724	0.2596	0.0000	0.2568	0.0000
16727	0.3361	0.0000	0.3388	0.0000
16760	0.1530	0.0004	0.1530	0.0004
16791	0.2186	0.0000	0.2213	0.0000
16840	0.3169	0.0000	0.3169	0.0000
16851	0.1967	0.0000	0.1995	0.0000
16854	0.3060	0.0000	0.3060	0.0000

Figure 6a presents the percentage of correctly identified HEs by ERA5 per station. The percentages range between 34.30% and 54.17%. Some stations, such as 16614, 16654, 16710, and 16791, exhibit relatively higher precision, suggesting that ERA5 is more reliable in identifying HEs. On the other hand, stations 16665, 16675, and 16724 presented the lowest percentages. This variability highlights that while ERA5-Land data are moderately effective in distinguishing HEs also captured by HNMS stations, its effectiveness is not uniform across all stations. Furthermore, Figure 6b illustrates the percentage of HEs successfully captured by ERA5 per station, regardless of false alarms. These percentages range between 47.46% (16613) and 72.63% (16724). This behavior suggests that ERA5-Land data tend to capture the majority of HNMS-derived HEs, although they sometimes overestimate their occurrence. The overall trend indicates that the system prioritizes sensitivity (detecting most events) over precision (avoiding false positives).

TABLE III. KS TEST RESULTS BETWEEN INTERPOLATED AND MEASURED CLIMATOLOGICAL INDICES.

Station Code	HF KS Statistic	HD KS Statistic	HS KS Statistic	HS p-value
16606	0.2600	0.3293	0.1713	0.0280
16613	0.2788	0.2317	0.0769	0.7186
16614	0.2614	0.2770	0.0857	0.5570
16618	0.3274	0.2449	0.0776	0.7056
16619	0.3774	0.3198	0.1004	0.4232
16628	0.3423	0.2904	0.0698	0.7408
16632	0.3358	0.2578	0.1371	0.1279
16642	0.3206	0.3461	0.1189	0.1855
16645	0.3561	0.2578	0.1137	0.2924
16648	0.3859	0.3017	0.1070	0.3797
16654	0.3386	0.3037	0.0816	0.6169
16665	0.3965	0.3712	0.1282	0.4628
16672	0.3785	0.2642	0.1593	0.0296
16674	0.3882	0.3431	0.1715	0.0346
16675	0.4100	0.3492	0.0892	0.6616
16699	0.3424	0.3736	0.1565	0.0752
16710	0.3959	0.2783	0.2137	0.0012
16715	0.4176	0.3106	0.0733	0.8369
16718	0.4358	0.2704	0.1390	0.1531
16724	0.4448	0.3664	0.0693	0.8687
16727	0.4198	0.3448	0.2301	0.0012
16760	0.3214	0.4390	0.2262	0.0032
16791	0.3871	0.3288	0.1520	0.0564
16840	0.3430	0.2911	0.1161	0.1790
16851	0.3428	0.3647	0.1423	0.0413
16854	0.2639	0.3109	0.2401	0.0001

The present study provides an overview of the ability of the ERA5-Land dataset to capture the occurrence of HEs. The agreement observed between ERA5-Land and station-based daily TX time series, as well as the reliable representation of TX95 values, is consistent with other studies that highlight ERA5-Land's accuracy in capturing general temperature patterns and extreme hot temperatures across Europe [12, 32]. Furthermore, the observation that ERA5-Land is valuable in areas with limited station coverage, particularly mountainous regions, is supported by other research highlighting the utility of reanalysis data in such data-sparse environments [20].

However, statistically significant discrepancies were identified in the HF and HD indices between the two datasets in all cases, despite good agreement in HS. Studies have indicated that while reanalysis products can accurately represent the magnitude of temperature extremes, they often struggle with the precise timing, frequency, and duration of HEs, especially in regions with complex or heterogeneous terrains [33]. The inherent smoothing effect of gridded datasets and the challenges in capturing finer-scale atmospheric phenomena in such diverse topographies, like those found in Greece, may lead to such discrepancies [23, 24, 34]. Despite these limitations, the strong temporal correspondence observed in

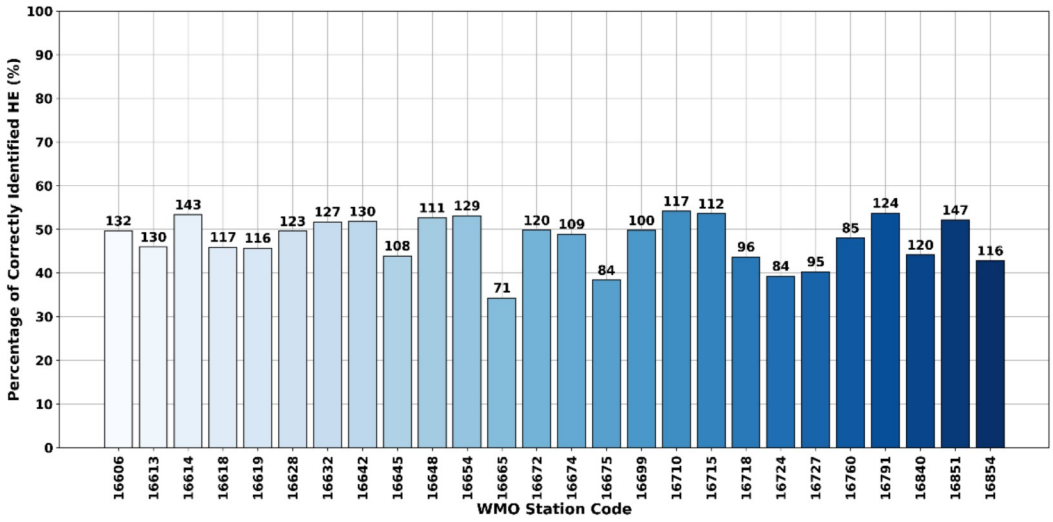

(a)

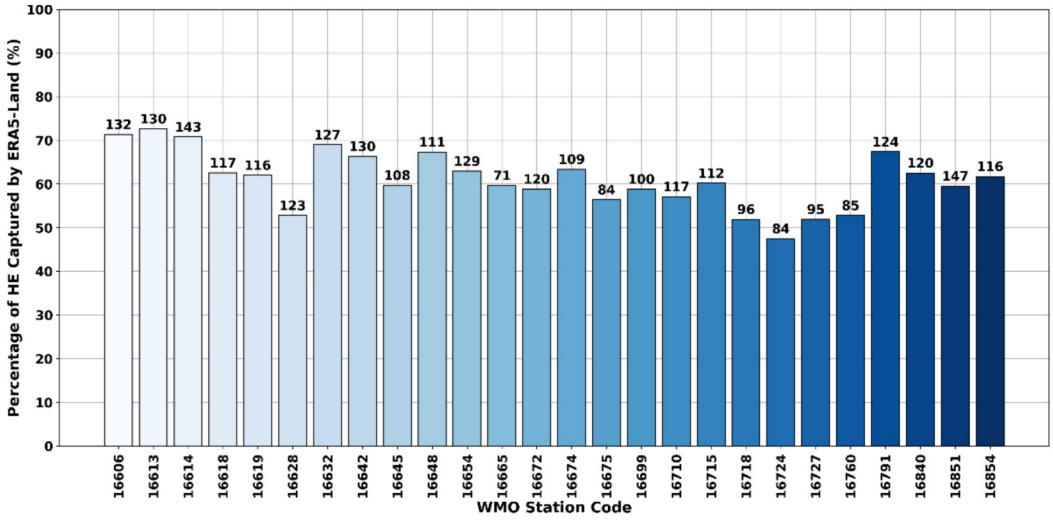

(b)

(a) Percentage of correctly identified HEs and (b) percentage of HEs captured by ERA5-Land dataset across different weather stations.Numbers above each bar indicate the exact number of HEs.

heatwave detection in this study reinforces the utility of ERA5-Land for identifying the occurrence and persistence of heatwaves.

IV. Conclusions

This study evaluated the ability of the spatially interpolated dataset, generated using the Inverse Distance Weighting (IDW) method, from the ERA5-Land reanalysis values from 1950 to present to replicate the measured daily Maximum Temperature (TX) and heatwave characteristics in Greece. The interpolated data were compared against measurements from the Hellenic National Meteorological Service (HNMS) weather station network.

The comparison of raw TX time series demonstrated strong agreement, with values distributed closely along the line of equality and Cumulative Distribution Functions (CDFs) exhibiting nearly identical shapes. In addition, Kolmogorov–Smirnov (KS) test statistics highlighted statistically significant results with low KS values (0.0560–0.2133) and near-zero p-values, indicating that ERA5-Land provides a robust reproduction of daily TX values across stations.

The assessment of daily 95th-percentile TX thresholds (TX95) further confirmed this reliability. ERA5-Land closely follows measurements, with only a few deviations, particularly at lower TX values. KS statistics indicated statistically significant but generally small discrepancies, consistent with the expected smoothing of localized extremes in gridded datasets. Similarly, the analysis of climatological indices highlighted systematic differences in HD and HF, with KS statistics often exceeding 0.3. These results suggest that ERA5-Land underestimates the temporal extent and recur-

rence of heatwaves, a limitation attributed to spatial averaging. In contrast, HS values showed far closer agreement, with small KS values but higher p-values.

Despite these systematic biases in HD and HF, the evaluation of HE detection revealed a moderate temporal correspondence between ERA5 and HNMS observations. The percentage of temporally correctly identified HEs ranged from 34.30% to 54.17%, while the percentage of HEs successfully captured by ERA5-Land ranged from 47.46% to 72.63%. This indicates that the ERA5-Land dataset can be utilized to identify the occurrence and persistence of heatwaves, but its limitations should be carefully considered. For precise temporal and recurrence analyses, however, the specific limitations of ERA5-Land concerning HF and HD should be acknowledged.

Overall, ERA5-Land is concluded to be a reliable dataset for assessing and identifying HEs in Greece, especially in areas with limited station coverage. While there are systematic biases in HD and HF , the dataset offers a reliable representation of extreme temperature intensity and a robust reproduction of heatwave occurrence. These findings highlight the suitability of ERA5-Land for climatological and risk assessment applications, while also underscoring the continued importance of station-based observations for capturing localized extremes.

References

[1] D. Arsenović, S. Savić, Z. Lužanin, I. Radić, D. Milošević, and M. Arsić, "Heat-related mortality as an indicator of population vulnerability in a mid-sized Central European city (Novi Sad, Serbia, summer 2015)," *Geographica Pannonica*, vol. 23, no. 4, pp. 204–215, 2019, https://doi.org/10.5937/gp23-22680.

[2] S. K. Behera, "Understanding the impact of climate change on extreme events," *Frontiers in Science*, vol. 2, Oct. 2024, https://doi.org/10.3389/fsci.2024.1433766.

[3] D. García-León, A. Casanueva, G. Standardi, A. Burgstall, A. D. Flouris, and L. Nybo, "Current and projected regional economic impacts of heatwaves in Europe," *Nature Communications*, vol. 12, no. 1, Oct. 2021, Art. no. 5807, https://doi.org/10.1038/s41467-021-26050-z.

[4] P. T. Nastos *et al.*, "Review article: Risk management framework of environmental hazards and extremes in Mediterranean ecosystems," *Natural Hazards and Earth System Sciences*, vol. 21, no. 6, pp. 1935–1954, June 2021, https://doi.org/10.5194/nhess-21-1935-2021.

[5] E. Tejedor, G. Benito, R. Serrano-Notivoli, F. González-Rouco, J. Esper, and U. Büntgen, "Recent heatwaves as a prelude to climate extremes in the western Mediterranean region," *npj Climate and Atmospheric Science*, vol. 7, no. 1, Sept. 2024, Art. no. 218, https://doi.org/10.1038/s41612-024-00771-6.

[6] F. G. Kuglitsch *et al.*, "Heat wave changes in the eastern Mediterranean since 1960," *Geophysical Research Letters*, vol. 37, no. 4, 2010, https://doi.org/10.1029/2009GL041841.

[7] M. O. Molina, E. Sánchez, and C. Gutiérrez, "Future heat waves over the Mediterranean from an Euro-CORDEX regional climate model ensemble," *Scientific Reports*, vol. 10, no. 1, May 2020, Art. no. 8801, https://doi.org/10.1038/s41598-020-65663-0.

[8] K. Tolika, "Assessing Heat Waves over Greece Using the Excess Heat Factor (EHF)," *Climate*, vol. 7, no. 1, Jan. 2019, Art. no. 9, https://doi.org/10.3390/cli7010009.

[9] K. Pantavou, V. Kotroni, G. Kyros, and K. Lagouvardos, "Thermal bioclimate in Greece based on the Universal Thermal Climate Index (UTCI) and insights into 2021 and 2023 heatwaves," *Theoretical and Applied Climatology*, vol. 155, no. 7, pp. 6661–6675, July 2024, https://doi.org/10.1007/s00704-024-04989-5.

[10] N. Politi, D. Vlachogiannis, A. Sfetsos, and P. T. Nastos, "High resolution projections for extreme temperatures and precipitation over Greece," *Climate Dynamics*, vol. 61, no. 1, pp. 633–667, July 2023, https://doi.org/10.1007/s00382-022-06590-w.

[11] C. A. Ramseyer and P. W. Miller, "Atmospheric Flash Drought in the Caribbean," Nov. 2023, https://doi.org/10.1175/JHM-D-22-0226.1.

[12] L. A. Espinosa, M. M. Portela, L. M. Moreira Freitas, and S. Gharbia, "Addressing the Spatiotemporal Patterns of Heatwaves in Portugal with a Validated ERA5-Land Dataset (1980–2021)," *Water*, vol. 15, no. 17, Jan. 2023, Art. no. 3102, https://doi.org/10.3390/w15173102.

[13] O. Lhotka and J. Kyselý, "The 2021 European Heat Wave in the Context of Past Major Heat Waves," *Earth and Space Science*, vol. 9, no. 11, 2022, Art. no. e2022EA002567, https://doi.org/10.1029/2022EA002567.

[14] P. A. Dirmeyer, G. Balsamo, E. M. Blyth, R. Morrison, and H. M. Cooper, "Land-Atmosphere Interactions Exacerbated the Drought and Heatwave Over Northern Europe During Summer 2018," *AGU Advances*, vol. 2, no. 2, 2021, Art. no. e2020AV000283, https://doi.org/10.1029/2020AV000283.

[15] C. M. Gouveia, J. P. A. Martins, A. Russo, R. Durão, and I. F. Trigo, "Monitoring Heat Extremes across Central Europe Using Land Surface Temperature Data Records from SEVIRI/MSG," *Remote Sensing*, vol. 14, no. 14, Jan. 2022, Art. no. 3470, https://doi.org/10.3390/rs14143470.

[16] I. Markantonis, D. Vlachogiannis, A. Sfetsos, and I. Kioutsioukis, "Investigation of the extreme wet–cold compound events changes between 2025–2049 and 1980–2004 using regional simulations in Greece," *Earth System Dynamics*, vol. 13, no. 4, pp. 1491–1504, Nov. 2022, https://doi.org/10.5194/esd-13-1491-2022.

[17] I. Markantonis, D. Vlachogiannis, A. Sfetsos, and I. Kioutsioukis, "Atmospheric preconditions investigation of wet-cold compound events in Greece between 1980 and 2004," *Theoretical and Applied Climatology*, vol. 155, no. 8, pp. 8151–8163, Aug. 2024, https://doi.org/10.1007/s00704-024-05122-2.

[18] J. Aschauer and C. Marty, "Evaluating methods for reconstructing large gaps in historic snow depth time series," *Geoscientific Instrumentation, Methods and Data Systems*, vol. 10, no. 2, pp. 297–312, Nov. 2021, https://doi.org/10.5194/gi-10-297-2021.

[19] B. Zellou, N. El Moçayd, and E. H. Bergou, "Review article: Towards improved drought prediction in the Mediterranean region – modeling approaches and future directions," *Natural Hazards and Earth System Sciences*, vol. 23, no. 11, pp. 3543–3583, Nov. 2023, https://doi.org/10.5194/nhess-23-3543-2023.

[20] P. Zhao, Z. He, D. Ma, and W. Wang, "Evaluation of ERA5-Land reanalysis datasets for extreme temperatures in the Qilian Mountains of China," *Frontiers in Ecology and Evolution*, vol. 11, Feb. 2023, https://doi.org/10.3389/fevo.2023.1135895.

[21] D. Power, M. A. Rico-Ramirez, S. Desilets, D. Desilets, and R. Rosolem, "Cosmic-Ray neutron Sensor PYthon tool (crspy 1.2.1): an open-source tool for the processing of cosmic-ray neutron and soil moisture data," *Geoscientific Model Development*, vol. 14, no. 12, pp. 7287–7307, Nov. 2021, https://doi.org/10.5194/gmd-14-7287-2021.

[22] G. Duveiller *et al.*, "Getting the leaves right matters for estimating temperature extremes," *Geoscientific Model Development*, vol. 16, no. 24, pp. 7357–7373, Dec. 2023, https://doi.org/10.5194/gmd-16-7357-2023.

[23] R. Paranunzio and F. Marra, "Open gridded climate datasets can help investigating the relation between meteorological anomalies and geomorphic hazards in mountainous areas," *Global and Planetary Change*, vol. 232, Jan. 2024, Art. no. 104328, https://doi.org/10.1016/j.gloplacha.2023.104328.

[24] I. Petrou and P. Kassomenos, "Local factors contributing to daytime, nighttime, and compound heatwaves in the Eastern mediterranean," *Theoretical and Applied Climatology*, vol. 156, no. 4, Mar. 2025, Art. no. 194, https://doi.org/10.1007/s00704-025-05429-8.

[25] J. A. Guijarro, "Homogenisation of Climatic Series with Climatol." 2021, https://climatol.eu.

[26] J. Muñoz Sabater *et al.*, "ERA5-Land post-processed daily statistics from 1950 to present." Copernicus Climate Change Service Climate Data Store, 2024, https://doi.org/10.24381/cds.e9c9c792.

[27] World Meteorological Organization, *Guidelines on the Definition and Characterization of Extreme Weather and Climate Events*. Geneva, Switzerland: World Meteorological Organization, 2023.

[28] Intergovernmental Panel on Climate Change, *Climate Change 2021 – The Physical Science Basis: Working Group I Contribution to the Sixth Assessment Report of the Intergovernmental Panel on Climate Change*. Cambridge, UK: Cambridge University Press, 2023.

[29] X. Zhang, G. Hegerl, F. W. Zwiers, and J. Kenyon, "Avoiding Inhomogeneity in Percentile-Based Indices of Temperature Extremes," June 2005, https://doi.org/10.1175/JCLI3366.1.

[30] P. A. Burrough and R. A. McDonnell, *Principles of Geographical Information Systems*. Oxford, UK: Oxford University Press, 1998.

[31] D. S. Wilks, *Statistical Methods in the Atmospheric Sciences*. Amsterdam, Netherlands: Elsevier Inc., 2020.

[32] K. Velikou, G. Lazoglou, K. Tolika, and C. Anagnostopoulou, "Reliability of the ERA5 in Replicating Mean and Extreme Temperatures across Europe," *Water*, vol. 14, no. 4, Jan. 2022, Art. no. 543, https://doi.org/10.3390/w14040543.

[33] E. Coughlan de Perez, J. Arrighi, and J. Marunye, "Challenging the universality of heatwave definitions: gridded temperature discrepancies across climate regions," *Climatic Change*, vol. 176, no. 12, Nov. 2023, Art. no. 167, https://doi.org/10.1007/s10584-023-03641-x.

[34] S. Sy, F. Madonna, F. Serva, I. Diallo, and B. Quesada, "Assessment of NA-CORDEX regional climate models, reanalysis and in situ gridded-observational data sets against the U.S. Climate Reference Network," *International Journal of Climatology*, vol. 44, no. 1, pp. 305–327, 2024, https://doi.org/10.1002/joc.8331.

Proceedings of the International Conference on Engineering, Technology and Applied Science Innovations pp. 29–32
DOI: 10.15439/2025I14
ISSN 2300-5963 ACSIS, Vol. 46

Depth Dependent Chemical Information in the Liquid-Solid Interface of Nanoparticles in Solutions by Conventional X-ray Photoelectron Spectroscopy

Stavros Karakalos
Research Core Facilities UC Merced
Merced, California 95343
skarakalos@ucmerced.edu

***Abstract*—Iron oxides are promising materials for a wide range of applications including photocatalytic water splitting, energy storage, and heterogeneous catalysis. However, understanding the interaction between iron oxide nanoparticles (Fe_2O_3 nps) and liquid water at the molecular level remains challenging due to the limitations of conventional surface analysis techniques. In this study, we present an in-situ X-ray Photoelectron Spectroscopy (XPS) investigation of Fe_2O_3 nps suspended in aqueous solution using a custom-designed environmental cell (e-cell), sealed with ultrathin silicon nitride (SiN) membranes. The attenuation of Fe 2p photoelectrons through 3–5 nm thick membranes was modeled and experimentally verified, enabling successful detection of chemical states within the aqueous suspension. Depth relevant information revealed a layered structure of the nps, with surface hydroxide species, an Fe_2O_3 core, and an intermediate FeOx phase. Spectra close to the valence band region confirmed the liquid nature of the encapsulated solution via the detection of water molecular orbitals, while ionic Na^+ signals further demonstrated the method's capability for detecting dissolved species. This approach provides a powerful platform for real-time chemical analysis of solid-liquid interfaces under ambient-like conditions, with broad implications for catalysis, electrochemistry, and environmental science.**

***Index Terms*—In-situ XPS, Iron oxide nps, Solid-liquid interface, Environmental cell, Aqueous suspension, Redox chemistry, Dissolved ions**

I. Introduction

IRON oxides possess a combination of attractive characteristics—such as low toxicity, robust stability, and low cost—that make them suitable for numerous emerging technologies. For instance, α-Fe_2O_3 has a band gap that is nearly optimal for driving solar-powered water splitting, carried out through the reaction:

$$H_2O \rightarrow 1/2O_2 + H_2$$

enabling the conversion of sunlight into chemical fuel and providing a significant pathway for hydrogen generation.[1] Additionally, α-Fe_2O_3 is being explored for energy-storage applications, particularly as an anode material in lithium-ion batteries, as well as in various heterogeneous catalytic processes.[2]

Understanding how water dissociatively chemisorbs on solids is a central topic in surface science, as surface hydroxyls can strongly modify surface characteristics and strongly influence reactivity. [3] Beyond its relevance to electrochemical and photoelectrochemical water splitting—where external conditions drive the breaking of O–H bonds—the basic mechanisms by which water interacts with clean, well-defined surfaces remain under active investigation. Although debates persist in certain systems regarding whether water adsorbs intact or dissociates upon adsorption, it is widely recognized that surface imperfections, especially on metal-oxide substrates, can promote the spontaneous cleavage of water molecules.

The aforementioned applications make fundamental understanding of Iron (Fe and FexOy) reactivity at the liquid/solid interface, crucial for rational design of materials. A number of experimental approaches for the study of liquids at the molecular level, with the use of surface sensitive techniques, have been proposed during the last two decades. X-Ray Photoelectron Spectroscopy (XPS) has been applied on liquids using different experimental setups like: ambient pressure XPS[4], use of environmental cells, consisting of a few layers thick graphene[5, 6], grapheme oxide[7], or silicon nitride membranes[8] and with the use of liquid-microjets [9].

II. Experimental

In the present study the approach used to study the liquid/solid interface, was proposed by Raimu Endo et al.[8] We created an environmental cell (e-cell) in which a liquid can be sealed inside a cavity, using a 5nm thick SiN membrane as a window, quasi-transparent for X-rays/photoelectrons, that separates the vacuum from the environment (Figure 1). The nanoparticle (np) suspension used, is the alpha-Fe_2O_3 10nm np 15wt% water dispersion (99.9% purity, Orange-Red) from US Research Nanomaterials, Inc. The np suspension was encapsulated in silicon microchips (SiMPore, Inc.), with a 25 x 25 μm window covered by a 5 nm-thick SiN membrane at the center of the 3-mm-long microchip. The microchips were used as received, without any further treatment before the introduction in the Ultra High Vacuum (UHV) chamber.

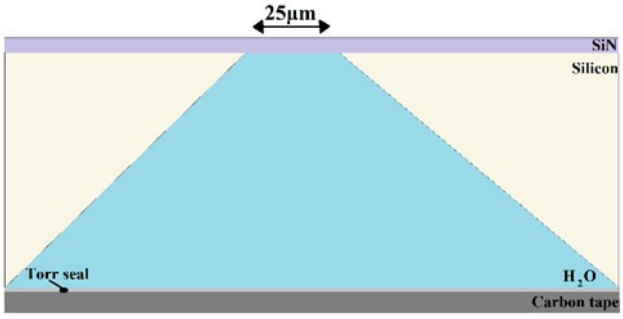

Figure 1. Cross-sectional schematic representation of the Si chip filled with H_2O, sealed on the top side by a SiN membrane and with Torr seal glue on the bottom side.

The XPS measurements were performed using a Kratos AXIS Ultra DLD XPS system with a hemispherical energy analyzer and a conventional lab-based monochromatic Al Kα source, operated at 15 keV and 150 W. The X-rays were incident at an angle of 45° with respect to the surface normal. Analysis was performed at a pressure ~$3x10^{-9}$ mbar. High resolution core level spectra were measured with a Pass Energy (PE) of 40 eV, except Fe 2p regions that were recorded with 80 ev PE. The XPS experiments on the e-cell were performed without the use of an electron gun (e-gun), although for the dried samples on HOPG an e-gun was used and directed electrons on the sample for charge neutralization. Ion sputtering was performed by accelerating Ar^+ ions (4 kV, 15 mA emission) towards the e-cell's surface for 40 sec. The estimated thickness of the removed layer under the sputtering conditions used in this study, is 2nm for each 40 sec cycle.

The 25 μm wide SiN window of 5 nm thickness, can hold 2.25 atm of pressure according to the manufacturer's standards, which is more than twice the ambient pressure inside the e-cell. It is expected that SiN thickness of ~2.5 nm could still hold more than 1 atm of pressure. The attenuation ratio, I_{exp} / I_0, of photoelectrons for the Fe 2p peak can be calculated by the equation:

$$I_{exp} / I_0 = \exp (d / \lambda_{IMFP} \cdot \cos \theta) \quad (1)$$

where d, λ_{IMFP}, and θ are the thickness of the membrane, the inelastic mean free path of Fe 2p and the take-off angle of photoelectrons, respectively. The λ_{IMFP} for photoelectrons with kinetic energy of ~776.0 eV ($E_{kin} = hv - E_{binding}$, hv = 1486.6 eV) below a layer of inorganic compound, is 2.7 nm. Angle θ in the experimental setup used in these measurements is 0° (cos θ = 1), because the electron analyzer was placed parallel to the surface normal of the e-cell surface.

Figure 2 shows that the experimental setup used for these studies is expected to permit 15.7% of the inelastic emitted Fe 2p photoelectrons from the solution to pass a 5 nm thick SiN membrane. When the SiN is thinner, around 3 nm thick, the 33.0% of the inelastic emitted Fe 2p photoelectrons from the solution are expected to pass through the membrane. These theoretical calculations clearly demonstrate that recording of the Fe 2p peak through a thin SiN membrane is possible when using conventional X-Rays. In order to improve the signal to noise ratio, long recorded times might be needed.

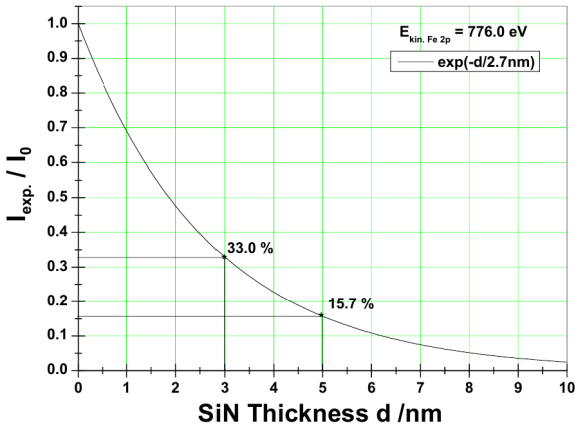

Figure 2. Attenuation ratio of the Fe 2p photoelectron intensity (I_{exp} / I_0) passing through the SiN membrane as a function of the membrane thickness.

III. Results & Discussion

he Fe 2p peaks that were recorded through the SiN window are shown in Figure 3 in comparison to the Fe 2p spectrum acquired from the dried Fe_2O_3 np aqueous suspension on HOPG. The as-received window was contaminated mainly by SiO_2 and Carbon preventing the recording of the XPS signal from the suspension inside the e-cell. After removing surface atomic layers with Ar^+ sputtering, the Fe 2p peaks were recorded, for the 5nm and 3nm thick windows. Peak deconvolution of the data, showed in both cases the existence of three chemical states of iron in the suspension. It is obvious that Fe_2O_3 np were able to dissociate water inside the solution, creating iron hydroxide species on the np surface. Signal for the Fe_2O_3 state is detected in the Fe 2p region and also a lower BE contribution at ~708.0 eV attributed to FeO_x with $x < 1$. It is known that water interaction with Fe_2O_3 reduces iron from Fe^{3+} to Fe^{2+} due to the creation of oxygen vacancies,[10] but in the present study we recorded that inside the aqueous solution, iron oxide is reduced even to lower oxidation state than Fe (II). The same solution that was dried in the ambient on HOPG, shows that the reduction caused from water is from Fe (III) to Fe(II) as reported in the literature.

The lower than Fe (II) oxidation state of Fe2O3 suspension in water, indicates stronger water-np interaction that was not previously observed. XPS studies on dried samples were not able to capture the real oxidation state of Iron inside the solution making the current experimental approach invaluable for in-situ measurements. The presence of hydroxides on the dried sample is expected in the literature [11], as hydroxides are stable enough to be detected on metals under Ultra High Vacuum conditions.

By removing ~2 nm of SiN layer on top of the np suspension, we are able to record Fe 2p photoelectrons from ~2nm

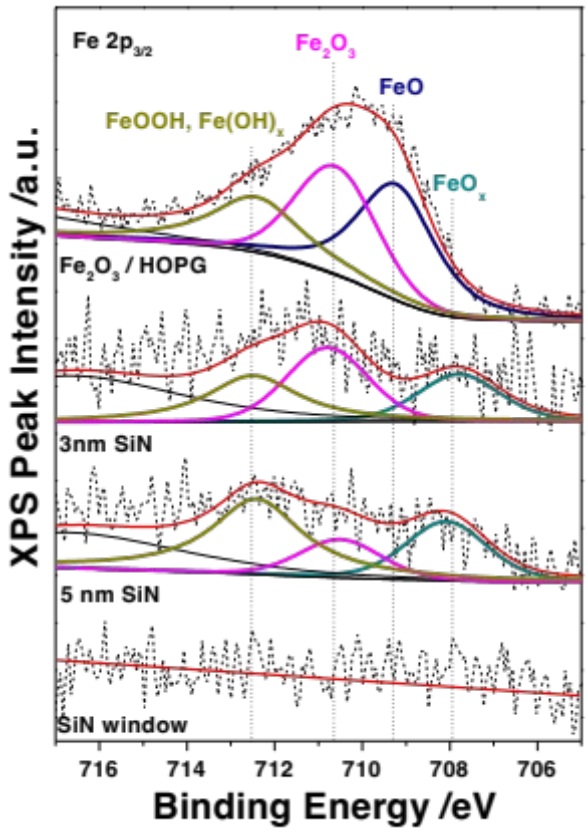

Figure 3. Fe 2p photoelectron spectra acquired from the e-cell filled with Fe2O3 np aqueous suspension without charge neutralization in comparison to the Fe 2p spectrum acquired from the dried Fe2O3 np aqueous suspension on HOPG.

deeper. This depth dependent information (Figure 4) showed that the intensity ratio of the Fe 2p peak contributions changes as a function of the depth of analysis. The hydroxide contribution to the overall Fe 2p signal reduces as we get information from deeper inside the np, the Fe2O3 contribution increases and the FeOx is almost stable (Figure 4).

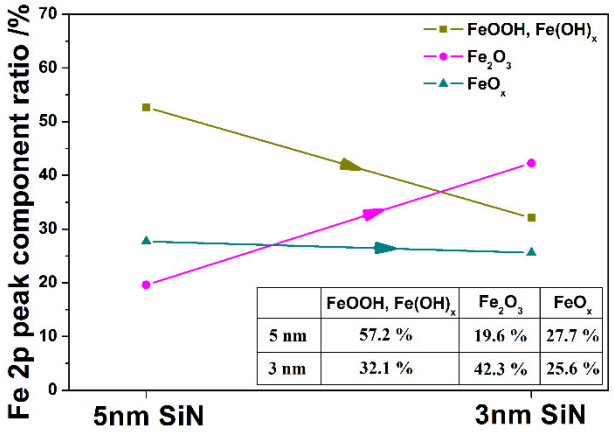

	FeOOH, Fe(OH)x	Fe2O3	FeOx
5 nm	57.2 %	19.6 %	27.7 %
3 nm	32.1 %	42.3 %	25.6 %

Figure 4. Depth-dependence of the Fe 2p intensity of the different iron chemical states.

The information provided by these changes in the peak intensity ratio, indicate a layered structure of the np due to the interaction with liquid water (Scheme 1). The nps consist of a surface layer of iron hydroxide and a Fe_2O_3 core. The FeOx state of iron, extends within the other two iron states, almost homogeneously from the outer surface layers close to the Fe_2O_3 core.

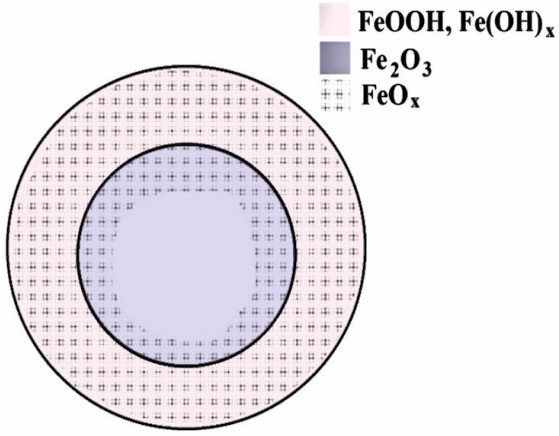

Scheme 1. Chemical characterization of layered structure of Fe2O3 np in water.

Finally, the strength and the relevance of the current experimental approach is demonstrated by recording the region at low Binding Energies close to the valence band (Figure 5). The electronic structure of liquid water has been the focus of extensive theoretical and experimental investigation, yielding a well-established description of its five filled and three lowest empty molecular orbitals: $(1a_1)^2$ $(2a_1)^2$ $(1b_2)^2$ $(3a_1)^2$ $(1b_1)^2$ $(4a_1)^0$ $(2b_2)^0$ $(3b_2)^0$. The two orbitals at the lowest energies—$1a_1$ (non-bonding) and $2a_1$ (bonding)—originate primarily from the oxygen atom's 1s (entirely) and 2s (predominantly) atomic orbitals. These features are characteristic signatures of liquid-phase water, and detecting them serves as evidence that the sample indeed exhibits liquid-like behavior.

We have to note here that photoelectrons with low Binding Energy have the highest Kinetic Energy possible for the excitation energy of the X-Rays used for conventional XPS. For that reason, the percentage of the inelastic photoelectrons that are expected to pass through the SiN membrane and reach the analyzer, is much higher than the Fe 2p photoelectrons. For that reason, the peak Intensity in the recorded region close the Valence band is much higher than the peak intensity of the region of the Fe 2p peak.

In Figure 5 we can clearly see that the 2α1 molecular orbital of liquid water was recorded for both SiN thicknesses presented in these studies, indicating that the liquid solution was present inside the cell during the measurements.[12, 13] An additional bonus feature is that we were able to record dissolved ions into the liquid. The Na^+ (2p) peak was recorded indicating the presence of Na ions in the solution. [14, 15] The capability of recording the presence of elements in their ionic state in liquids can have tremendous impact to environmental studies making the current experimen-

tal approach valuable to studies form other fields than catalysis.

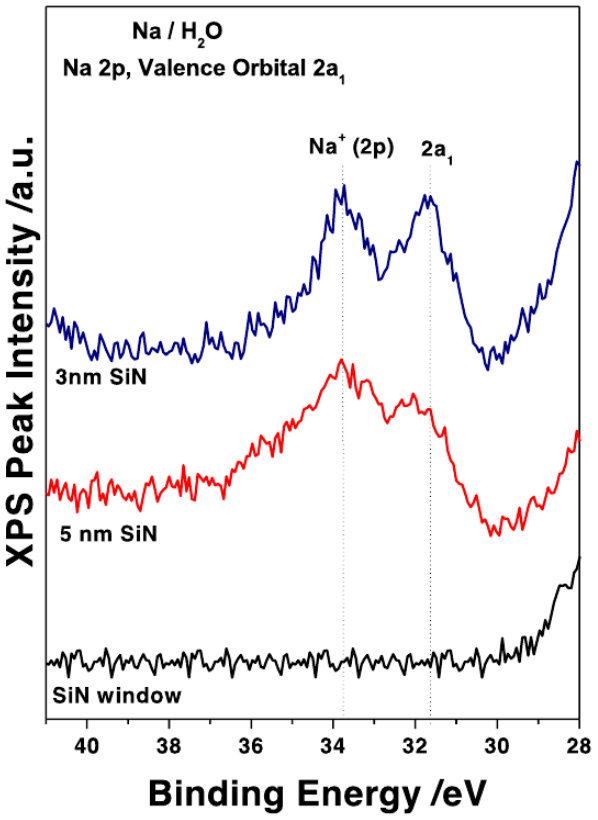

Figure 5. Liquid water orbital $2a_1$ recorded from the solution inside the E-cell. The ionic state Na^+ (2p) was also recorded from the solution indicating the presence of dissolved ions into the water.

IV. Conclusions

We have demonstrated a robust in-situ experimental method for probing the chemical state of iron oxide nanoparticles in aqueous environments using XPS through ultrathin SiN membranes. Our findings reveal that Fe_2O_3 nps interact strongly with liquid water, leading to partial reduction of Fe^{3+} to Fe^{2+} and even lower oxidation states, which cannot be captured by traditional XPS analysis of dried samples. Depth-resolved measurements show a stratified structure composed of an outer hydroxide layer, a Fe_2O_3 core, and a stable FeOx intermediate. Additionally, the detection of liquid-phase molecular orbitals and dissolved Na^+ ions confirms the presence and analyzability of the liquid environment inside the e-cell. This work validates the use of SiN-based e-cells for in-situ XPS analysis of solid-liquid interfaces and opens new possibilities for studying redox reactions, surface chemistry, and ionic species in fields ranging from catalysis and energy storage to environmental science.

Acknowledgment

The author would like to thank Phasma Labs Inc. for funding the research and providing the XPS experimental capabilities.

References

[1] N. Lahiri *et al.*, "Interplay between Facets and Defects during the Dissociative and Molecular Adsorption of Water on Metal Oxide Surfaces," *J. Am. Chem. Soc.,* vol. 145, p. 2930−2940, 2023, doi: 10.1021/jacs.2c11291.

[2] Y.-M. Lin, P. R. Abel, A. Heller, and C. B. Mullins, "α-Fe2O3 Nanorods as Anode Material for Lithium Ion Batteries," *J. Phys. Chem. Lett.,* vol. 2, pp. 2885–2891, 2011, doi: 10.1021/jz201363j.

[3] H. Xu *et al.*, "Splitting Water on Metal Oxide Surfaces," *J. Phys. Chem. C,* vol. 115, pp. 19710–19715, 2011, doi: 10.1021/jp2032884.

[4] D. Shah *et al.*, "Liquid water, by near-ambient pressure XPS," *Surface Science Spectra,* vol. 26, p. 024003, 2019, doi: 1055-5269/2019/26(2)/024003/6.

[5] J. Kraus *et al.*, "Photoelectron Spectroscopy of Wet and Gaseous Samples through Electron Transparent Graphene Membranes," *Nanoscale,* vol. 6, pp. 14394-14403, 2014, doi: 10.1039/C4NR03561E.

[6] R. S. Weatherup, B. Eren, Y. Hao, H. Bluhm, and M. B. Salmeron, "Graphene Membranes for Atmospheric Pressure Photoelectron Spectroscopy," *J. Phys. Chem. Lett.,* vol. 7, p. 1622−1627, 2016, doi: 10.1021/acs.jpclett.6b00640.

[7] A. Kolmakov *et al.*, "Graphene oxide windows for in situ environmental cell photoelectron spectroscopy," *Nat. Nanotechnology* vol. 6, pp. 651–657, 2011, doi: 10.1038/NNANO.2011.130.

[8] R. Endo, D. Watanabe, M. Shimomura, and T. Masuda, "In situ X-ray photoelectron spectroscopy using a conventional Al-Kα source and an environmental cell for liquid samples and solid-liquid interfaces," *Appl. Phys. Lett.,* vol. 114, p. 173702, 2019, doi: 10.1063/1.5093351.

[9] J. P. Bruce and J. C. Hemminger, "Characterization of Fe2+ Aqueous Solutions with Liquid Jet X-ray Photoelectron Spectroscopy: Chloride Depletion at the Liquid/ Vapor Interface Due to Complexation with Fe2+," *J. Phys. Chem. B,* vol. 123, p. 8285−8290, 2019, doi: 10.1021/acs.jpcb.9b06515.

[10] S. Poulin, R. Franca, L. M.-B. ´langer, and E. Sacher, "Confirmation of X-ray Photoelectron Spectroscopy Peak Attributions of Nanoparticulate Iron Oxides, Using Symmetric Peak Component Line Shapes," *J. Phys. Chem. C,* vol. 114, pp. 10711–10718 2010, doi: 10.1021/jp100964x.

[11] P. Zhao and B. E. Koel, "Water Oxidation Catalysis: E ects of Nickel Incorporation on the Structural and Chemical Properties of the α-Fe2O3(0001) Surface," *ACS Appl. Mater. Interfaces,* vol. 6, p. 22289−22296, 2014, doi: dx.doi.org/10.1021/am5062773.

[12] B. Winter, R. Weber, W. Widdra, M. Dittmar, M. Faubel, and I. V. Hertel, "Full Valence Band Photoemission from Liquid Water Using EUV Synchrotron Radiation," *J. Phys. Chem. A,* vol. 108, pp. 2625-2632, 2004, doi: 10.1021/jp030263q.

[13] B. Jagoda-Cwiklik, P. Slavıcek, D. Nolting, B. Winter, and P. Jungwirth, "Ionization of Aqueous Cations: Photoelectron Spectroscopy and ab Initio Calculations of Protonated Imidazole," *J. Phys. Chem. B, Letters,* vol. 112, pp. 7355-7358, 2008, doi: 10.1021/jp802454s.

[14] N. Ottosson, M. Faubel, S. E. Bradforth, P. Jungwirth, and B. Winter, "Photoelectron spectroscopy of liquid water and aqueous solution: Electron effective attenuation lengths and emission-angle anisotropy," *Journal of Electron Spectroscopy and Related Phenomena,* vol. 177, pp. 60–70, 2010, doi: 10.1016/j.elspec.2009.08.007.

[15] B. Winter *et al.*, "Electron Binding Energies of Aqueous Alkali and Halide Ions: EUV Photoelectron Spectroscopy of Liquid Solutions and Combined Ab Initio and Molecular Dynamics Calculations," *J. AM. CHEM. SOC.,* vol. 127, pp. 7203-7214, 2005, doi: 10.1021/ja042908l.

Proceedings of the International Conference on Engineering, Technology and Applied Science Innovations pp. 33–38
DOI: 10.15439/2025I29
ISSN 2300-5963 ACSIS, Vol. 46

Ground Resistance Measurements and Evaluation of Grounding Electrodes Performance

Konstantinos Koutras
School of Electrical and Computer Engineering
Technical University of Crete
Chania, Greece
kkoutras@tuc.gr

Eleni Tsolou
Department of Electrical & Computer Engineering
University of Patras
Patras, Greece
eletso@gmail.com

Georgios Peppas
School of Electrical and Computer Engineering
Technical University of Crete
Chania, Greece
peppas@tuc.gr

Apostolos Samiotis
Department of Electrical & Computer Engineering
University of Patras
Patras, Greece
up1072779@ac.upatras.gr

Eleftheria Pyrgioti
Department of Electrical & Computer Engineering
University of Patras
Patras, Greece
e.pyrgioti@ece.upatras.gr

***Abstract*—This paper presents an experimental study on grounding resistance measurements carried out at the University of Patras. Seven case studies are examined to analyze the impact of soil type, electrode geometry, and grounding system configuration on measured resistance values. The findings highlight key factors affecting grounding performance and provide a basis for optimizing system design in varying soil conditions.**

***Index Terms*—Earth Electodes; Grounding system; Ground Resistance; Soil Resistivity.**

I. Introduction

THE primary purpose of an electrical grounding system is to ensure safety, support reliable operation, and extend the longevity of electrical installations. It provides a low-resistance path for fault currents, thereby preventing electric shock, reducing fire hazards, stabilizing system voltage, and protecting sensitive equipment. Grounding effectiveness is typically assessed through resistance measurements, as low grounding resistance enhances safety and mitigates back flashover risk due to lightning surges.

Ground resistance (R_g) is determined by the grounding system's geometry and the soil resistivity (ρ) in which it is embedded. Key factors influencing R_g include electrode characteristics (length, diameter, burial depth, shape, material, and number), soil resistivity, moisture content, and temperature.

This study investigates the variation of grounding resistance across seven experimental configurations, considering different soil types, electrode parameters, and grounding system arrangements. The experiments were conducted at a designated site within the University of Patras, where six ground electrodes were installed. Resistance measurements were taken from October 2024 to May 2025. Results for each case are analyzed and compared, providing quantitative insight into electrode performance, with observed deviations from theoretical predictions further discussed.

II. The Location Under Study

The experimental process of measurement of grounding resistance was carried out in the area of the University of Patras and more specifically in the area opposite of the Department of Electrical Engineering. In figure 1 the selected area is indicated by red colour.

Figure 1. Location of the expirement.

The selected location is well-suited for repeated measurements, as it is an open, unoccupied area within the University of Patras, free from interference by other departments. Its large size enhances the validity and accuracy of the measurements by allowing sufficient spacing between test points. Six ground electrodes were installed at different positions to capture variations in soil conditions: three were placed in an open, tree-covered area, and the remaining three near the High Voltage Laboratory building.

III. Materials and Methods

A. Materials and Equipment

In this study for all the six different cases the materials used to conduct the experiment was copper rod 1.5 meters long and 16 millimeters in diameter as presented in figure 2 below.

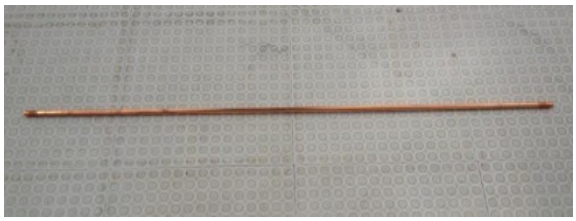

Figure 2. Copper rod 16×1500 mm

Whereas the following equipment and tools were used in carrying out the resistivity measurement as seen in Figure 3 below:

- Digital - Earth Resistance Tester
- Meter Hammer (to drive probes)
- Measuring tape
- Test Electrodes three insulated wire conductors

Figure 3. Resistivity Measurement / Test Equipment

B. Resistance Measurement Method

In this experiment the drop voltage method is adopted for measuring the earthing resistance of an earth electrode. Fall-of-Potential measuring technique [7] is the most recognized method for measuring the resistance to earth of a grounding system, or the ground system performance. This method is based on an IEEE standard [1] and is suitable for use in transmission line structure earths, or areas of difficult terrain. Furthermore, it provides a very accurate result when properly performed.

Figure 4 presents the measurement of the earth resistance using the fall of potential method. First, the Earth Resistance Tester is connected to the earth electrode of interest (T) whose resistance is to be measured. Then two auxiliary electrodes (A) and (P) are placed in the ground in a direct line – away of the earth electrode. The distance T-A is large compared to the length of the earth electrode. A known current (I) generated by the Earth Resistance Tester flows between the auxiliary electrode (A) and the earth electrode (T). Furthermore the drop in voltage potential is measured between the auxiliary electrode (P) and the earth electrode (T). Using Ohm's Law ($U = IR$), the tester automatically calculates the resistance of the earth electrode. Therefore, the resistance value will be U/I.

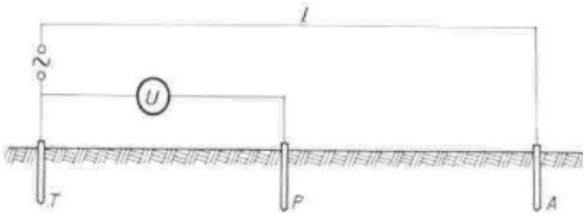

Figure 4. Fall of Potential Method

When performing a measurement, the aim is to position the auxiliary electrode (A) far enough away from the earth electrode under test so that the auxiliary electrode (P) will lay outside the effective resistance areas of both the ground system and the other test electrode.

IV. Experimental Procedure

The experimental procedure of this study was based on seven different cases depending on the grounding system

TABLE I. Experimental Study Cases

	EXPERIMENT CASE STUDY TABLE					
	Test Ground Electrodes common characteristics					
	Material			***Diameter***		
	Copper			16mm		
Case Study	**Case Studies Parameters**					
	Rod No	***Resistance (Ohm)***	***Grounding System***	***Electrode***		***Type of Soil***
				Length	***Depth***	
1	1	R1	Single rod	1.50	1.30	Soft & Sifted & Dry
2	2	R2	Single rod	1.50	1.10	Stoney
3	3	R3	Single rod	1.50	1.30	Stoney Soil with TERRAFFIL improved materials
4	1	R4	Single rod	1.50	1.30	Soft & Sifted & Wet
5	4	R5	Ending of an active 6x8 grounding grid, placed at a depth of 4m, which consists the active laboratory grounding.	1.50	1.30	soft
6	5	R6	Single rod	2.0	2.0	Stoney
7	6	R7	Single rod	2.0	2.0	Stoney

used, the test electrode depth and the type soil. In table I below each of the seven study cases is presented. During the collection of resistance data, the values of the grounding electrode resistance are recorded for each case study.

Case Study 4 is a variation of Case Study 1, with the addition of 1 liter of water applied to the soil to simulate wet conditions and assess the impact of moisture on grounding resistance. In Case Study 3, the electrode was installed in stony soil that had previously been treated with TERRAFFIL, a material used to lower soil resistivity. As the treatment occurred some time ago, this case evaluates whether TERRAFFIL's effectiveness persists over time.

Case Studies 6 and 7 involve electrodes with identical characteristics placed in similar soil conditions. However, construction activity around Electrode 6 led to partial soil removal, leaving the rod partially exposed. This case examines how incomplete soil coverage affects grounding resistance.

For all seven case studies, resistance measurements were conducted twice daily at 12:00 and 15:00, from October 2024 to May 2025, resulting in 29 measurements per case. Ambient temperature and precipitation were also recorded during the measurement period to support analysis of environmental influences on the results.

V. Results

Table II presents the collected grounding resistance data. Grey-shaded cells indicate measurements taken during wet periods with recorded precipitation, while white cells correspond to dry periods. The wet period includes December, March, April, and selected days in May, whereas the dry period comprises October, November, and the remaining days of May. No measurements were taken in January and February.

The table also highlights the maximum and minimum resistance values for each case study. In general, resistance values peak during dry periods and reach their lowest during wet conditions. An exception is observed for electrode R5, whose maximum and minimum values both occurred during the wet period. Notably, while minimum resistance values are spread across the wet months, maximum values are predominantly recorded in October. This observation aligns with reports from the Hellenic Meteorological Service, which characterized October as unusually warm with minimal rainfall [5].

A. Variation of Value of Grounding Resistance in regards to Temperature

In Figure 5 the variation of the average resistance value in relation to temperature during the wet and dry periods is illustrated.

According to Figure 5, the recorded resistance values during wet period are much lower than the ones during dry period. However, this is not the case for the average resistance values (R5) of electrode 4, as the average values in the month of March and April (wet period) are higher than the ones recorted in dry period of time.

Table II. Recorded data

Recoded Data							
Temperature (°C)	***Electrode Resistance R (Ω)***						
	R1	R2	R3	R4	R5	R6	R7
19	440	850	560	400	1.37	350	200
19	400	850	600	370	1	350	150
18	400	1000	700	350	0,9	350	180
18	350	1000	600	320	1,1	400	175
19	400	1100	650	350	1,1	400	150
17	450	1250	700	400	0,8	395	170
17	440	1350	720	400	1	400	180
16	450	1150	750	400	0,75	400	150
16	400	1250	750	350	0,7	350	180
16	505	1535	800	467	1,35	420	173
16	550	1590	840	460	0,5	**500 max**	**200 max**
16	546	**1855 max**	**898 max**	**495 max**	0,95	418	176
11	**619 max**	743	378	440	1,1	436	182
10	222	285	231	208	0,35	107	88
10	161	465	**146 min**	105	0,23	89	83,3
10	146	**194 min**	209	93	**0,19 min**	85	74,5
10	141	203	198	123	0,55	83	77,1
6	185	500	258	171	0,48	**76 min**	61,4
7	189	204	178	176	1,91	113	84
13	**105 min**	519	427	**92 min**	0,35	92	79
14	122	285	179	108	4,5	112	84,4
8	114	237	182	102	**4,9 max**	131	87,5
12	107	232	172	95	1,47	86	58,4
11	112	230	232	101	3,63	90	**56,5 min**
8	132	321	251	112	1,21	101	71,3
23	342	1145	567	319	0,35	234	133
16	361	1261	577	339	0,34	231	144,1
21	375	1280	575	356	0,33	240	153,1
24	345	1310	453	328	0,68	260	140

Furthermore, the value of the grounding resistance varies proportionally with temperature. During the wet period of time the increase of temperature from 10 oC to 19,5 oC results in the increase of grounding resistance. Similarly, the fluctuation of temperature during dry period results in grounding resistance value variation. This finding is in accordance to theory [1, 4].

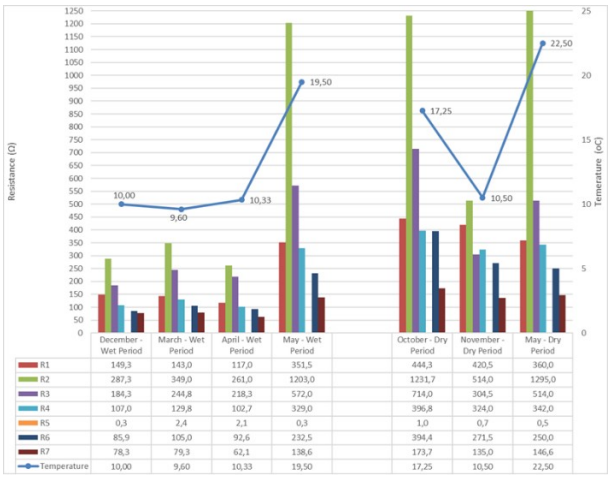

Figure 5. Variation of the Resistance value in relation to temperature during the wet and dry periods.

B. Variation Grounding Resistance depending on Electrode Depth

The investigation of the impact of test electrode depth on the value of grounding resistance is based on the comparison of three of the seven case studies. Namely, case study 2, 3 and 7 are selected from table I because the remaining parameters (earthing system and type of soil) that these study cases are built on are similar. Specifically, for all the three case studies, the type of soil is stoney and the grounding system is single rod.

In figure 6 below the variation of value of earthing resistances R2, R3 and R7 is illustrated. Additionaly, the maximum and the minimum value of each resistance is depicted.

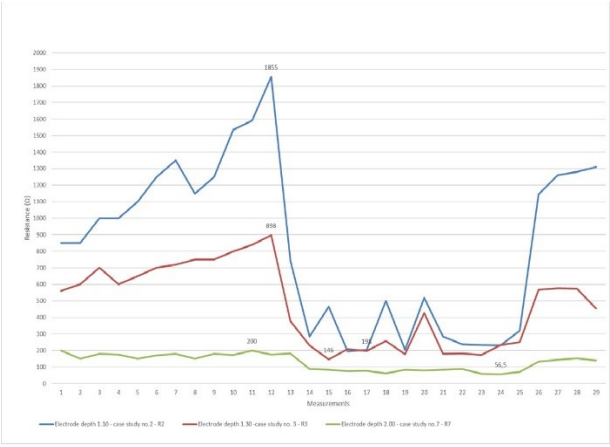

Figure 8. Variation of grounding resistance value in regards to electrode depth

As shown in Figure 6, the earthing resistance of Case Study 7 (Table I and II), corresponding to a 2.00 m electrode depth, consistently exhibits significantly lower values throughout the measurement period compared to those of Case Studies 2 and 3. The highest resistance values are recorded in Case Study 2, which corresponds to a 1.10 m electrode depth. This observation aligns with theoretical principles, which indicate that grounding resistance decreases with increasing electrode depth due to higher moisture content and more stable temperature conditions at greater depths, enhancing soil conductivity [1–3].

To isolate the effect of electrode depth from moisture influence, Figure 7 presents grounding resistance values for single-rod electrodes at fixed soil resistivity. For a soil resistivity of 218 Ω·m, an electrode depth of 1.10 m results in a resistance of 167.4 Ω. Increasing the depth to 1.30 m reduces the resistance by 13%, while a further increase to 2.00 m results in a total reduction of 39%.

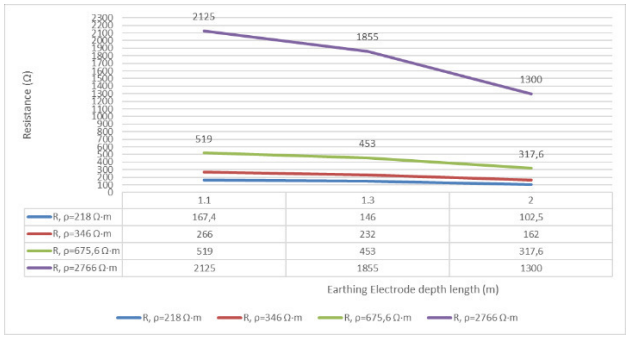

Figure 7. Variation of grounding resistance value in regards to electrode depth – moisture effect disabled

Similarly, for a soil resistivity of 346 Ω·m, an electrode depth of 1.10 m results in a grounding resistance of 266 Ω. This value decreases by 13% when the depth increases to 1.30 m, and by 39% when extended to 2.00 m. The same trend is observed for the remaining two cases presented in Figure 7, confirming the consistent influence of electrode depth on grounding resistance across different soil resistivities.

C. Variation of Grounding Resistance in regards to Ground Moisture

The effect of soil moisture on grounding resistance is examined through Case Studies 1 and 4, both involving Electrode 1. The key difference lies in the application of 1 liter of

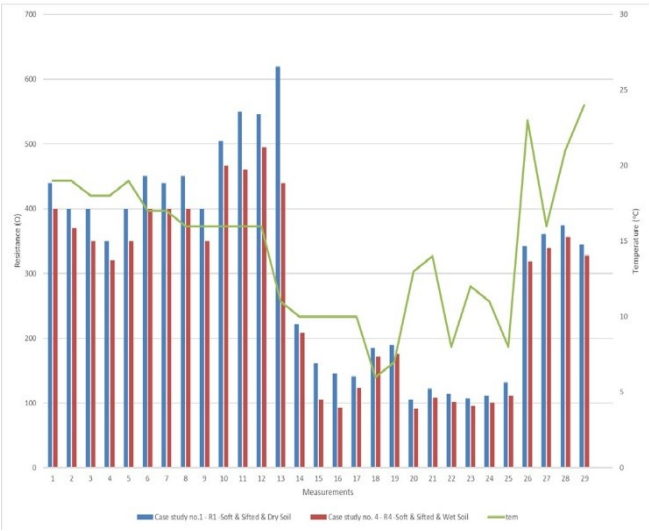

Figure 9. Ground Moisture effect on Grounding Resistance

water in Case Study 4 to simulate increased moisture content.

Figure 9 illustrates the variation in grounding resistance for Electrode 1 before and after water addition. A clear reduction in resistance is observed following the increase in soil moisture. These experimental results confirm that higher soil moisture, along with elevated ambient temperature, contributes to a decrease in grounding resistance.

D. Variation of Grounding Resistance in regards to type of Soil

The following line chart present the variation of the grounding resistance value in regards to type of soil for all case studies with single rod grounding system. Therefore, figure 10 depicts all the case studies besides no. 5.

In order to to disable the depth length effect of grounding electrode on grounding resistance value, the grounding resistance values are calculated with grounding electrode depth length equal to 2.00m, as it results in the maximum grounding resistance decrease. Therefore, for all the 29 measurements and for the five case studies where depth length is 1.10m and 1.30m the soil resistivity (ρ) is calculated. Based on the calculated soil resistivity (ρ) the grounding resistance values is calculated with grounding length equal to 2.00m.

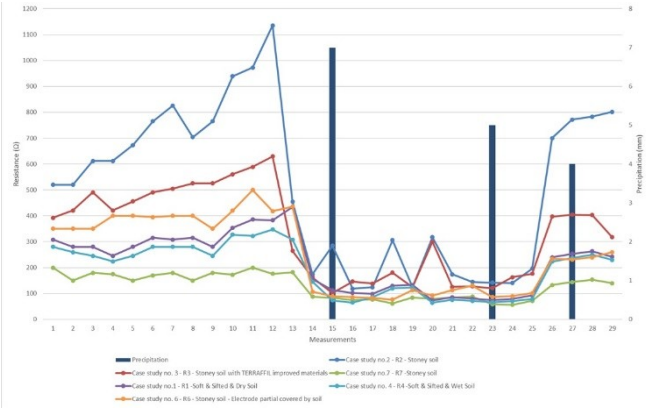

Figure 10. Type of Soil effect on Grounding Resistance – depth length effect of grounding electrode disabled

According to Figure 10, the R_2 grounding resistance has recorded the highest values, followed in most measurement period by R3 grounding resistance which refers to stoney soil with TERRAFFIL improved materials, which in its turns followed by R6 grounding resistance which is measured in stoney soil but there is a lack of soil around the corresponding electrode 6. Afterwards, ground resistance R1, which is measured in soft, sifted and dry soil, follows and then resistance R4, which is measured in soft, sifted but wet soil, is recorded. Finally, the lowest grounding resistance values are recorded for electrode 7.

Furthermore, Figure 10 illustrates rainfall data at the bar column. It is worth mentioned that during wet period of time, where the higher rainfalls occurred, there are slight variations in the aforementioned ranking of grounding resistances. This finding is explained by the increase of moisture content in the soil affect, which affects soil resistivity.

Table III below summarize the aforementioned ranking of grounding resistance values in descending order.

TABLE III. RANKING GROUNDING RESISTANCES

Ranking of grounding resistance values in descending order		
Resistance	***Type of Soil***	***Reference to case study in Table I***
R2	Stoney	Case study no. 2
R3	Stoney Soil with TERRAFFIL improved materials	Case study no. 3
R6	Stoney with lack of soil around the grounding electrode 6	Case study no. 6
R1	Soft & Sifted & Dry Soil	Case study no. 1
R4	Soft & Sifted & Wet Soil	Case study no. 4
R7	Stoney	Case study no. 7

According to Table III stoney soil is reporded as high earthing resistance soil, which become higher during dry seasons. Stoney soil with TERRAFFIL improved materials comes second in ranking, which is explained by the decreased effect of TERRAFIL on stoney soil during time. Soft, sifted and dry soil comes fourth in ranking and it is followed by the soft, sift and wet soil. The stoney soil surrounding electrode 7 results in the lowest grounding resistance. Data in table III are in accordance with theory.

E. Variation of Grounding Resistance in regards to grounding system

Two grounding systems were investigated in the case studies: a single rod system and a grounding grid system. The grounding grid, shown in Figure 11, is an active 6 m × 8 m grid installed at a depth of 4 m and serves as the laboratory's primary grounding system. Case Study 5 evaluates the effect of this grounding grid on earthing resistance.

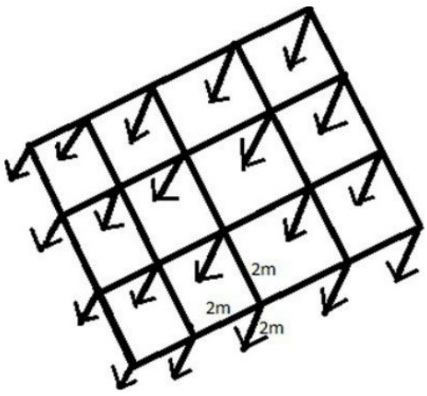

Figure 11. Grounding system based on 6mx8m grounding grid

Table IV below summarize the variation of the mean values of grounding resistance in regards to grounding system.

TABLE IV. RANKING GROUNDING RESISTANCES

Ranking of grounding resistance values in descending order			
Resistance	***Mean Grounding Resistance Values (Ω)***	***Grounding System***	***Reference to case study in Table I***
R1	314	Single Rod	Case study no. 1
R2	834	Single Rod	Case study no. 2
R3	475	Single Rod	Case study no. 3
R4	277	Single Rod	Case study no. 4
R5	1	Grounding grid	Case study no. 5
R6	252	Single Rod	Case study no. 6
R7	129	Single Rod	Case study no. 7

According to Table IV, grounding system with grid results in the lowest earthing resistance value. This finding is explained due to the larger contact area of grounding grid with the ground and the uniform distribution of the leakage current. Furthermore, the grounding grid is less sensitive to local changes in soil conditions such as drought and frost than a single electrode, ensuring a more stable and reliable grounding.

VI. CONCLUSIONS

The analysis of grounding resistance was conducted across seven experimental cases, considering soil type, electrode characteristics, and grounding system configuration, while also accounting for ambient temperature and soil moisture effects.

Results show that grounding resistance varies proportionally with temperature and is significantly lower during wet periods compared to dry seasons. Increased soil moisture consistently reduces grounding resistance.

Regarding electrode depth, measurements confirm that resistance decreases with greater burial depth, attributed to higher moisture content and more stable temperatures at depth, which improve soil conductivity [1–3].

In terms of soil type, stony soil exhibited the highest grounding resistance, particularly during dry seasons. Stony soil treated with TERRAFFIL ranked second, reflecting a diminished long-term effectiveness of the material. Soft, sifted dry soil ranked fourth, followed by soft, sifted wet soil. The stony soil around Electrode 7 produced the lowest resistance values among soil types tested.

Finally, the grounding system with a grid demonstrated the lowest earthing resistance, due to its larger contact area and more uniform leakage current distribution. This system also offers greater stability and reliability, being less affected by variations in soil conditions.

REFERENCES

[1] Guide for Safety in AC Substation Grounding (2000) ANSI/IEEE Std 80.

[2] IEEE Std 81-1983, “IEEE guide for measuring earth resistivity, ground impedance, and earth surface potentials of a ground system”, 11 March 1983.

[3] Manal Maged Awad and El-Sayed Soliman A. Said, “Effect of both ambient temperature and soil moisture on the earthing resistance”, Journal of Al Azhar University Engineering Sector, vol.13, No. 49, pp. 1300-1310, 2018.

[4] Tatum, J. (2024). *Electricity and Magnetism.* Ανακτήθηκε από: https://commons.libretexts.org/store/product/phys-5409

[5] *Meteo: Weather review of 2024: The records of the NWS meteorological stations and other notable figures of the year (2025).* Ανακτήθηκε από: *https://www.meteo.gr/article_view.cfm?entryID=3533*

[6] Theophilus E. Edeko and Eseosa Omorogiuwa, “Soil Resistivity, its Impact on Optimum Depth of Electrodes in Earthing System– Case Study University of Port Harcourt Residential Staff Quarters”, International Journal of Research and Innovation in Applied Science (IJRIAS), vol. VII, Issue XII, 2022.

[7] Arfah Ahmad, Mohd Rizal Ahmad Saroni, Intan Azmira Wan Abdul Razak, Suziana Ahmad, “A Case Study on Ground Resistance Based on Copper Electrode vs. Galvanized Iron Electrode”.IEEE International Conference Power & Energy (PECON), 2014.

[8] Fani E. Asimakopoulou, George J. Tsekouras, Ioannis F. Gonos, Ioannis A. Stathopulos, “Estimation of seasonal variation of ground resistance using Artificial Neural Networks”, Electric Power Systems Research, vol.94, pp. 113-121, January 2013.

[9] Ap. Samiotis, (2024). *Earth Resistance Measurements.* University of Patras.

Proceedings of the International Conference on Engineering, Technology and Applied Science Innovations pp. 39–45 DOI: 10.15439/2025I30 ISSN 2300-5963 ACSIS, Vol. 46

Neurocognitive Approaches to Fraction Learning: Integrating EEG, fMRI, and Eye Tracking in Mathematics Education

Eleni Lekati
Department of Informatics
Ionian University
Corfu, Greece
elenlekati@ionio.gr

Konstantinos Lazarou
Department of Informatics
Ionian University
Corfu, Greece
Lakonstant@ionio.gr

Aristidis Vrahatis
Department of Informatics
Ionian University
Corfu, Greece
aris.vrahatis@ionio.gr

Spyridon Doukakis
Department of Informatics
Ionian University
Corfu, Greece|
sdoukakis@ionio.gr

***Abstract*—This paper reviews neurocognitive studies using EEG, fMRI, and eye-tracking to investigate how learners understand fractions. While challenges with fractions are well documented, most research has focused on adults, leaving children underrepresented. The review highlights how the brain processes symbolic and nonsymbolic fractions, the involvement of regions such as the intraparietal sulcus, and the role of visual attention and neural timing in mathematical reasoning. It also examines how targeted instruction can reshape brain activity related to fraction magnitude estimation. Emphasis is placed on the promise of portable EEG devices for real-time classroom use, supporting personalized and responsive teaching. The findings underscore the potential of educational neuroscience to inform more effective and developmentally appropriate practices in mathematics education.**

***Index Terms*—educational neuroscience, fractions, EEG, fMRI, eye tracking, mathematical cognition, precision education.**

I. Introduction

EDUCATIONAL neuroscience has emerged at the intersection of psychology, neurology, and pedagogy, aiming to deepen our understanding of how individuals learn while also contributing to the refinement of teaching methods and learning environments. Despite the considerable body of research developed since the early 20th century, difficulties in mathematical understanding persist across age groups, affecting both children and adults [1]. Drawing on expertise from psychology, neuroscience, and education, recent research applies neuroscientific tools and experimental methodologies to address fundamental challenges in learning and instruction. As an interdisciplinary field, educational neuroscience enriches educational research by introducing innovative techniques that can inform more effective teaching practices and foster optimized learning environments. Technologies such as magnetic resonance imaging (MRI), electroencephalography (EEG), and near-infrared spectroscopy, alongside eye-tracking systems, facial expression analysis, and wearable devices like smartwatches, provide access to neurophysiological data under naturalistic conditions. These tools also support the identification of digital biomarkers and contribute to a better understanding of memory mechanisms [2].

In parallel, data mining techniques offer valuable insights into cognitive processes, behavioral patterns, and the factors influencing academic performance [3,4]. Such analyses facilitate the development of personalized learning strategies tailored to individual needs and learning profiles [5]. Neuroimaging studies have further enhanced this effort by identifying brain regions involved in understanding mathematical constructs like fractions, thereby providing a foundation for more targeted instructional design [6,7]. While neuroscience may not yield directly applicable classroom strategies, it can inform educational practice by integrating knowledge about brain function and cognitive development into pedagogical contexts [8,9]. It can also assist teachers in selecting instructional methods aligned with student characteristics and adapting their practices based on learners' cognitive profiles [10].

This evolving dialogue between educational research and cognitive neuroscience points to a dynamic, reciprocal relationship. Both disciplines contribute to a broader methodological framework aimed at shaping a new educational paradigm, where insights from neuroscience on brain development are actively used to enhance and enrich pedagogical practices [11]. Against this backdrop, the present paper synthesizes empirical findings from studies using EEG, fMRI, and eye-tracking technologies to uncover key neurocognitive patterns in mathematical thinking, with a specific focus on fraction understanding. By combining these complementary approaches, the paper aims to illuminate how the brain processes mathematical concepts and to explore how this knowledge can inform the creation of developmentally appropriate and cognitively attuned instructional strategies in mathematics education.

II. Neural Foundations of Mathematical Skills

Mathematical cognition is supported by a complex neural architecture involving multiple brain regions. Among these, the parietal cortex plays a central role. Specifically, mathe-

matical tasks activate areas within and around the horizontal intraparietal sulcus (IPS), which has been consistently implicated in number processing [12, 13, 14]. Neuropsychological models suggest that numerical concepts are represented bilaterally, within cortical regions surrounding the IPS, using symbolic formats [15]. While the left parietal regions are primarily involved in quantity estimation regardless of format, the right parietal cortex appears to specialize in the processing of non-symbolic numerical information. These findings point to the existence of two functionally distinct but overlapping neural systems involved in mathematical cognition [16]. Importantly, IPS activation is not uniform across tasks. Studies have shown that it varies inversely with numerical distance; the closer two numbers are, the greater the activation observed in this region [17, 18].

In addition to the parietal cortex, the prefrontal cortex (PFC) also plays a key role in mathematical thinking, including even simple arithmetic tasks [16, 19]. The fronto-parietal network is thus considered essential for mathematical reasoning [20, 21]. Within this system, algebra and arithmetic both activate bilateral parietal areas but rely on distinct cognitive systems: algebra is more strongly associated with semantic networks, while arithmetic is linked to phonological and visuospatial processing [20].

Beyond these regions, additional cortical structures have been implicated in mathematical processing. These include the claustrum, the insula, and the cingulate gyrus, which contribute to broader executive and motivational processes [21]. The insula, in particular, appears to be crucial for children's mathematical computations, given its role in intrinsic motivation, emotional goal-setting, and attentional control [21]. Notably, increased activation in the insula has also been observed in adults and children when they face challenges in processing numerical magnitude [22]. Finally, mathematical error processing engages a distributed network including the anterior cingulate cortex (ACC), pre-supplementary motor area (pre-SMA), bilateral insula, thalamus, and the right inferior parietal lobule, regions associated with cognitive control, conflict monitoring, and attentional adjustment [23].

A. Neurocognitive Data on Fraction Processing

In recent years, research efforts have increasingly focused on understanding the cognitive mechanisms involved in the processing and acquisition of fractions. Studies have shown that symbolic representations of fractions are particularly challenging to comprehend and often lead to systematic errors. These difficulties are largely attributed to pre-existing cognitive biases that stem from the habitual use of whole number knowledge, observed in both children and adults. However, the specific stages of fraction perception and processing at which these difficulties arise remain unclear [24]. Despite growing interest in this area, investigations into the neurocognitive mechanisms underlying fraction processing are still relatively limited.

B. Eye-Tracking Investigations in Fraction Processing

One of the principal methods for exploring how learners process fractions is eye-tracking technology, which has been widely employed in research on mathematical cognition. It is an established tool in educational research, particularly in mathematics education [25, 26]. The most commonly used form of eye tracking relies on infrared light to non-invasively record eye movements and provide real-time data on visual attention and fixation points. This technique is grounded in the "eye–mind hypothesis" [27], which posits that eye movements reflect the ongoing cognitive processes of the viewer. As such, eye tracking offers insights into the problem-solving strategies employed by individuals when engaging with mathematical tasks [28], while also acknowledging certain methodological limitations related to interpretation and resolution [29].

A pioneering study by [30] examined how eight adults approached both simple and complex fraction comparison problems. Participants demonstrated flexible, problem-adapted strategies, adjusting their methods based on task complexity. Additionally, shorter fixation durations were observed for larger numerical ratios, supporting earlier findings on the relationship between numerical proximity and reaction time [31]. In contrast, [32] found that denominators attracted significantly more fixations than numerators, regardless of problem type—suggesting greater difficulty in processing denominators. Similarly, [33] reported that in complex fraction addition tasks with unlike denominators, participants exhibited increased fixations and saccades between denominators, indicating heightened cognitive demand.

Complementing these findings, [34] found that in fraction comparison tasks without shared elements, participants tended to focus more on numerators—likely reflecting an underlying natural number bias, where whole-number reasoning interferes with accurate fraction interpretation. Taken together, eye-tracking studies have made substantial contributions to our understanding of fraction processing. They have revealed how learners extract information from numerators and denominators and how they adjust their strategies based on the specific demands of each task. Moreover, findings indicate that participants frequently rely on simplified cognitive strategies or heuristics to navigate mathematical challenges, highlighting the role of intuitive reasoning in fraction understanding [24].

C. Neuroimaging Studies of Fraction Processing: Insights from fMRI

Over the past three decades, extensive research has been conducted on the neural correlates of whole number processing. In contrast, studies focusing on the neural mechanisms involved in the processing of fractions and proportional reasoning remain relatively scarce. Only a limited number of investigations have explored these mechanisms in adults using functional magnetic resonance imaging (fMRI). These studies have addressed various dimensions of fractional reasoning, including proportional comparisons [35, 36], the

cognitive processing of fractions [38, 39, 35, 7, 37], and the influence of instructional interventions on neural activation patterns [6] .

Functional magnetic resonance imaging (fMRI) is a widely used non-invasive technique for evaluating brain activity, offering several key advantages. Its high spatial resolution enables the detailed mapping of small brain structures, allowing for comprehensive assessment of both cortical and subcortical regions. This makes fMRI particularly valuable for studying the distributed neural networks involved in mathematical cognition. However, its relatively limited temporal resolution, approximately two seconds to capture whole-brain activity, limits the ability to resolve rapid changes in neural processing. The inherent delay of the BOLD (blood-oxygen-level-dependent) signal further constrains the interpretation of fast, transient cognitive events. In the context of fraction-related tasks, where quick shifts in numerical comparison or proportional reasoning are crucial, these temporal limitations hinder a precise understanding of the timing and sequence of cognitive processes [24]. Neuroimaging findings have consistently identified the intraparietal sulcus (IPS) as playing a central role in the representation of both symbolic and nonsymbolic numerical magnitudes. Developmental neuroimaging studies in adults further support the IPS as a key hub for numerical cognition [19, 40].

[42] investigated how the neuronal recycling hypothesis may apply to the cognitive systems that process nonsymbolic fractions. They also examined how these systems could contribute to the development of abilities required for understanding symbolic fractions. Their study builds upon the theoretical framework of neuronal recycling proposed by [41], which suggests that the brain repurposes pre-existing cognitive systems—originally evolved for other purposes—to integrate culturally acquired concepts like symbolic fractions [42].

Building on these findings, [7] investigated the developmental trajectory of fraction understanding in school-aged children. They proposed that conceptual knowledge of fractions emerges gradually, beginning with an early sensitivity to nonsymbolic ratios—such as length comparisons—even before formal instruction. By Grade 2, children can interpret nonsymbolic proportions by drawing on innate magnitude perception skills, without using numerical symbols. By Grade 5, children develop the capacity to process symbolic fractions (e.g., 1/2, 3/4) through experience, engaging neural networks that were originally associated with nonsymbolic reasoning. This developmental shift supports the idea that symbolic fraction understanding builds upon earlier, magnitude-based representations.

In Grade 2, tasks involving nonsymbolic fraction comparisons were found to activate a neural network centered in the right ventral prefrontal cortex, including the right IPS and nearby prefrontal regions. By Grade 5, activation became more bilaterally distributed, engaging a broader ventral prefrontal network during both symbolic and nonsymbolic fraction tasks. This transition reflects a more integrated and efficient use of neural resources [7]. The IPS, a region critically involved in numerical cognition, is sensitive to the magnitude difference between fractions. It encodes proportional distance, thereby supporting both nonsymbolic and symbolic fraction processing. These findings underscore the brain's ability to reorganize existing cognitive systems to accommodate new mathematical concepts introduced through instruction [7].

[24] conducted a pioneering study to examine the effects of a structured educational intervention on the neural processing of fraction magnitudes in 48 adults. Over five consecutive days, participants engaged in a training program focused on estimating the placement of fractions on a number line ranging from 0 to 1. Each daily session included 96 tasks, with the possibility of up to 12 repetitions depending on individual performance. To assess changes in neural activation, participants performed symbolic fraction comparison tasks, line segment comparison tasks, and fraction-to-line matching tasks both before and after the intervention. Pretraining results showed that the numerical distance effect—a phenomenon in which smaller differences between numerical values require more cognitive effort—modulated IPS activity during line segment comparisons and fraction-to-line matching, but not during symbolic fraction comparisons. These findings indicate that symbolic fractions initially engaged distinct neural pathways compared to nonsymbolic magnitude tasks.

After the intervention, brain activation patterns for the non-symbolic tasks (line and line-to-fraction matching) remained stable. In contrast, symbolic fraction comparisons showed a marked change: the distance effect now influenced IPS activation, indicating that participants had started to engage magnitude-related neural resources when working with symbolic fractions. This shift suggests that training in numerical magnitude estimation may reshape neural processing and enhance fraction understanding at a conceptual level. Findings from fMRI studies underscore the complexity of fraction processing and its dynamic developmental trajectory. Research indicates that non-symbolic and symbolic fraction processing engages distinct yet partially overlapping neural mechanisms. Notably, [6] highlight the neuroplasticity of these systems, demonstrating how learning experiences can refine brain activity associated with mathematical skill development.

While fMRI provides valuable spatial insights into which brain regions are involved in fraction-related tasks, it lacks the temporal resolution needed to capture rapid neural processes occurring within milliseconds. This limitation makes it difficult to pinpoint the precise sequence of cognitive events during fast-paced tasks such as numerical comparisons or proportional reasoning. To overcome this challenge, researchers have increasingly adopted electroencephalography (EEG). With its high temporal resolution, EEG enables the real-time tracking of brain activity, making it especially suitable for exploring the fine-grained temporal dynamics of

mathematical cognition. As a result, EEG complements fMRI by offering a more comprehensive understanding of how the brain processes complex concepts like fractions.

D. Investigating Fraction Perception Using EEG

Electroencephalography (EEG) is a non-invasive neuroimaging technique that records electrical activity along the scalp, capturing brain signals generated by neural oscillations with millisecond precision. Because of its high temporal resolution, EEG is particularly effective for studying mathematical cognition, offering valuable insights into the neural dynamics underpinning numerical reasoning and problem solving. For example, [43] demonstrated that EEG signals can reliably distinguish between verbal and mathematical cognitive processes, especially through variations observed in the theta frequency band. These findings underscore EEG's utility in detecting subtle distinctions in brain activity across different types of symbolic and domain-specific tasks, including arithmetic operations.

EEG-based research has advanced our understanding of the neural processes underlying mathematical thinking by revealing distinct patterns of brain activity associated with task complexity and type. Notably, studies by [44] & [45] have emphasized the role of the beta, gamma, and delta frequency bands in supporting cognitive effort, attentional control, and error detection during mathematical tasks. Additionally, [46] applied graph theory to EEG data and found that as mathematical tasks become more challenging, the brain organizes into more efficient and cohesive networks particularly within frontoparietal regions. These findings suggest that various mathematical processes, from simple arithmetic to complex reasoning, elicit distinct neural signatures that EEG can detect with high reliability.

While prior neuroimaging research has shown that processing fractions and decimals activates both shared and distinct brain regions, the precise timing of these processes remained poorly understood. [47] addressed this gap by employing Event-Related Potentials (ERPs) to examine the neural dynamics associated with fraction and decimal processing. Their study focused on comparing symbolic formats and investigating how numerical distance (i.e., whether numbers were numerically close or far apart) influenced ERP components such as P1/N1, P2, and N2.

The results revealed distinct ERP patterns for the two numerical formats. Decimal numbers elicited a larger N1 and a smaller P1 component in the parietal cortex compared to fractions. Moreover, the numerical distance effect significantly influenced the fronto-central P2 component for fractions, while a similar effect emerged in the left anterior N2 component for decimals. These patterns indicate that different cognitive systems are engaged in processing each format. Decimal recognition appears to rely more heavily on visual cortical areas, enabling faster and more efficient identification. Conversely, understanding fractions—which requires more elaborate cognitive operations—involves fronto-central brain regions responsible for fine-grained magnitude manipulation. The study also highlighted that these neural processing differences emerge within the first 100 milliseconds following stimulus presentation, demonstrating the importance of ERP techniques in capturing the rapid temporal dynamics of mathematical cognition.

[48] investigated the neural mechanisms underlying fraction understanding using EEG recordings in a sample of 24 adults engaged in fraction comparison tasks. Their results revealed distinct neural patterns, including longer reaction times for nonequivalent fractions and two specific ERP components: an early frontal N270 for nonequivalent fractions and a late parietal P300 for equivalent ones. These findings suggest that fraction processing involves cognitive operations similar to those used in arithmetic tasks, with nonequivalent fraction comparisons requiring greater cognitive effort and resource allocation. This study highlights the potential of ERP techniques in examining the temporal dynamics of fraction processing, offering valuable insights into the timing and sequence of brain activity during numerical reasoning.

In this context, [49] study was among the first to explore fraction learning processes through EEG in a school-aged population. A total of 512 fifth-grade students participated, of whom 44 (22 high-performing and 22 low-performing based on a diagnostic test on fractions) were selected for EEG recording during the execution of fraction-related tasks. High-performing students exhibited more balanced, bilateral theta band activation (4–7.5 Hz), in contrast to their low-performing peers, who showed greater reliance on the right hemisphere—particularly during the initial phases of problem solving. Moreover, in the beta1 frequency band (13–18 Hz), low-performing students demonstrated increased activity in the left hemisphere, especially when working on tasks involving discrete sets and area models. These findings suggest that high-performing students engage their brains more efficiently when processing fractions, drawing upon both hemispheres in a coordinated manner. Conversely, low-performing students appear to employ less effective cognitive strategies, resulting in greater cognitive effort and reduced efficiency in solving fraction problems. The differences in theta and beta1 activity highlight distinct neural processing patterns associated with performance levels and learning competence in fraction understanding.

III. Comparing Neuroimaging Methods (fMRI & EEG) in Fraction Processing and Educational Implications

Recent neuroimaging research has significantly advanced our understanding of the neural mechanisms underlying fraction comprehension. Functional Magnetic Resonance Imaging (fMRI), in particular, has been instrumental in identifying the brain regions involved in symbolic numerical processing. Numerous studies have demonstrated that the intraparietal sulcus (IPS) plays a central role in representing numerical magnitudes [19, 40, 14] . Moreover, the frontoparietal network has been shown to support complex arithmetic

operations and proportional reasoning [35, 36, 38, 39, 7, 42, 6].

While fMRI offers crucial insights into the spatial organization of brain activity, its limited temporal resolution constrains our ability to capture the rapid neural processes that underlie numerical cognition [24]. To address this limitation, electroencephalography (EEG) has been proposed as a complementary method, offering millisecond-level temporal precision. Notably, studies using Event-Related Potentials (ERPs) have begun to uncover the temporal dynamics of processing different numerical formats, such as fractions and decimals, revealing distinct neural activation patterns and clear timing differences [47, 48]. EEG findings suggest that decimal numbers and fractions engage different cognitive and neural pathways. Decimal processing appears to rely mainly on visual brain areas, enabling faster and more automatic recognition. In contrast, fraction processing demands greater cognitive effort and engages fronto-central brain regions associated with complex and abstract numerical reasoning [47].

In support of this, [48] reported that comparisons involving nonequivalent fractions resulted in longer reaction times and increased brain activity, as reflected by the early frontal ERP component N270. Conversely, equivalent fractions were associated with the late parietal P300 component, linked to cognitive control and recognition of numerical relationships. These results suggest that fraction processing recruits neurocognitive mechanisms similar to those used in arithmetic operations, with nonequivalent comparisons requiring higher cognitive resource allocation. Despite substantial progress in understanding the neural underpinnings of fraction processing, a notable research gap remains regarding how these processes unfold in children. Most existing studies focus on adult participants and predominantly employ fMRI, leaving the developmental trajectory of mathematical thinking in childhood—a critical period for acquiring fraction knowledge—relatively underexplored. As [7] note, children's understanding of fractions evolves from an early sensitivity to nonsymbolic ratios into the ability to manipulate symbolic representations through structured educational experiences.

Utilizing EEG to investigate the neural basis of this developmental progression could provide valuable insights into how children's brains adapt during fraction learning. Furthermore, identifying the temporal characteristics of fraction processing may inform the design of educational interventions that align with the natural course of cognitive development in children. In conclusion, fMRI research has laid a strong foundation for elucidating the neural mechanisms of fraction processing, yet its limitations underscore the importance of further EEG-based studies—particularly involving elementary-aged learners. The combined application of fMRI and EEG can offer a more complete picture of the cognitive and neural systems underlying fraction comprehension. Future EEG research with children holds promise for informing evidence-based instructional practices aimed at improving the acquisition of mathematical concepts.

IV. Discussion and Proposals for Future Educational Research

The integration of neuroimaging tools such as functional magnetic resonance imaging (fMRI) and electroencephalography (EEG) into educational research has significantly expanded the understanding of the cognitive processes that underpin learning, particularly in domains such as arithmetic reasoning and fraction comprehension [53]. These technologies allow for precise observation of brain activity and offer critical insights into how learners process mathematical content, with variations depending on symbolic representation, task complexity, and individual cognitive profiles. However, current research has predominantly centered on adult populations or older students, resulting in a notable gap in understanding how mathematical concepts are acquired during the early stages of education. The classroom, where foundational learning takes place, remains an underutilized setting for applying such neuroimaging techniques. Moreover, the practical challenges associated with traditional EEG setups have limited their deployment in real-world educational environments [53].

This gap is especially evident in the context of fraction learning—a core mathematical concept introduced in the primary school curriculum and one that is often associated with persistent difficulties for young learners. Investigating how children's brains respond to both symbolic and nonsymbolic representations of fractions can offer valuable direction for the design of early instructional strategies. Addressing this need calls for the use of portable, wireless EEG technologies, such as the Muse 2 headset, which offer improved ergonomics and feasibility for use in school settings. These devices make it possible to collect reliable neurocognitive data with minimal disruption to classroom activities. In doing so, researchers can gain real-time access to measures of cognitive engagement and mental fatigue, enabling the development of more accurate and responsive learner profiles.

This approach aligns with the broader vision of precision education, which aims to tailor instruction to the specific needs of each learner by leveraging objective neurophysiological indicators. The integration of affordable, user-friendly neurotechnologies into routine classroom practice holds the potential to transform mathematics education by informing the development of personalized interventions and promoting educational equity. EEG-derived data—including markers of attention, engagement, and cognitive fatigue—can support the design of individualized learning pathways that are responsive to each student's cognitive state [50, 51]. The use of portable EEG systems like the Muse 2 also allows for continuous, non-intrusive monitoring within everyday teaching contexts, ensuring that insights from neuroscience can be seamlessly embedded into educational practice [7, 52].

By extending neuroscience beyond the laboratory and into the classroom, educators and researchers can co-develop real-time, developmentally appropriate strategies to support young learners—especially those struggling with abstract mathematical concepts such as fractions. Future research should prioritize the inclusion of primary-aged students in neurocognitive investigations and explore how emerging neurotechnologies can be effectively employed to support mathematical learning from the earliest stages. Bridging the gap between neuroscience and education through accessible, classroom-compatible tools offers a promising path toward more equitable and personalized instruction. Aligning neurocognitive data with instructional design not only enhances fraction learning but also contributes to the creation of more inclusive and effective learning environments. Realizing this vision will require sustained interdisciplinary collaboration, continued investment in research, and a renewed commitment to reimagining mathematics education for the challenges of the twenty-first century.

Acknowledgment

The authors declare that they have no acknowledgments.

References

[1] M. I. Fandiño Pinilla, “Fractions: conceptual and didactic aspects,” *Acta Didactica Universitatis Comenianae. Mathematics*, vol. 7, pp. 81–115, 2007.

[2] P. Giannopoulou, M. A. Papalaskari, and S. Doukakis, “Neuroeducation and computer programming: A review,” in *GeNeDis 2018*, pp. 59–66. Springer, 2020. [Online]. Available: https://doi.org/10.1007/978-3-030-35249-3_8

[3] M. S. Schwarz, V. Hinesley, Z. Chang, and J. M. Dubinsky, “Neuroscience knowledge enriches pedagogical choices,” *Teaching and Teacher Education*, vol. 83, pp. 87–98, Apr. 2019. [Online]. Available: https://doi.org/10.1016/j.tate.2019.04.002

[4] M. Tissenbaum and J. D. Slotta, “Data-driven iteration of a collaborative inquiry curriculum,” *Journal of the Learning Sciences*, vol. 28, no. 1, pp. 84–126, 2019. [Online]. Available: https://doi.org/10.1080/10508406.2018.1522253

[5] W. Strielkowski, V. Grebennikova, A. Lisovskiy, G. Rakhimova, and T. Vasileva, “AI-driven adaptive learning for sustainable educational transformation,” *Sustainable Development*, vol. 33, no. 2, pp. 1921–1947, 2025.

[6] S. M. Wortha, J. Bloechle, M. Ninaus, K. Kiili, A. Lindstedt, J. Bahnmueller, … E. Klein, “Neurofunctional plasticity in fraction learning: An fMRI training study,” *Trends in Neuroscience and Education*, vol. 21, p. 100141, 2020.

[7] Y. Park, P. B. Kalra, Y. S. Chuang, J. V. Binzak, P. G. Matthews, and E. M. Hubbard, “Developmental changes in nonsymbolic and symbolic fractions processing: A cross-sectional fMRI study,” *Developmental Science*, vol. 28, no. 5, p. e70042, 2025.

[8] Z. Chang, M. S. Schwartz, V. Hinesley, and J. M. Dubinsky, “Neuroscience concepts changed teachers’ views of pedagogy and students,” *Frontiers in Psychology*, vol. 12, p. 685856, 2021.

[9] M. S. Thomas, D. Ansari, and V. C. Knowland, “Annual research review: Educational neuroscience: Progress and prospects,” *Journal of Child Psychology and Psychiatry*, vol. 60, no. 4, pp. 477–492, 2019

[10] P. Toscani, “Éditorial du dossier ‘Neurosciences et éducation’,” *Éducation et Socialisation. Les Cahiers du CERFEE*, no. 49, 2018.

[11] D. A. Turner, “Which part of ‘two-way street’ did you not understand? Redressing the balance of neuroscience and education,” *Educational Research Review*, vol. 6, no. 3, pp. 224–232, 2011. [Online]. Available: https://doi.org/10.1016/j.edurev.2011.04.001

[12] S. Dehaene, M. Piazza, P. Pinel, and L. Cohen, “Three parietal circuits for number processing,” in *The Handbook of Mathematical Cognition*, pp. 433–453. Psychology Press, 2005.

[13] M. Piazza and E. Eger, “Neural foundations and functional specificity of number representations,” *Neuropsychologia*, vol. 83, pp. 257–273, 2016.

[14] M. Arsalidou, M. Pawliw-Levac, M. Sadeghi, and J. Pascual-Leone, “Brain areas associated with numbers and calculations in children: Meta-analyses of fMRI studies,” *Developmental Cognitive Neuroscience*, vol. 30, pp. 239–250, 2018.

[15] D. Ansari, N. Garcia, E. Lucas, K. Hamon, and B. Dhital, “Neural correlates of symbolic number processing in children and adults,” *Neuroreport*, vol. 16, no. 16, pp. 1769–1773, 2005.

[16] H. M. Sokolowski, W. Fias, A. Mousa, and D. Ansari, “Common and distinct brain regions in both parietal and frontal cortex support symbolic and nonsymbolic number processing in humans: A functional neuroimaging meta-analysis,” *Neuroimage*, vol. 146, pp. 376–394, 2017.

[17] R. Cohen Kadosh, A. Henik, O. Rubinsten, H. Mohr, H. Dori, V. Van de Ven, *et al.*, “Are numbers special? The comparison systems of the human brain investigated by fMRI,” *Neuropsychologia*, vol. 43, pp. 1238–1248, 2005.

[18] L. Kaufmann, S. E. Vogel, M. Starke, C. Kremser, M. Schocke, and G. Wood, “Developmental dyscalculia: compensatory mechanisms in left intraparietal regions in response to nonsymbolic magnitudes,” *Behavioral and Brain Functions*, vol. 5, pp. 1–6, 2009.

[19] R. W. Emerson and J. F. Cantlon, “Continuity and change in children’s numerical cognition,” *Child Development Perspectives*, vol. 9, no. 3, pp. 152–156, 2015.

[20] Y.-L. Cheng, M. C. Cheung, C. S.-H. Ho, and T. K. Ng, “A systematic review of neuroimaging studies on mathematical processing,” *Neuroscience & Biobehavioral Reviews*, vol. 132, pp. 556–572, 2022.

[21] M. Arsalidou, M. Pawliw-Levac, M. Sadeghi, and J. Pascual-Leone, “Brain areas associated with numbers and calculations in children: Meta-analyses of fMRI studies,” *Developmental Cognitive Neuroscience*, vol. 30, pp. 239–250, 2018.

[22] G. Vatansever, S. Üstün, N. Ayyıldız, and M. Çiçek, “Developmental alterations of the numerical processing networks in the brain,” *Brain and Cognition*, vol. 141, p. 105551, 2020.

[23] R. Hester, C. Fassbender, and H. Garavan, “Individual differences in error processing: a review and reanalysis of three event-related fMRI studies using the GO/NOGO task,” *Cerebral Cortex*, vol. 14, no. 9, pp. 986–994, 2004.

[24] S. M. Wortha, A. Obersteiner, and T. Dresler, “Neurocognitive foundations of fraction processing,” in *Handbook of Cognitive Mathematics*, pp. 1–27, 2021.

[25] M. L. Lai, M. J. Tsai, F. Y. Yang, C. Y. Hsu, T. C. Liu, S. W. Y. Lee, … C. C. Tsai, “A review of using eye-tracking technology in exploring learning from 2000 to 2012,” *Educational Research Review*, vol. 10, pp. 90–115, 2013.

[26] A. R. Strohmaier, K. J. MacKay, A. Obersteiner, and K. M. Reiss, “Eye-tracking methodology in mathematics education research: A systematic literature review,” *Educational Studies in Mathematics*, vol. 104, pp. 147–200, 2020.

[27] M. A. Just and P. A. Carpenter, “A theory of reading: from eye fixations to comprehension,” *Psychological Review*, vol. 87, no. 4, p. 329, 1980.

[28] K. Holmqvist, M. Nyström, R. Andersson, R. Dewhurst, H. Jarodzka, and J. Van de Weijer, *Eye Tracking: A Comprehensive Guide to Methods and Measures*. Oxford, U.K.: OUP Oxford, 2011.

[29] M. Carrasco, “Visual attention: The past 25 years,” *Vision Research*, vol. 51, no. 13, pp. 1484–1525, 2011.

[30] A. Obersteiner, G. Moll, J. T. Beitlich, C. Cui, M. Schmidt, T. Khmelivska, and K. Reiss, “Expert mathematicians' strategies for comparing the numerical values of fractions—Evidence from eye movements,” *North American Chapter of the International Group for the Psychology of Mathematics Education*, 2014.

[31] A. Obersteiner and C. Tumpek, “Measuring fraction comparison strategies with eye-tracking,” *ZDM*, vol. 48, pp. 255–266, 2016.

[32] S. Huber, K. Möller, and H. C. Nuerk, “Adaptive processing of fractions—Evidence from eye-tracking,” *Acta Psychologica*, vol. 148, pp. 37–48, 2014.

[33] A. Obersteiner and I. Staudinger, “How the eyes add fractions: Adult eye movement patterns during fraction addition problems,” *Journal of Numerical Cognition*, vol. 4, no. 2, pp. 317–336, 2018.

[34] M. Hurst and S. Cordes, “Rational-number comparison across notation: Fractions, decimals, and whole numbers,” *Journal of Experimen-*

tal Psychology: Human Perception and Performance, vol. 42, no. 2, p. 281, 2016.

[35] S. N. Jacob and A. Nieder, "Tuning to non-symbolic proportions in the human frontoparietal cortex," *European Journal of Neuroscience*, vol. 30, no. 7, pp. 1432–1442, 2009.

[36] J. Mock, S. Huber, J. Bloechle, J. Bahnmueller, K. Moeller, and E. Klein, "Processing symbolic and non-symbolic proportions: Domain-specific numerical and domain-general processes in intraparietal cortex," *Brain Research*, vol. 1714, pp. 133–146, 2019.

[37] M. R. Lewis, P. G. Matthews, and E. M. Hubbard, "Neurocognitive architectures and the nonsymbolic foundations of fractions understanding," in *Development of Mathematical Cognition*, pp. 141–164. Elsevier, 2016.

[38] M. DeWolf, J. N. Chiang, M. Bassok, K. J. Holyoak, and M. M. Monti, "Neural representations of magnitude for natural and rational numbers," *NeuroImage*, vol. 141, pp. 304–312, 2016.

[39] A. Ischebeck, M. Schocke, and M. Delazer, "The processing and representation of fractions within the brain: An fMRI investigation," *NeuroImage*, vol. 47, no. 1, pp. 403–413, 2009.

[40] I. M. Lyons, H. C. Nuerk, and D. Ansari, "Rethinking the implications of numerical ratio effects for understanding the development of representational precision and numerical processing across formats," *Journal of Experimental Psychology: General*, vol. 144, no. 5, p. 1021, 2015.

[41] S. Dehaene and L. Cohen, "Cultural recycling of cortical maps," *Neuron*, vol. 56, no. 2, pp. 384–398, 2007.

[42] R. M. Lewis, L. K. Gibbons, E. Kazemi, and T. Lind, "Unwrapping students' ideas about fractions," *Teaching Children Mathematics*, vol. 22, no. 3, pp. 158–168, 2015.

[43] E. V. Chemerisova, M. S. Atanov, I. N. Mikheev, and O. V. Martynova, "Classification of verbal and mathematical mental operations based on the power spectral density of EEG," *Psychology*, vol. 15, no. 2, pp. 268–278, 2018.

[44] E. V. Chemerisova, M. S. Atanov, I. N. Mikheev, and O. V. Martynova, "Classification of verbal and mathematical mental operations based on the power spectral density of EEG," *Psychology*, vol. 15, no. 2, pp. 268–278, 2018.

[45] F. J. Alvarado-Rodríguez, K. P. Ibarra-González, C. Eccius-Wellmann, H. Vélez-Pérez, and R. Romo-Vázquez, "Electrophysiological brain response to error in solving mathematical tasks," *Mathematics*, vol. 10, no. 18, p. 3294, 2022.

[46] M. A. Klados, K. Kanatsouli, I. Antoniou, F. Babiloni, V. Tsirka, P. D. Bamidis, and S. Micheloyannis, "A graph theoretical approach to study the organization of the cortical networks during different mathematical tasks," *PLoS One*, vol. 8, no. 8, p. e71800, 2013.

[47] P. Lin, Y. Zhu, X. Zhou, Y. Bai, and H. Wang, "Neural dissociations between magnitude processing of fractions and decimals," in *2021 43rd Annual International Conference of the IEEE Engineering in Medicine & Biology Society (EMBC)*, Nov. 2021, pp. 92–95. IEEE.

[48] B. Rivera and F. Soylu, "Incongruity in fraction verification elicits N270 and P300 ERP effects," *Neuropsychologia*, vol. 161, p. 108015, 2021.

[49] O. P. Hoon, "Neuroscience in mathematics: An electroencephalographic study on fraction learning," *Journal of Science and Mathematics Education in Southeast Asia*, vol. 25, no. 2, pp. 15–31, 2002.

[50] S. D'Urso, R. Luongo, and F. Sciarrone, "Enhancing educational outcomes through EEG-based cognitive indices and supervised machine learning: A methodological framework," in *2024 28th International Conference Information Visualisation (IV)*, Jul. 2024, pp. 1–6. IEEE.

[51] N. Kosmyna and P. Maes, "AttentivU: an EEG-based closed-loop biofeedback system for real-time monitoring and improvement of engagement for personalized learning," *Sensors*, vol. 19, no. 23, p. 5200, 2019.

[52] J. G. Cruz-Garza, J. A. Brantley, S. Nakagome, K. Kontson, M. Megjhani, D. Robleto, and J. L. Contreras-Vidal, "Deployment of mobile EEG technology in an art museum setting: Evaluation of signal quality and usability," *Frontiers in Human Neuroscience*, vol. 11, p. 527, 2017.

[53] E. Lekati and S. Doukakis, "Neuroeducation and mathematics: The formation of new educational practices," in *Worldwide Congress on Genetics, Geriatrics and Neurodegenerative Diseases Research*, Cham: Springer International Publishing, 2022, pp. 91–96

Proceedings of the International Conference on Engineering, Technology and Applied Science Innovations pp. 47–52
DOI: 10.15439/2025I25
ISSN 2300-5963 ACSIS, Vol. 46

A New Approach to the Beam Calculus Made of Functionally Graded Materials

Vasile Nastasescu
Department of Integrated Aviation Systems and Mechanics
Ferdinand I Military Technical Academy
Bucharest, Romania
vasile.nastasescu@mta.ro

Dragos Gabriel Zisopol
Mechanical Engineering Department Petroleum-Gas University of Ploiesti
Ploiesti, Romania
zisopold@upg-ploiesti.ro
(corresponding author)

Mihaela Badea
National University of Sciences and Technologies Politehnica,
Bucharest, Romania
radu.cristianamihaela@gmail.com

***Abstract*—The use of functionally graded materials is increasingly used, from the simplest structural elements to the most complex or dedicated ones, in more and more fields of engineering creation. Under these conditions, both the manufacture of these materials and the development of their calculation are also in an appropriate development. This work is placed in the field of developing the calculation of mechanical structures from functionally graded materials, in conditions of accuracy, efficiency, economy and accessibility for designers and scientific researchers in the field. The beam we researched is the Euler-Bernoulli beam - the type most approached in mechanical engineering constructions. The new approach proposed by the authors is based on the use of two concepts (defined and used) original for the field addressed: the concept of multilayer material and the concept of equivalent material. In this work, the research results refer only to the calculation of displacements in bars subjected to bending. In the research carried out, the variation (according to the material law) of both Young's modulus and Poisson's ratio was taken into account. The method, methodology and models presented are theoretically substantiated and supported by practical examples, with general validity. The validation of the new approach in the calculation of bent beams is carried out on simple examples, with well-known analytical solutions, by applying both to the beam made of homogeneous and isotropic material, and to the beam made of a functionally graded material, made according to the power law of the material, for different values of the power coefficient. An important aspect of the authors' research is the fact that the approach to the calculation of bent bars made of functionally graded materials is accessible to numerical calculation without developing an appropriate software, but using general calculation programs using the finite element method. Based on our research, we state, without demonstrating in this paper, that the proposed approach is also suitable for calculation by numerical methods of the meshless and meshfree type. The work is distinguished by its novelty and originality and is part of the general effort to develop the calculation of structures made of functionally graded materials.**

***Index Terms*—Functionally Graded Materials; finite element method; beam calculus.**

I. Introduction

THIS paper is the result of my own scientific research in the field of calculation of structures from functionally graded materials. The structural element presented in this paper is a straight beam, of the Euler-Bernoulli type, loaded in bending.

The beam is a very widespread structural element in engineering constructions and also a structural element very suitable to be built from functionally graded materials [1], [2], [3]. The calculation of structures from functionally graded materials represents a problem with great mathematical difficulties stemming from the variation according to a certain law of its properties. There are several material laws [4], [5], the most used, to which our work also refers, is the power law. This work proposes to solve the calculation of the displacements of bent bars in an original, accessible and efficient way by introducing the concepts of multilayer material and equivalent material. The two concepts can be used independently or in combination. The models, methodology and examples that are presented make the calculation of functionally graded bars (FGB) an accessible problem for both analytical and numerical calculation, such as the finite element method but also other methods such as the Galerkin Free Element Method, the Smoothed Particle Hydrodynamics Method, etc. can be used. The numerical solutions in this paper are carried out with the finite element method - the most well-known and used method - and the use of the Ansys program (the highly reliable software product), so that accessibility is as high as possible, using common programs. The illustrative examples are based on the well-known case for the calculation of bent straight bars made of homogeneous and isotropic materials, namely the bar simply supported at the ends, loaded with a uniformly distributed load. Considering the possibilities offered by the use of the two concepts (multilayer material and equivalent material), our research also considered the evaluation of taking into account the influence of the Poisson's ratio, as a constant value or with a variable value according to the material law. The concepts and methodology presented in this paper are of a general nature, which allows those interested to develop research for other structural elements. The authors' achievements include published works on the calculation of other structures, such as plates, thick-walled tubes, etc. The intro-

duction of the two concepts of approach to calculus, through their originality and especially through the proposed methodology, represents the original and novel part, which makes the calculation of functionally graded bars an accessible and efficient calculation, with current means within the reach of any researcher.

II. Research Object

Our research focuses on a straight beam made of a functionally graded material according to the power law, based on two materials: alumina and aluminum. Their properties are presented in Table I.

Table I. Material Properties

Materials	Ceramic material (Al_2O_3)	Aluminum (Al)
Position	Top	Bottom
E [Pa]	$3.8\cdot10^{11}$	$7\cdot10^{10}$
$\nu[-]$	0.22	0.33
$\rho[kg/m^3]$	3960	2700

The functionally analyzed graded beam has the characteristics presented in Figure 1. The power law [3] is represented by the relation (1), with reference to Young's modulus (E). Analogously, the relation is written with reference to Poisson's ratio (ν). Analogously, the power law is written for any other properties, for which the values on the extreme faces are known.

$$E(y) = E_b + (E_t - E_b)\left(0.5 + \frac{y}{h}\right)^k \qquad (1)$$

The indices "t" and "b" signify the "top" and "bottom" positions, respectively, in relation to the beam – Figure 1. The parameter "k" is called the power coefficient, which theoretically can have values from zero to infinity.

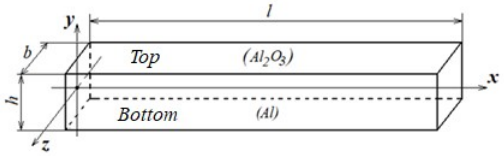

Fig. 1. Functionally graded beam

It is also found that small values of the power coefficient ($k<1$) lead to an increased influence of the material with superior characteristics (the ceramic material in this case).

For the value one of the power coefficient, the variation of all properties is linear. Figures 2 and 3 also show us a different curvature of the material properties variation curves, for the power coefficient value ranges: $k<1$, respectively $k>1$.

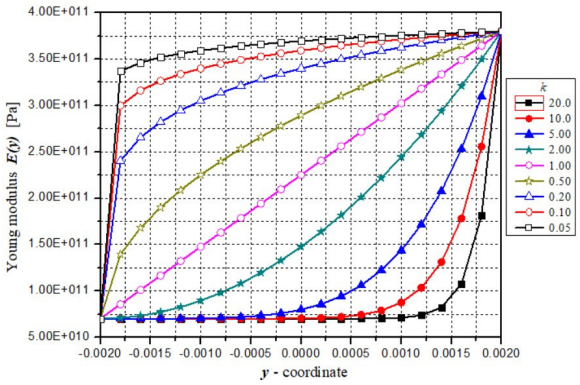

Fig. 2. Variation of Young's modulus over the height of the section

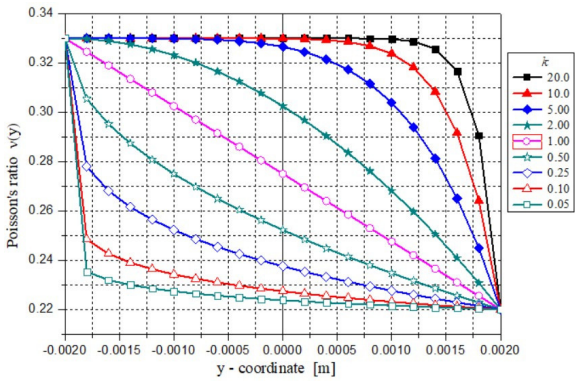

Fig. 3. Variation of Poisson's ratio over the height of the section

The dimensions of the analyzed beam have the values: $l=0.20$ m si $b=h=0.004$ m The distributed load is $p=1\cdot10^5$ N/m.

III. The Concept of Multilayer Material

The concept of multilayer material considers that the functionally graded material is composed of a number of layers of different materials, with homogeneous and isotropic properties (Figure 4) [6]. Each layer (j) is assigned the material properties calculated with the relation (1).

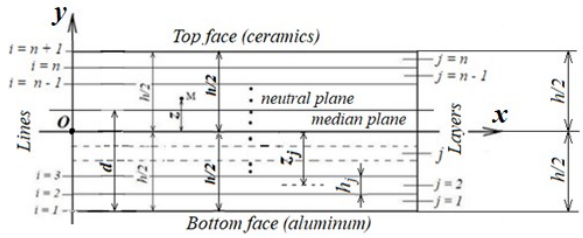

Fig. 4. Illustration of the multilayer material concept

For an infinite number of layers, the variation of the properties becomes continuous, according to the adopted law. In practice, one must work with a finite number of layers.

This concept causes the continuous variation of the properties to be replaced by a step variation, as exemplified in Figure 5, regarding the variation of the Young's modulus.

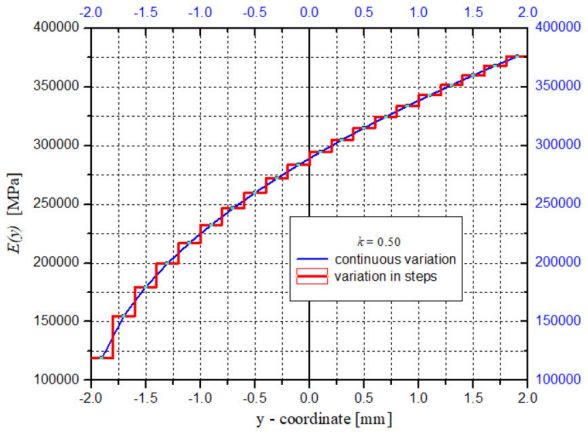

Fig. 5. Stepwise variation of Young's modulus

TABLE II. THE LAYERS VALUES OF ELASTIC CONSTANTS

Layers	*E(y)*	ρ*(y)*	ν*(y)*
1	3.278E+11	3747.77	0.311
2	3.423E+11	3806.94	0.317
3	3.494E+11	3835.58	0.319
4	3.541E+11	3854.84	0.321
5	3.577E+11	3869.44	0.322
6	3.606E+11	3881.24	0.323
7	3.631E+11	3891.15	0.324
8	3.652E+11	3899.70	0.325
9	3.670E+11	3907.23	0.325
10	3.687E+11	3913.96	0.326
11	3.702E+11	3920.05	0.327
12	3.715E+11	3925.61	0.327
13	3.728E+11	3930.73	0.327
14	3.740E+11	3935.48	0.328
15	3.751E+11	3939.90	0.328
16	3.761E+11	3944.04	0.329
17	3.770E+11	3947.94	0.329
18	3.779E+11	3951.62	0.329
19	3.788E+11	3955.10	0.330
20	3.796E+11	3958.41	0.330
Average values	3.654E+11	3900.84	0.325

The property values assigned to each layer (homogeneous and isotropic) are presented in Table II. These values are calculated for the power coefficient $k = 0.05$.

$$t_{\max} \le \frac{h}{20}[m] \tag{2}$$

The number of layers is adopted based on one's own experience, by calculating the maximum thickness of the layers. Using relation (2), it resulted $t_{\max} = 0.0002$ m.

A. *Calculus of bending stiffness*

From the study of straight bars subjected to bending, the relationships (2) and (3) are known [7], [8]:

$$u = -z\frac{\mathrm{d}w}{\mathrm{dx}} \tag{2}$$

$$\varepsilon_x = \frac{\mathrm{d}u}{\mathrm{dx}} = -y\frac{\mathrm{d}^2 \mathrm{v}}{\mathrm{dx}^2} \tag{3}$$

Since the stress state in the beam is linear (monoaxial), for each layer k the following relationship can be written [9]:

$$(\sigma_x)_k = E_k \cdot (\varepsilon_x)_k = -y \cdot E_k \frac{\mathrm{d}^2 \mathrm{v}}{\mathrm{dx}^2} \tag{4}$$

In the cross section of the multilayer beam, the relationship between bending moment and stresses is written [7]:

$$M_z = \sum_k \int_{y_{k-1}}^{y_k} (\sigma_x)_k \cdot (y - y_c) \cdot dy \tag{5}$$

In relation (5), $y_c = d$ is the coordinate that defines the position of the neutral plane (Figure 4).

Its calculation is done [10] with the relation,

$$y_c = \frac{\sum_k S_k}{\sum_k A_k} \tag{6}$$

representing the ratio between the static moment of the each layer area with respect to the lower side of the cross-section and the static moment of the entire section with respect to the same side. By introducing relation (6) into relation (5), after some mathematical operations, the relation is obtained:

$$M_z = -\frac{\sum_k E_k \cdot \frac{y_k^3 - y_{k-1}^3}{3} \cdot \sum_k E_k \cdot (y_k - y_{k-1}) - \left(\sum_k E_k \cdot \frac{y_k^2 - y_{k-1}^2}{2}\right)^2}{\sum_k E_k \cdot (y_k - y_{k-1})} \cdot \frac{\mathrm{d}^2 \mathrm{v}}{\mathrm{dx}^2} \tag{7}$$

Comparing relation (7) with the differential equation of the deformed average fiber, we arrive at the identification of the bending stiffness:

$$EI = K = \frac{A \cdot C - B^2}{A} \tag{8}$$

In relation (8) the following notations were made:

$$A = \sum_k E_k \cdot (y_k - y_{k-1}) \tag{9}$$

$$B = \sum_k E_k \frac{y_k^2 - y_{k-1}^2}{2} \tag{10}$$

$$C = \sum_k E_k \cdot \frac{y_k^3 - y_{k-1}^3}{3} \tag{11}$$

For the considered FGB and for the power coefficient $k = 0.05$, $A = 1.46178 \cdot 10^9$ N/m, $B = 2.97939 \cdot 10^6$ N and $C = 7997.95$ Nm, resulting in bending stiffness:

$$K = 1925.3795 \text{ Nm}^2 \tag{12}$$

Knowing the bending stiffness allows the calculation of the displacements of bent straight bars with the known relations for homogeneous and isotropic straight bars. The relations depend on the mode of support and are well known in the literature.

IV. The Concept of Equivalent Material

The concept of equivalent material allows the replacement of a functionally graded material (multilayer) with a fictitious, homogeneous and isotropic one, which has the same behavior as the real material. For the calculation of the displacements of bent straight bars, the equivalent material must have the same bending stiffness. For the calculation of the equivalent bending stiffness $(EI)_{ech} = K_{ech}$, we will define the bending stiffness by analogy with the multilayer plate [7].

Thus,

- for a homogeneous and isotropic plate,

$$D = \frac{Eh^3}{12(1-\nu^2)} = \frac{E \cdot I}{1-\nu^2} \tag{13}$$

- for the multilayer plate, we can write,

$$D^* = \frac{E_t I^*}{1-\nu^2} \tag{14}$$

where the parameter I^* (axial moment of inertia for width equal to unity) is defined by the relation,

$$I^* = \int_{-h/2}^{h/2} \frac{E_k}{E_t} y_k^2 \, \mathrm{d}y \tag{15}$$

where y_k represents the distance of the average fiber of the layer k from the neutral axis, and the ratio E_k / E_t is a constant c_k with different values from one layer to another. In relation (14), we recognize the calculus relation of the axial inertia moment of each laye area, with the equivalent width of each layer equal to c_k, from the neutral axis. In the case of bars, being a monoaxial state of tension, the denominator $(1-\nu^2)$ is replaced by the value one. Therefore, for the calculation of the bending stiffness of functionally graded straight bars we can write:

$$D^* = E_t I^* = K_{ech} \tag{16}$$

$$I^* = \int_{-h/2}^{h/2} c_k \cdot y_k^2 \cdot \mathrm{d}y \tag{17}$$

$$c_k = \frac{E_k}{E_t} \tag{18}$$

After performing the integrals, for n layers we can write:

$$I^* = \left[\frac{c_1 h_1^3}{12} + c_1 h_1 d_{G1}^2 \right] + \left[\frac{c_2 \cdot h_2^3}{12} + c_2 h_2 d_{G2}^2 \right] + \ldots \\ \ldots + \left[\frac{c_n h_n^3}{12} + c_n h_n d_{Gn}^2 \right] \tag{19}$$

For the considered FGB, for the power coefficient $k = 0.05$, the calculus of the equivalent inertia moment leads to the value $I^* = 5.07240 \cdot 10^{-9}$ m^4.

Using the relation $D^* = E_t I^* = K_{ech}$, the equivalent bending stiffness is:

$$K_{ech} = 1925.3804 \text{ Nm}^2 \tag{20}$$

The values of bending stiffness found for those two concepts are practically identical (error of 0.00013%). The two methods, concepts are therefore concordant.

V. Numerical Approach

The numerical analysis is performed with the finite element method [13], [14], [15], based on the concept of multilayer material, using data of Table II. The finite element used is SOLID185 from the Ansys program library [16], [17].

This finite element (8-node brick) is used in two variants: with the multilayer finite element option (Figure 6) and with the structural finite element option (regular) [11], [12]. The finite element model is performed considering the beam made up of 20 different layers, without sliping between them.

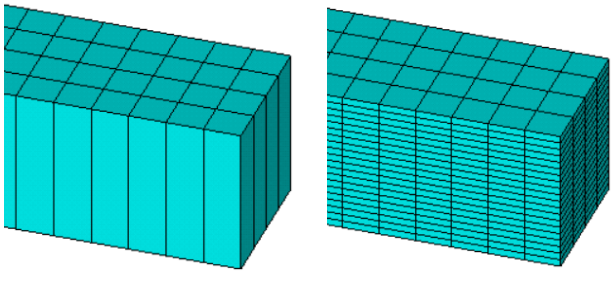

Fig. 6. Details of multilayer finite element modeling

The deformed state of the functionally graded bar shown in Figure 7, where the maximum displacement $v_{max} = 0.001083$ represents the case of the beam made of

the material with the power coefficient $k = 0.05$ and Poisson's ratio $\nu = 0$.

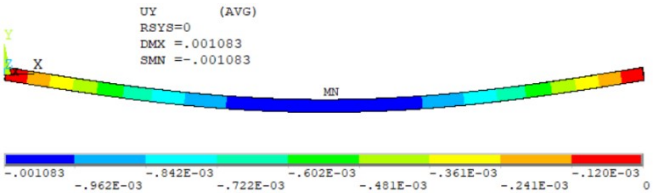

Fig. 7. Deformed state of the functionally graded beam

TABLE III. BENDING STIFFNESS

k	A	B	C	$EI = K$
[-]	$[\mathrm{N/m}] \cdot 10^9$	[N]	[Nm]	$[\mathrm{Nm}^2]$
0.05	1.46178	2979385.67	7997.95	1925.3779
0.10	1.40854	2921669.24	7892.75	1832.4824
0.25	1.27346	2763964.10	7596.60	1597.6017
0.50	1.10745	2543269.04	7159.49	1318.8262
1.00	0.90000	2212300.00	6449.20	1011.1208
2.00	0.69307	1798451.83	5454.45	787.6744
4.00	0.52748	1384085.15	4316.06	684.3028
6.00	0.45637	1176390.67	3681.88	649.4752
8.00	0.41675	1051368.99	3276.87	624.4811

TABLE IV. EQUIVALENT BENDING STIFFNESS

Layer No.	E_k	y_{Gk}	$c_k = b$	I_k
[-]	[Pa] $\cdot 10^{11}$	[m]	[-]	[m^4] $\cdot 10^{-10}$
1	3.27786	-0.0019	0.862594737	6.48663
2	3.42342	-0.0017	0.900900000	5.44986
3	3.49388	-0.0015	0.919442105	4.35704
4	3.54128	-0.0013	0.931915789	3.34392
5	3.57721	-0.0011	0.941371053	2.44537
6	3.60622	-0.0009	0.949005263	1.67699
7	3.63060	-0.0007	0.955421053	1.04766
8	3.65164	-0.0005	0.960957895	5.63107
9	3.67017	-0.0003	0.965834211	2.27382
10	3.68673	-0.0001	0.970192105	4.35278
11	3.70172	0.0001	0.974136842	1.39352
12	3.71540	0.0003	0.977736842	1.40545
13	3.72800	0.0005	0.981052632	4.24977
14	3.73967	0.0007	0.984123684	8.68612
15	3.75055	0.0009	0.986986842	1.47265
16	3.76074	0.0011	0.989668421	2.23814
17	3.77033	0.0013	0.992192105	3.16603
18	3.77937	0.0015	0.994571053	4.25715
19	3.78794	0.0017	0.996826316	5.51228
20	3.79608	0.0019	0.998968421	6.93211
			$I_{ech} = \sum_k I_k =$	50.6679
			$D^* = E_t I^* = K_{ech} =$	1925.3804

TABLE V. COMPARATIVE EVALUATION OF STIFFNESS

k	$EI = K$	$K_{ech}(k)$	E_{rr}.
[-]	$[\mathrm{Nm}^2]$	$[\mathrm{Nm}^2]$	[%]
0.05	1925.3779	1925.3804	-0.00013
0.10	1832.4824	1832.4822	0.00001
0.25	1597.6017	1597.6045	-0.00018
0.50	1318.8262	1318.8237	0.00019
1.00	1011.1208	1011.1208	0.00000
2.00	787.6744	787.6768	-0.00030
4.00	684.3028	684.3033	-0.00007
6.00	649.4752	649.4762	-0.00015
8.00	624.4811	624.4782	0.00046

VI. COMPARATIVE RESULTS

For a series of values of the power coefficient k, Table III presents the values of some intermediate parameters and the value of the bending stiffness $K = EI$ of the beam, according to the concept of multilayer material. Table IV presents the values of some parameters and of equivalent bending stiffness $K_{ech} = (EI)_{ech}$ in accordance with the concept of equivalent material, all of this for the power coefficient $k = 0.05$.

Repeating the calculations in Table IV for the other values of the power coefficient, we find the values in Table V, comparatively with the stiffness values in Table III.

Rezultatele calculului analitic si numeric sunt prezentate sintetic, comparativ, in Tabelul VI, pentru mai multe valori ale coeficientului putere, pentru diferite valori ale coeficientului Poisson, pentru cazul barei simplu rezemate la capete, incarcata cu o sarcina uniform distribuita. Relatia analitica de calcul este:

$$v_{\max} = \frac{5}{384} \cdot \frac{pl^4}{EI} = \frac{5}{384} \cdot \frac{pl^4}{K} \qquad (21)$$

VII. CONCLUSIONS

The paper deals, in an original manner, with a topic of great relevance and importance for mechanical engineering – the calculation of beams made of functionally graded materials.

The originality and consequently the novelty brought by the work lies in the manner of solving, by using the concepts of equivalent material and multilayer material. These concepts can be used both independently and in combinations, leading to the greatest possible efficiency of the calculation.

The numerical exemplification of the use of the presented concepts, methods and methodologies validates their use for calculating the displacements of functionally graded beams.

The values in Table VI demonstrate through quantitative arguments that the influence of the Poisson's ratio is small, but it exists and can be evaluated.

TABLE VI. COMPARATIVE EVALUATION OF STIFFNESS

k	$v_{max}^{analytical}$	v_{max}^{FEM}	E_{rr}
[-]	[m]	[m]	[%]
$\nu = 0$			
0.05	0.001082	0.001083	*0.19*
0.10	0.001137	0.001138	*-0.27*
0.25	0.001304	0.001305	*-0.46*
0.50	0.001580	0.001581	*-0.02*
1.00	0.002060	0.002062	*0.02*
2.00	0.002645	0.002648	*0.19*
4.00	0.003044	0.003048	*0.15*
6.00	0.003208	0.003211	*-0.07*
8.00	0.003336	0.003340	*-0.12*
		Average error =	***-0.04***
$\nu = 0.30$			
0.05	0.001082	0.001084	*-0.18*
0.10	0.001137	0.001139	*-0.19*
0.25	0.001304	0.001306	*-0.15*
0.50	0.001580	0.001582	*-0.15*
1.00	0.002060	0.002063	*-0.13*
2.00	0.002645	0.002649	*-0.15*
4.00	0.003044	0.003050	*-0.18*
6.00	0.003208	0.003213	*-0.16*
8.00	0.003336	0.003342	*-0.18*
		Average error =	***-0.16***
$\nu = \nu(k)$			
0.05	0.001082	0.001084	*-0.18*
0.10	0.001137	0.001138	*-0.10*
0.25	0.001304	0.001305	*-0.07*
0.50	0.001580	0.001579	*0.04*
1.00	0.002060	0.002058	*0.12*
2.00	0.002645	0.002641	*0.15*
4.00	0.003044	0.003042	*0.08*
6.00	0.003208	0.003206	*0.05*
8.00	0.003336	0.003334	*0.06*
		Average error =	***0.02***

Although for the three cases of considering the Poisson's ratio the errors are below 1%, the case closest to the analytical calculation is the one in which the Poisson's ratio is considered in accordance with the law of variation – $\nu = \nu(k)$ – when the average error is the smallest, reaching the value of 0.02%.

In this paper we have only referred to the calculation of displacements, but the concepts, methods and methodologies presented are generally valid for the calculation of rotations or taking into account the effects of shear force. Also, our way of solving functionally graded beams is independent of the beam support mode.

This new approach to the calculation of bars made of functionally graded materials has been used for other structural elements as well.

The results of our research, although presented synthetically in this paper, highlight the validity, efficiency and accessibility of the new way of approaching the calculation of functionally graded beams

REFERENCES

[1] Anju, M.; Subha, K. A Review on Functionally Graded Plates. Int. Res. J. Eng. Technol. 2018, 5.

[2] Nastasescu, V., Barsan, Gh., Mocian, O., Calculul unor elemente structurale din materiale gradate funcțional, Editura Academiei Române, București, 2025, ISBN: 978-973-27-3950-1.

[3] Toudehdehghan, A.; Lim, J.W.; Foo, K.E.; Ma'Arof, M.; Mathews, J., A Brief Review of Functionally Graded Materials. MATEC Web Conf. 2017, 131, 03010. [CrossRef]

[4] Pradhan, K.K.; Chakraverty, S. Overview of functionally graded materials. In Computational Structural Mechanics; Elsevier: Amsterdam, The Netherlands, 2019; pp. 1–10.

[5] Mahamood, R.M.; Akinlabi, E.T.; Shukla, M.; Pityana, S.L. Functionally graded material: An overview. In Proceedings of the World Congress on Engineering, London, UK, 4–6 July 2012; Volume 3.

[6] Năstăsescu, V., Research and Developments in Engineering Research, Volume 8, Chapter 1: Study about Calculus of Functionally Graded Plates by using Multylayer Plate Concept, Print ISBN 978 81-19761-42-5, eBook ISBN 978-81-19761-53-1, DOI: 10.9734/bpi/rader/v8, Print ISBN: 978-81 19217-45-8, eBook ISBN: 978-81-19217-47-2, DOI: 0.9734/bpi/rader/v3/19159D.

[7] Szilard, R., Theories and Applications of Plate Analysis: Classical, Numerical and Engineering Methods. Appl. Mech. Rev. 2004, 57, B32–B33. [CrossRef].

[8] Timoshenko, S. P., Theory of Elasticity, 3rd Edition, Tokyo, London, New York, McGraw-Hill, 1970.

[9] Bia, C., Ille, V., Soare, M. V., Rezistența materialelor și teoria elasticității, București, Editura Didactică și Pedagogică, 1983.

[10] Bassin, M. G., Brodsky, S. M., Wolkoff, H., Statics and Strength of Materials, Third Edition, McGraw-Hill Book Company, 1979.

[11] Alshorbagy, A.E.; Eltaher, M.; Mahmoud, F. Free Vibration Characteristics of a Functionally Graded Beam by Finite Element Method. Appl. Math. Model. 2010, 35, 412–425. [CrossRef].

[12] Ramu, I.; Mohanty, S., Modal Analysis of Functionally Graded Material Plates Using Finite Element Method. Procedia Mater. Sci. 2014, 6, 460–467. [CrossRef].

[13] Bathe, K., J., Finite Element Procedures; Prentice-Hall, Inc.: Hoboken, NJ, USA, 1996.

[14] Huebner, K., H.; Dewhirst, D., L.; Smith, D.E.; Byrom, T., G., The Finite Element Method for Engineers, 3rd ed.; John Willey and Sons, Inc.: Hoboken, NJ, USA, 1995.

[15] Zienkiewicz, O.C.; Taylor, R.L.; Zhu, J.Z. The Finite Element Method, 4th ed.; McGraw-Hill Book Company: New York, NY, USA, 2005.

[16] * * * Theory Reference for the Mechanical APDL and Mechanical Applications, Ansys Inc., Release 12, 2009

[17] * * * Ansys Theory Reference, Ansys Inc., Release 5.6, 1999.

Proceedings of the International Conference on Engineering, Technology and Applied Science Innovations pp. 53–59
DOI: 10.15439/2025I28
ISSN 2300-5963 ACSIS, Vol. 46

Regulatory and Governance Aspects of 5G and Beyond

Dionysia Varvarigou
University of Patras
Patras, Greece
dvarvarigou@upatras.gr

Kostas Lampropoulos
University of Patras
Patras, Greece
klamprop@ece.upatras.gr

Spyros Denazis
University of Patras
Patras, Greece
sdena@upatras.gr

Paris Kitsos
University of Patras,
University of Peloponnese
Patras, Greece
pkitsos@ieee.org

***Abstract*—The rapid deployment of 5G networks introduces new opportunities for digital transformation while exposing critical vulnerabilities across technical and regulatory domains. This paper offers a comprehensive exploration of the European cybersecurity landscape for 5G and beyond, analyzing how legislative frameworks such as GDPR, the EECC, and NIS2 shape telecom security practices. It examines the roles of key actors including ENISA, national regulatory authorities, and international bodies, and discusses how telecom operators can implement and operationalize these frameworks. The paper further presents a practical use case demonstrating how the SAND5G platform supports compliance and incident response through contextualized risk assessment and real-time threat mitigation. Looking ahead, it outlines future governance challenges and emerging technologies—such as quantum cryptography, zero trust architectures, and AI-driven security—required to secure next-generation networks like 6G. The study underscores the need for dynamic, multi-layered, and forward-looking cybersecurity strategies that balance innovation with resilience.**

***Index Terms*—SAND5G Platform, 5G Security, Cybersecurity Regulations.**

I. Introduction

THE SAND5G project is a European research initiative dedicated to advancing the security analysis of 5G and beyond networks. This paper builds upon the comprehensive findings of SAND5G, particularly those presented in Deliverable D2.1 "Security analysis for 5G and beyond networks," to provide a critical overview of the multifaceted evolution of 5G technology, its associated security implications, regulatory frameworks, and strategic perspectives for future telecommunications.

The project underscores a dual strategy that leverages both technical advancements and regulatory policies to fortify network security. It highlights the pioneering roles of standardization bodies such as 3GPP, ETSI, and ITU-T, alongside collaborative projects and initiatives focused on securing 5G infrastructures. The analysis addresses emerging security challenges introduced by 5G adoption, including vulnerabilities linked to IoT proliferation, the convergence of IT and telecom infrastructures, and complexities arising from software-defined networking and virtualization.

The global deployment of 5G networks marks a critical milestone in telecommunications, enabling unprecedented speeds, massive device connectivity, and ultra-low latency that power innovative applications from smart cities to Industry 4.0. However, these advancements bring new complexities in security and privacy that require comprehensive governance frameworks. Europe's approach emphasizes harmonizing rapid technological progress with robust protection of data and infrastructure resilience. The SAND5G project contributes to this endeavor by integrating technical innovation with regulatory insight, ensuring that security is embedded not only in network design but also in policy and operational practices. This paper examines the European regulatory environment alongside emerging security strategies, highlighting the challenges and opportunities of securing 5G and paving the way for future generations such as 6G.

This work advocates a holistic approach that integrates technical solutions, governance frameworks, and international collaboration to navigate the evolving security landscape of 5G and beyond. The subsequent sections provide an in-depth background on standardization and innovations in 5G, explore the intricate security landscape shaped by novel architectures and extensive connectivity, examine regulatory compliance and data protection considerations, and review existing security mechanisms. The paper further presents the European Union's strategic response through initiatives such as the 5G toolbox and concludes with insights into future telecommunications innovations including 6G and beyond.

To ensure the secure and resilient deployment of 5G networks, regulatory frameworks play a pivotal role alongside technical safeguards. Within the European Union, the security and privacy of telecommunications infrastructure are guided by a complex yet comprehensive set of regulations and directives. These legal instruments not only define the responsibilities of operators and service providers but also establish mechanisms for oversight, coordination, and enforcement. Understanding this evolving regulatory landscape is essential for aligning technical innovation with legal compliance and public trust. The following section outlines

This article describes work undertaken in the context of the SAND5G project, "Security Assessments for Networks anD services in 5G" which has received funding from the European Union's Digital Europe programme under grant agreement No 101127979 and is supported by European Cybersecurity Competence Center. Views and opinions expressed are however those of the author(s) only and do not necessarily reflect those of the European Union. Neither the European Union nor the granting authority can be held responsible for them

the most relevant EU legislation shaping the 5G cybersecurity domain.

II. Existing European Regulatory Framework

Regulatory compliance, particularly in the context of European legislation, plays a significant role in shaping user-centric security considerations for 5G networks. In the European Union (EU), several key regulations and directives govern cybersecurity and data protection, impacting how 5G networks are deployed, managed, and secured. Here are some important aspects of regulatory compliance in the EU [1].

GDPR [2] is one of the most comprehensive data protection regulations globally and significantly impacts the security and privacy of user data in 5G networks. GDPR applies to the processing of personal data by organizations operating within the EU or offering goods and services to individuals in the EU. It imposes strict requirements on data controllers and processors, including obligations related to data protection principles, lawful processing, data subject rights, data breach notification, and privacy by design and by default. Compliance with GDPR is essential for safeguarding user privacy and avoiding hefty fines and penalties for non-compliance.

The ePrivacy Directive [3] governs the processing of personal data and the protection of privacy in the electronic communications sector. While not specifically tailored to 5G networks, it applies to the collection and use of data transmitted over these networks, including metadata generated by communication services. The forthcoming ePrivacy Regulation, intended to replace the current directive, aims to modernize and strengthen privacy rules for electronic communications, further impacting the security and privacy of 5G networks.

The European Electronic Communications Code (EECC) [4] is the main EU policy framework for the telecom sector. Adopted in 2018, these rules apply to all electronic communications services and networks in the EU. Currently, the EECC has been transposed by most EU countries, with the Commission supporting Member States in the implementation process.

Security requirements for the telecom sector are contained in Article 40 of the EECC (which replaces Article 13a of the Framework Directive). Article 40 asks Member States to ensure that operators take “appropriate” cybersecurity measures and report significant incidents to the national authorities; Article 41 asks Member States to ensure that the national competent authority, for instance a telecom national regulatory agency (NRA) or a cybersecurity agency, depending on the national setting, has the powers to audit telecom operators and to enforce measures in case of cybersecurity deficiencies.

In terms of supervision of these security requirements, Member States have taken diverse approaches. For instance, where binding rules apply to mobile network operators, they may cover different types of technical and organizational measures. In Member States where security measures are further clarified in more technical and practical detail (often via secondary legislation), they often refer to the ENISA framework of detailed technical telecom security measures, which was developed with all Member States to implement the EECC and contains a detailed list of relevant telecom security measures.

The NIS1 [5] establishes cybersecurity standards for operators of essential services (OES) and digital service providers (DSPs) within the EU. It requires member states to adopt national cybersecurity strategies, designate competent authorities, and establish incident reporting mechanisms for significant cyber incidents. Compliance with the NIS Directive involves implementing appropriate security measures, conducting risk assessments, and reporting cybersecurity incidents to national authorities.

The revised NIS Directive, referred to as NIS2 [6], will repeal and replace Articles 40 and 41 of the EECC, with effect from 18 October 2024, streamlining the cybersecurity policy framework, adding providers of public electronic communications networks and providers of publicly available electronic communications services to the ‘digital infrastructure’ sector. The NIS2 Directive establishes: (a) obligations requiring Member States to adopt national cyber security strategies and to designate or set up competent authorities, cyber crisis management authorities, cyber security single points of contact and computer security incident response teams (CSIRTs), (b) cybersecurity risk management measures and reporting obligations for entities of the type referred to in Annexes I and II of the NIS2 Directive, (c) rules and obligations regarding the exchange of cybersecurity information and (d) Member States' obligations regarding supervision and enforcement. Under the NIS2 Directive, the Commission has to issue implementing acts on security measures and incident reporting, for several entities under the NIS2 digital infrastructure sector, including TLDs, DNS, and content delivery networks (CDNs). The NIS Cooperation Group already published detailed technical security measures for TLD registries [7] and is drafting a guideline on security measures for the DNS providers. In addition, the NIS2 allows the NIS Cooperation Group, together with the Commission and ENISA, to conduct EU-wide risk assessments in critical supply chains.

The Resilience of Critical Entities (CER) Directive [8] covers the physical resilience of critical entities against man-made and natural hazards, in coherence with the NIS2 Directive which covers cybersecurity risks. This Directive focuses on all relevant non-cyber natural and man-made risks, including cross-sectoral or cross-border, that may affect the provision of essential services, such as natural disasters, accidents, public health emergencies and antagonistic threats, including terrorist offences, sabotage and hybrid threats. It covers eleven sectors, including digital infrastructure.

The EU Cybersecurity Act [9] introduces a certification framework for cybersecurity products, services, and processes, including those related to 5G networks. The frame-

work enables the voluntary certification of ICT products, ICT processes, and ICT services based on common cybersecurity standards and schemes recognized across the EU. A European cybersecurity certification scheme may specify one or more of the following assurance levels for ICT products, ICT services and ICT processes: 'basic', 'substantial' or 'high'. The assurance level shall be commensurate with the level of the risk associated with the intended use of the ICT product, ICT service or ICT process, in terms of the probability and impact of an incident. Compliance with cybersecurity certification requirements can enhance the trustworthiness and security of 5G products and services, fostering consumer confidence and market competitiveness.

The Cyber Resilience Act (CRA) [10], for which a provisional political agreement has been reached in December 2023, requires manufacturers of connectable software and hardware products intended for the EU market to ensure that such products are developed in line with security-by-default and security-by-design principles and that their security is maintained throughout their lifetime, for instance through testing and security updates. The CRA covers a wide range of products deployed by network operators, such as routers and switches. It has the potential to increase transparency on the security of such products and facilitate supply chain security management for critical infrastructure covered by the NIS2 Directive, including operators of public electronic communications networks and core Internet infrastructure. The agreement reached is, as of February 2024, subject to formal approval by both the European Parliament and the Council.

While the European regulatory framework sets the foundation for securing 5G networks, its effective implementation and coordination depend on the efforts of specialized institutions. Among them, the European Union Agency for Cybersecurity (ENISA) plays a pivotal role in translating policy into practice. As the EU's dedicated cybersecurity body, ENISA supports member states and stakeholders by developing technical guidelines, facilitating collaboration, and strengthening collective preparedness. The following section explores ENISA's multifaceted contributions to securing 5G and beyond.

III. European Union Agency for Cybersecurity (ENISA)

ENISA [11] plays a key role in enhancing cybersecurity and resilience across the EU, particularly within the telecommunications sector. It provides guidance, best practices, and recommendations to strengthen the security of telecom networks and infrastructure.

ENISA collaborates with telecom stakeholders to collect threat intelligence, analyze emerging risks, and share actionable information to improve situational awareness. It works closely with EU institutions, national cybersecurity agencies, industry groups, and international partners to coordinate efforts and address common cybersecurity challenges. This includes participation in working groups, joint initiatives, and information-sharing frameworks to bolster collective resilience.

The agency publishes security guidelines and technical standards covering network security, incident response, risk management, and security-by-design. ENISA also supports the telecom sector in developing incident response and crisis management capabilities through guidance, exercises, and simulations to improve preparedness.

Furthermore, ENISA contributes to cybersecurity certification schemes for telecom products and services, promoting common evaluation criteria and mutual recognition of certifications across EU member states.

To build capacity, ENISA organizes training, workshops, and awareness programs for telecom professionals, regulators, and policymakers, fostering knowledge sharing and improving the sector's overall cybersecurity posture.

ENISA's role extends beyond guidance and standard-setting. The agency actively coordinates large-scale cybersecurity exercises such as the annual European Cybersecurity Challenge, fostering readiness and collaboration among Member States. Through its Threat Landscape reports, ENISA provides up-to-date intelligence on evolving cyber threats, including those targeting 5G infrastructures. The agency also supports the implementation of the EU 5G Toolbox, assisting countries in adopting consistent risk mitigation measures. ENISA's collaboration with CERTs (Computer Emergency Response Teams) across Europe enhances rapid incident response and information sharing, critical for managing the complex threat environment in telecommunications.

While ENISA primarily operates within the EU context, its activities also intersect with broader international efforts aimed at securing global telecommunications infrastructure. As 5G networks are inherently cross-border in nature, threats targeting them often span jurisdictions. Consequently, cooperation with international organizations and standardization bodies becomes essential to ensure cohesive and interoperable security practices. Building on ENISA's regional contributions, the following section explores the EU's role in fostering global partnerships for 5G security and resilience.

IV. International Cooperation in 5G Security

Securing 5G networks is a global challenge that transcends regional boundaries. The European Union actively cooperates with international bodies such as the International Telecommunication Union (ITU), the Global System for Mobile Communications Association (GSMA), the 3rd Generation Partnership Project (3GPP), and other regional cybersecurity agencies to harmonize standards, develop secure-by-design architectures, and share threat intelligence. These collaborations facilitate the alignment of security frameworks, promote technical interoperability, and support coordinated responses to transnational cyber threats and large-scale incidents. Joint efforts—such as coordinated threat reporting, the development of shared risk assessment

methodologies, and participation in cross-border cybersecurity exercises—help enhance collective preparedness and resilience.

On the policy level, such cooperation also reinforces global consensus around key principles like transparency, accountability, and proportionality in cyber risk management. It further supports the development of trusted ICT supply chains through common evaluation schemes and coordinated vendor risk assessments, aiming to mitigate dependencies on untrusted suppliers and ensure strategic autonomy. These international efforts are crucial for sustaining long-term cybersecurity in a rapidly evolving technological landscape.

While international cooperation provides a broad framework for harmonizing 5G security practices across borders, effective implementation depends heavily on the actions of national regulatory authorities. These authorities serve as the operational arms of policy enforcement, translating international and regional strategies into concrete technical and organizational requirements. The next section examines the pivotal role played by national regulators in overseeing compliance, coordinating incident response, and fostering resilience at the member state level.

V. Regulatory Authorities

National regulatory authorities oversee 5G network security and enforce compliance with applicable laws and standards. While specific requirements vary by jurisdiction, authorities typically set security standards and guidelines that telecom operators must follow, covering areas such as authentication, encryption, access control, incident response, and risk management.

Operators are often required to conduct risk assessments, implement risk management processes, and promptly report significant cybersecurity incidents to authorities. Regulatory bodies monitor compliance through audits, inspections, and reporting, imposing penalties for non-compliance when necessary.

Authorities also promote collaboration and information sharing among operators, government agencies, and other stakeholders to address common cybersecurity threats. A key example of such international cooperation is ENISA's European Competent Authorities for Secure Electronic Communications (ECASEC) expert group [11]. This group plays a central role in aligning national efforts by agreeing on technical and organizational measures for the implementation of Articles 40 and 41 of the European Electronic Communications Code (EECC) and the provisions of the NIS2 Directive concerning telecom security and incident reporting. Furthermore, ECASEC facilitates the voluntary exchange of information among national experts on threats, cybersecurity incidents, lessons learned, applicable standards, and practical tools. The group also contributes to the development of ENISA's policy and technical outputs by reviewing and providing input on key documents, thereby reinforcing a coordinated and resilient approach across Member States.

While national authorities are responsible for setting and enforcing regulatory standards, the responsibility for practical implementation lies primarily with telecom operators. These operators act as the frontline of network security, translating legal and policy requirements into actionable security practices within their infrastructures. The following section explores how telecom providers operationalize compliance, establish robust governance structures, and deploy security controls to protect 5G networks against evolving cyber threats.

VI. Telecom Operators

For telecom operators, adhering to regulatory frameworks such as the EECC, the NIS Directive, and the GDPR is vital for maintaining secure and resilient 5G networks. To ensure compliance and mitigate risks, operators must begin by conducting comprehensive assessments to determine which regulatory requirements apply to their operations, enabling them to formulate an effective compliance strategy. Establishing robust governance frameworks is equally important, with clearly defined roles and the appointment of dedicated compliance officers to oversee implementation. Strong security and privacy controls should be deployed, including mechanisms for encryption, access management, intrusion detection, and data loss prevention. Operators are also expected to develop and communicate formalized policies and procedures that cover key areas such as data protection, incident response, risk management, and staff training.

To address privacy risks in particular, telecom companies should perform Data Protection Impact Assessments (DPIAs), ensuring that GDPR obligations are met throughout their service delivery. Incident response capabilities must be in place to allow for prompt reporting of cybersecurity events to both the relevant authorities and affected individuals. Additionally, third-party suppliers must be subject to rigorous security and compliance oversight, as they are often integral to the telecom ecosystem. Building a resilient security culture requires ongoing training and awareness programs for both employees and contractors. Finally, operators must implement continuous monitoring and regular audits to evaluate the effectiveness of security controls and update them as necessary to adapt to evolving threats and regulatory requirements. Through this proactive and structured approach, telecom operators can safeguard their infrastructure, meet legal obligations, and foster trust among users and regulators alike.

While telecom operators are expected to adopt comprehensive security and compliance strategies, the complexity of modern 5G infrastructures demands the support of advanced platforms that enable rapid detection, contextual analysis, and coordinated response. To demonstrate how such support is operationalized in practice, the following section presents a realistic scenario in which the SAND5G platform is employed to manage a security breach. This use

case illustrates how integrated tools and compliance workflows—aligned with both GDPR and NIS2—empower telecom actors to respond effectively and maintain regulatory assurance in the face of cyber incidents.

VII. Use Case: Security Breach Mitigation using the SAND5G Platform under GDPR/NIS2

In this illustrative scenario (see Figure 1), we demonstrate how the SAND5G platform supports a telecom operator in managing a security breach under GDPR and NIS2. When a potential intrusion is detected via integrated IDS (e.g., Snort3), SAND5G enriches the alert with contextual asset data and calculates impact scores. This enables the security analyst and Data Protection Officer (DPO) to quickly assess the situation, fulfill notification obligations within 72 hours (GDPR), and notify the NIS authority as required. If needed, users are informed and further steps are taken. The platform also logs mitigation activities and helps ensure post-incident compliance and policy updates.

While the SAND5G platform exemplifies how advanced tooling can support compliance and incident management under today's regulatory frameworks, it also establishes a solid foundation for the cybersecurity solutions of tomorrow. As networks transition toward 6G, platforms like SAND5G are expected to evolve, embracing increased complexity and integrating emerging technologies such as quantum security, zero-trust models, and AI-driven governance. The following section explores future governance models and security innovations that will be essential to support this next leap in telecommunications.

Figure 1: Security breach mitigation process using the SAND5G platform under GDPR and NIS2 directives.

VIII. Future Governance for 6G Security

The complexity and ubiquity of 6G networks introduce new security and resilience challenges. Adversaries are becoming more sophisticated, employing advanced AI techniques to launch novel attacks. To address these threats, 6G networks must achieve significantly higher levels of trustworthiness, dependability, and security, requiring advancements across multiple domains. Key approaches include the following subsections.

A. Physical Layer Security

Physical Layer Security (PLS) ([12],[13]) harnesses the physical characteristics of wireless channels to establish security, employing methods such as spread spectrum, frequency hopping, and directional antennas. It also emerges as a promising security technology for 6G due to its immunity to traditional cryptography vulnerabilities. Leveraging the physical attributes of wireless channels, PLS renders eavesdropping or interference by attackers exceedingly challenging.

B. Quantum Cryptography

Quantum cryptography ([14]) utilizes the principles of quantum mechanics to forge unbreakable encryption, offering a promising avenue for 6G security by evading vulnerabilities present in traditional cryptography. In addition, it stands out as a highly promising security solution for 6G networks, leveraging the distinct principles of quantum mechanics, which starkly contrast classical physics. This inherent distinction makes quantum cryptography resilient against attacks, even from formidable adversaries.

C. Zero Trust Security

Zero Trust Security ([15],[16]) operates under the assumption that no user or device is inherently trustworthy, necessitating comprehensive traffic inspection regardless of origin or destination. Zero Trust architecture provides a collection of concepts and ideas designed to minimize uncertainty in enforcing accurate, least privilege per-request access decisions in information systems and services in the face of a network viewed as compromised. It emphasizes continuous authentication, authorization, and validation, alongside granular access control and continuous monitoring. It presents a robust security paradigm that operates under the assumption that no user or device holds inherent trustworthiness. Consequently, all network traffic undergoes scrutiny, regardless of its origin or destination, offering potent defense mechanisms against attacks on 6G networks.

D. Artificial Intelligence and Machine Learning

AI and ML technologies [17],[18]) are poised to bolster 6G network security by swiftly identifying and mitigating intrusions, discerning malicious traffic patterns, and predicting potential attacks. They offer multifaceted avenues to bolster the security of 6G networks. These technologies can adeptly identify and mitigate intrusions, discern malicious traffic patterns, and forecast potential threats. While still

evolving, AI and ML hold considerable promise in revolutionizing the security landscape of 6G networks.

E. Enhanced Authentication and Authorization

6G will adopt advanced authentication and authorization methods [19],[20], including multi-factor authentication and biometric verification, strengthening identity and access management to protect networks.

F. Secure Network Slicing

Secure network slicing [21],[22] aims to create isolated virtual networks tailored to specific services or user groups, ensuring protection and resource separation across 6G infrastructures.

G. Quantum Key Distribution

Quantum Key Distribution (QKD) [23], based on quantum mechanics, enables secure key exchange between parties, safeguarding against eavesdropping and interception in 6G channels.

As 6G technology approaches realization, governance models must evolve to accommodate unprecedented technological complexity and agility. Future governance will likely incorporate adaptive regulatory frameworks enabled by real-time monitoring and AI-powered compliance tools, allowing for rapid responses to emerging threats. Moreover, ethical considerations surrounding AI deployment, user privacy, and digital sovereignty will demand multi-stakeholder engagement including industry, governments, academia, and civil society. Transparent mechanisms for accountability, certification, and cross-border cooperation will become critical. This dynamic governance approach aims to balance innovation acceleration with security assurance, fostering trust and sustainability in next-generation networks.

In light of these anticipated advancements, it becomes imperative to reflect on the regulatory foundations that must evolve in parallel. The following conclusion synthesizes the insights presented and outlines the key priorities for securing future networks.

IX. Conclusion

As 5G networks become the backbone of modern digital infrastructure, regulatory oversight remains essential to ensuring their security and resilience. The European Union's frameworks—GDPR, EECC, and the NIS Directives—provide a solid foundation for data protection, risk mitigation, and incident response. Institutions like ENISA, along with national authorities and international partners, play a vital role in guiding and enforcing these regulations.

This paper has illustrated how telecom operators can align with evolving compliance demands and has demonstrated the practical value of platforms like SAND5G in navigating real-world breaches. These tools enable actionable, risk-based decision-making and help bridge the gap between regulatory requirements and operational response.

However, as we move toward 6G, new threats and technological paradigms demand a shift in cybersecurity governance. Adaptive regulatory models, AI-enhanced security mechanisms, and quantum-safe solutions will be key to protecting next-generation networks. Moving forward, a holistic, collaborative, and proactive governance strategy will be essential—not only to safeguard infrastructure, but also to foster trust and innovation across the digital ecosystem.

REFERENCES

[1] Cybersecurity and resiliency of Europe's communications infrastructures and networks, Follow-up to the Nevers Call of 9 March 2022, NIS Cooperation Group, 21 February 2024.

[2] Regulation (EU) 2016/679 of the European Parliament and of the Council of 27 April 2016 on the protection of natural persons with regard to the processing of personal data and on the free movement of such data, and repealing Directive 95/46/EC (General Data Protection Regulation).

[3] Directive (EU) 2002/58 of the European Parliament and of the Council of 12 July 2002 concerning the processing of personal data and the protection of privacy in the electronic communications sector (Directive on privacy and electronic communications).

[4] Directive (EU) 2018/1972 of the European Parliament and the Council establishing the European Electronic Communications Code.

[5] Directive (EU) 2016/1148 of the European Parliament and of the Council of 6 July 2016 concerning measures for a high common level of security of network and information systems across the Union (NIS 1 Directive).

[6] Directive (EU) 2022/2555 of the European Parliament and of the Council of 14 December 2022 on measures for a high common level of cybersecurity across the Union, amending Regulation (EU) No 910/2014 and Directive (EU) 2018/1972, and repealing Directive (EU) 2016/1148 (NIS 2 Directive).

[7] NIS Cooperation Group, Technical Guideline: Security Measures for Top-Level-Domain Name Registries, 23 March 2022.

[8] Directive (EU) 2022/2557 of the European Parliament and of the Council of 14 December 2022 on the resilience of critical entities.

[9] Regulation (EU) 2019/881 of the European Parliament and of the Council of 17 April 2019 on ENISA (the European Union Agency for Cybersecurity) and on information and communications technology cybersecurity certification.

[10] Proposal for a Regulation of the European Parliament and of the Council on horizontal cybersecurity requirements for products with digital elements and amending Regulation (EU) 2019/1020, COM/2022/454 final.

[11] ENISA's ECASEC Expert Group portal, https://resilience.enisa.europa.eu/article-13.

[12] L. Mucchi et al., "Physical-Layer Security in 6G Networks," in IEEE Open Journal of the Communications Society, vol. 2, pp. 1901-1914, 2021, doi: 10.1109/OJCOMS.2021.3103735.

[13] E. O. Frimpong, B.-H Oh, T. Kim, I. Bang, "Physical-Layer Security with Irregular Reconfigurable Intelligent Surfaces for 6G Networks", Sensors 2023, 23, 1881. https://doi.org/10.3390/s23041881.

[14] C. R. García et al., "Secure and Agile 6G Networking – Quantum and AI Enabling Technologies", 23rd International Conference on Transparent Optical Networks (ICTON), Bucharest, Romania, 2023, pp. 1-4, doi: 10.1109/ICTON59386.2023.10207418.

[15] H. Sedjelmaci, K. Tourki and N. Ansari, "Enabling 6G Security: The Synergy of Zero Trust Architecture and Artificial Intelligence", in IEEE Network, doi: 10.1109/MNET.2023.3326003.

[16] M. A. Enright, E. Hammad and A. Dutta, "A Learning-Based Zero-Trust Architecture for 6G and Future Networks", 2022 IEEE Future Networks World Forum (FNWF), Montreal, QC, Canada, 2022, pp. 64-71, doi: 10.1109/FNWF55208.2022.00020.

[17] Abdulrahman Yarali, "Artificial Intelligence and Machine Learning in the Era of 5G and 6G Technology", in From 5G to 6G: Technologies, Architecture, AI, and Security , IEEE, 2023, pp.65-72, doi: 10.1002/9781119883111.ch4.

[18] M. M. Saeed, R. A. Saeed,M. Abdelhaq, R. Alsaqour, M. K. Hasan, R. A. Mokhtar, "Anomaly Detection in 6G Networks Using Machine Learning Methods", Electronics 2023, 12, 3300. https://doi.org/10.3390/electronics12153300.

[19] Samuthira Pandi V, Anitha Juliette Albert, K. Naresh Kumar Thapa, R. Krishnaprasanna, "A novel enhanced security architecture for sixth

generation (6G) cellular networks using authentication and acknowledgement (AA) approach", Results in Engineering, Vol. 21, 2024, doi:https://doi.org/10.1016/j.rineng.2023.101669.

[20] I. Darman, M. K. Mahmood, S. A. Chaudhry, S. A. Khan and H. Lim, "Designing an Enhanced User Authenticated Key Management Scheme for 6G-Based Industrial Applications," in IEEE Access, vol. 10, pp. 92774-92787, 2022, doi: 10.1109/ACCESS.2022.3198642.

[21] Z. Ren, X. Li, Q. Jiang, Y. Wang, J. Ma and C. Miao, "Network Slicing in 6G: An Authentication Framework for Unattended Terminals", in IEEE Network, vol. 37, no. 1, pp. 78-86, January/February 2023, doi: 10.1109/MNET.112.2100738.

[22] I. H. Abdulqadder and S. Zhou, "SliceBlock: Context-Aware Authentication Handover and Secure Network Slicing Using DAG-Blockchain in Edge-Assisted SDN/NFV-6G Environment", in IEEE Internet of Things Journal, vol. 9, no. 18, pp. 18079-18097, 15 Sept.15, 2022, doi:10.1109/JIOT.2022.3161838.

[23] Muhammad Zulfiqar Ali, etal, "Quantum for 6G communication: A perspective", IET Quantum Communication, Vol. 4, Issue 3, 2023, doi: https://doi.org/10.1049/qtc2.12060.

Proceedings of the International Conference on Engineering, Technology and Applied Science Innovations pp. 61–67
DOI: 10.15439/2025I26
ISSN 2300-5963 ACSIS, Vol. 46

Study on the influence of heat treatment on the mechanical tensile characteristics of parts additively manufactured by thermoplastic extrusion of PETG

Zisopol Dragos Gabriel
Mechanical Engineering Department
Petroleum-Gas University of Ploiesti
Ploiesti, Romania
zisopold@upg-ploiesti.ro

Minescu Mihail
Mechanical Engineering Department
Petroleum-Gas University of Ploiesti
Ploiesti, Romania
mminescu@upg-ploiesti.ro

Nastasescu Vasile
Department of Integrated Aviation Systems and Mechanics
Ferdinand I Military Technical Academy
Bucharest, Romania
vasile.nastasescu@mta.ro

Iacob Dragos Valentin
Doctoral School, Mechanical Engineering Department
Petroleum-Gas University of Ploiesti
Ploiesti, Romania
dragoshicb@gmail.com
(corresponding author)

***Abstract*—The paper presents the results of research on the influence of heat treatment on the mechanical tensile characteristics of parts manufactured additively by thermoplastic extrusion of PETG. For the study, 27 tensile specimens were made from PETG filament on the Anycubic 4Max Pro 2.0 3D printer, using layer height values Lh of 0.10; 0.15 and 0.20 mm and filling percentages Ip of 50%, 75% and 100%. The printed specimens were subjected to a heat treatment at 75 °C for 180 minutes. Subsequently, they were tested in tension on the Barrus White 20 kN universal machine. The results showed that the heat treatment generated an increase in tensile strength with values ranging between 5.90% and 17.88% compared to PETG specimens manufactured additively without heat treatment.**

***Index Terms*—FDM; heat treatment; experimental study; tensile strength.**

I. Introduction

THE technical performance of parts plays a crucial role in the smooth running of production processes, [1-7]. Increasing the technical performance of parts without significantly impacting the production cost is a continuous challenge in product development and innovation processes, and additive manufacturing technologies have created new opportunities in terms of efficient manufacturing, [8 – 16]. Additive manufacturing technology by extrusion of plastic masses is one of the most versatile additive technologies due to its simplicity in use, the range of materials and the low operating costs, [17 - 21]. Given the need to increase the technical performance and operational safety of additively manufactured parts, a bibliographic study was carried out that led to the appropriate solution for applying heat treatments to additively manufactured parts by thermoplastic extrusion. Heat treatments are used to modify the properties of materials and are mainly used for metallic materials, however, there is research that highlights the fact that the application of heat treatments on plastic materials brings improvements in durability and ductility, [22 - 29]. In the paper [26] Authors applied an annealing heat treatment on the specimens for the 3-point bending test made of additively manufactured PLA. The results of the study show that the annealing heat treatment resulted in an improvement in the 3-point bending strengths of the PLA specimens by (11 – 17)%. The study presented in the paper [27] demonstrates the viability of using the annealing heat treatment as a solution for improving the mechanical performance of additively manufactured parts made of PETG-CF. In the paper [28] the study on the influence of heat treatment on the impact strengths of additively manufactured PLA specimens is presented. The research results show that the impact resistance of heat-treated parts is (125.10 – 283.70)% higher than the impact resistance of non-heat-treated parts. Considering the promising results of studies conducted by other researchers, but also the gaps identified in the specialized literature, the authors conducted the present study, the novelty of which consists in evaluating the influence of thermoplastic extrusion parameters (L_h – layer height deposited in one pass and I_p – filling percentage) and heat treatment on the mechanical tensile characteristics of parts additively manufactured by thermoplastic extrusion of PETG filament.

II. Of the Influence of Heat Treatment on the Tensile Characteristics of Specimens Additively Manufactured From PETG Filament

A. Additive manufacturing of tensile specimens by thermoplastic extrusion of PETG filament

Using the CAD software Solidworks 2022, the 2D sketch of the tensile specimen was made according to the ISO 527-

1:2019 standard, subsequently the 2D sketch was transformed into a 3D model, and in the last stage the 3D model was converted into STL (Standard Triangle Language) format. Figure 1 shows the 2D model of the tensile specimen.

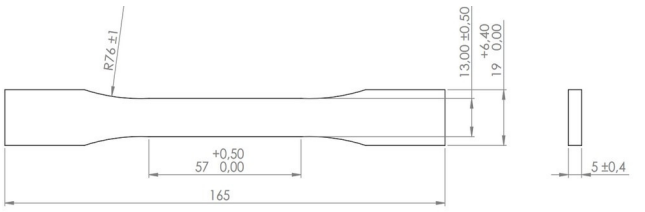

Fig. 1. 2D sketch of tensile sample.

The STL file of the tensile specimen was imported in Cura Slicer software. The thermoplastic extrusion parameters were set according to the data presented in Table 1. Based of these settings, 9 G-Code files were generated, each containing the neccessary instruction for additive manufacturing of the specimens using PETG filament. The G-Code files were transferred to the Anycubic 4 Max Pro 2.0 3D printer, where a total of 27 tensile specimens were produced by extruding Everfil PETG filament.

TABLE I. THERMOPLASTIC EXTRUSION PARAMETERS FOR ADDITIVE MANUFACTURING OF PETG FILAMENT TENSILE SPECIMENS

Constant parameters		**Variable parameters**		**Material**
		Layer height	**Infill percentage**	**PETG**
		L_h	I_p	-
Part orientation, P_o	X-Y	(mm)	(%)	(pieces)
Extruder temperature, E_t (°C)	250	0.10	100	27
			75	
			50	
Platform temperature, B_t (°C)	70	0.15	100	
			75	
			50	
Print speed, P_s (mm/s)	30	0.20	100	
			75	
Filling pattern, F_p	Grid		50	

Figure 2 shows the 27 tensile specimens additively manufactured on the Anycubic 4 Max Pro 2.0 3D printer by thermoplastic extrusion of PETG filament.

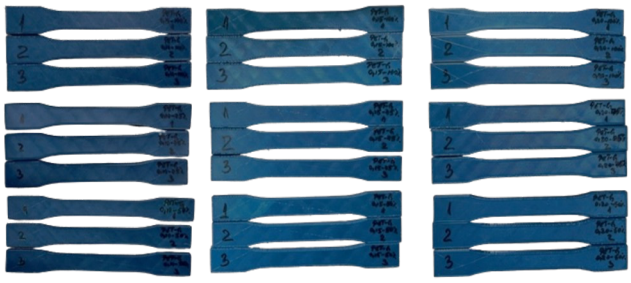

Fig. 2. Additive manufactured tensile samples by thermoplastic extrusion of PETG filament on 3D printer Anycubic 4 Max Pro 2.0.

B. Heat treatment of tensile specimens manufactured additively by thermoplastic extrusion of PETG filament

The 27 tensile specimens fabricated from PETG filament were placed in the ATS FAAR S110 FTE/D electric oven, where they were subjected to the annealing heat treatment. The parameters of the heat treatment applied to the tensile specimens fabricated from PETG filament are: temperature, T = 75 °C and duration, d = 180 minutes. Figure 3 shows the ATS FAAR S110 FTE/D electric oven, used to perform the heat treatment on the tensile specimens fabricated from PETG filament.

Fig. 3. Electrical convection oven ATS FAAR S110 FTE/D, used for heat treatment of tensile specimens made of PETG filament.

C. Impact of heat treatment and thermoplastic extrusion parameters on the tensile strength of additively manufactured specimens from PETG filament

The tensile specimens shown in Figure 2, made by thermoplastic extrusion of PETG filament on the Anycubic 4 Max Pro 2.0 printer, were tested on the Barrus White 20 kN testing machine (Fig. 4). Tensile tests were performed according to ISO 527-1:2019 standard, at a traverse speed of 5 mm/min [30].

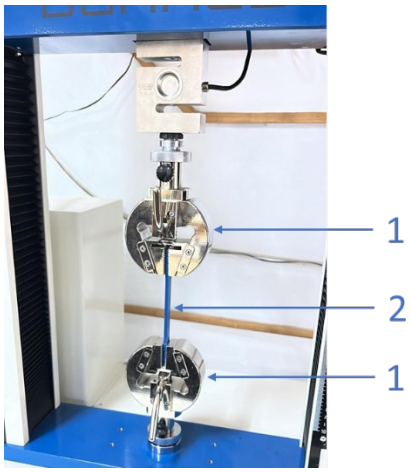

Fig. 4. Tensile testing of annelead samples on Barrus White 20 kN machine: 1 – grips; 2 – sample.

Figure 5 shows the 27 tensile specimens that underwent heat treatment after tensile testing on the Barrus White 20 kN machine.

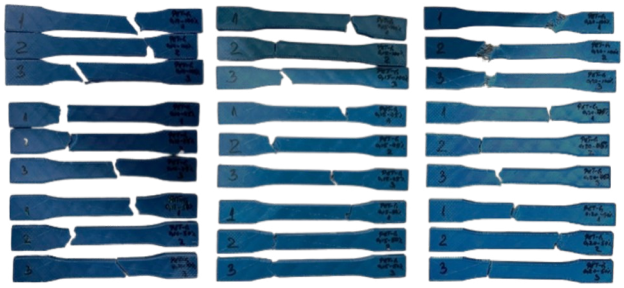

Fig. 5. Additive manufactured annealed tensile samples by thermoplastic extrusion of PETG filament on 3D printer Anycubic 4 Max Pro 2.0 after tensile testing on Barrus White 20 kN machine.

Figures 6 - 8 show the breaking strengths obtained for tensile specimens manufactured by thermoplastic extrusion of PETG filament and heat treated.

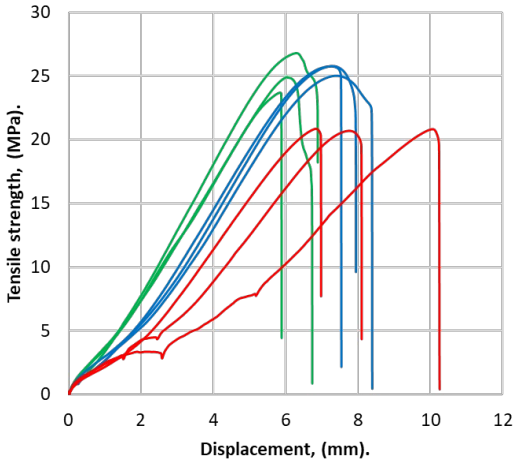

Lh (mm)	Ip (%)	Sample 1	Sample 2	Sample 3	Average (MPa)
0.10	50	20.69	20.86	20.83	**20.79**
	75	25.78	25.02	25.76	**25.52**
	100	23.69	24.92	26.80	**25.13**

Fig. 6. Breaking strength values for annealed PETG samples with L_h=0.10 mm and I_p= (50; 75; 100) %.

Analyzing the graph in Figure 6, it is possible to observe the influence of the filling percentage on the tensile strength of the specimens additively manufactured from PETG filament and subsequently heat-treated, using a constant layer height (L_h) of 0.10 mm. The maximum tensile strength of 25.52 MPa was recorded at a filling of 75%. Reducing the filling to 50% led to a loss of strength of 18.52%, and increasing it to 100% led to a slight reduction of 1.50%.

Analyzing figure 7, it can be observd how the filling percentages influence the tensile strengths of heat-treated and additively manufactured tensile specimens made PETG filament with L_h = 0.15 mm. The maximum average value of the tensile strengths (25.50 MPa) was recorded for the specimens manufactured with I_p = 100%. A reduction in the infilling percentage from 100% to 75% led to a 2.36% decrease in tensile strengths, while a reduction from 75% to 50% resulted in a tensile strength decrease of 28.17%.

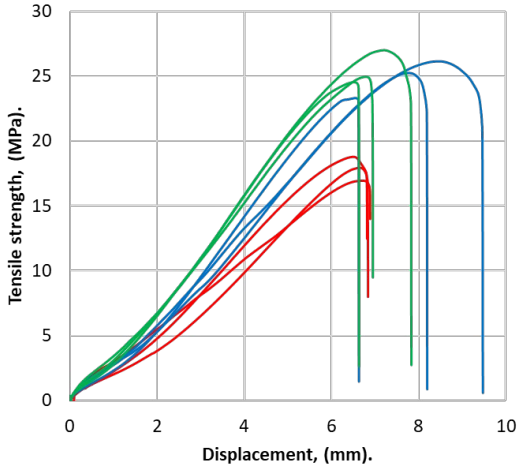

Lh (mm)	Ip (%)	Sample 1	Sample 2	Sample 3	Average (MPa)
0.15	50	18.78	17.94	16.94	**17.89**
	75	26.14	25.24	23.31	**24.90**
	100	27.00	24.54	24.96	**25.50**

Fig. 7 Breaking strength values for annealed PETG samples with L_h = 0.15 mm and I_p= (50; 75; 100) %.

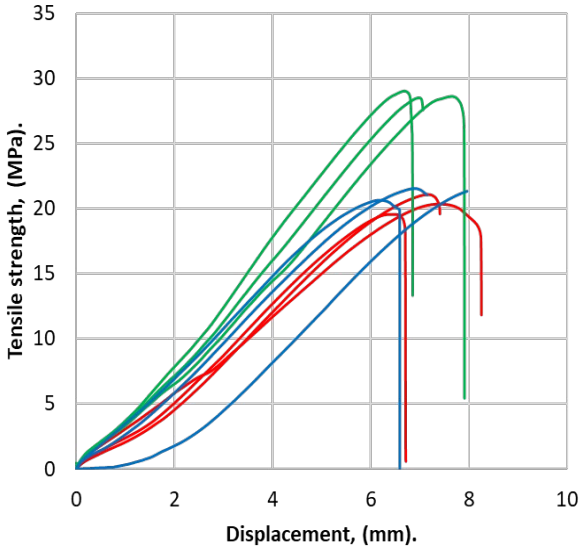

Lh (mm)	Ip (%)	Sample 1	Sample 2	Sample 3	Average (MPa)
0.20	50	20.34	21.08	19.55	**20.32**
	75	21.39	20.64	21.54	**21.19**
	100	29.03	28.62	28.51	**28.72**

Fig. 8. Breaking strength values for annealed PETG samples with L_h = 0.20 mm and I_p= (50; 75; 100) %.

Examining the graph in figure 8, we see the effects of filling percentages on the tensile strengths of thermally treated and additively manufactured tensile samples made from PETG filament with L_h = 0.20 mm. The highest average tensile strength value (28.72 MPa) was observed for the specimens produced with I_p = 100%. The reduction in the filling percentage from 100% to 75% led to a 26.21% decrease in

tensile strengths, while the reduction from 75% to 50% resulted in a 4.09% decrease in tensile strengths

Employing Minitab software, the tensile strength results of the tensile specimens produced from PETG filament with L_h = (0.10; 0.15; 0.20) mm and I_p = (50; 75; 100) %, followed by heat treatment, led to the creation of the Pareto chart in figure 8 and the contour chart in figure 9, illustrating the impact of the variable parameters of thermoplastic extrusion on tensile strengths, [31].

Examining the graphs in figures 9 and 10, we note that of the two parameters assessed, (A = L_h and B = I_p), the parameter that considerably affects the tensile strength results of the specimens produced from PETG filament and subjected to heat treatment is the parameter B = I_p.

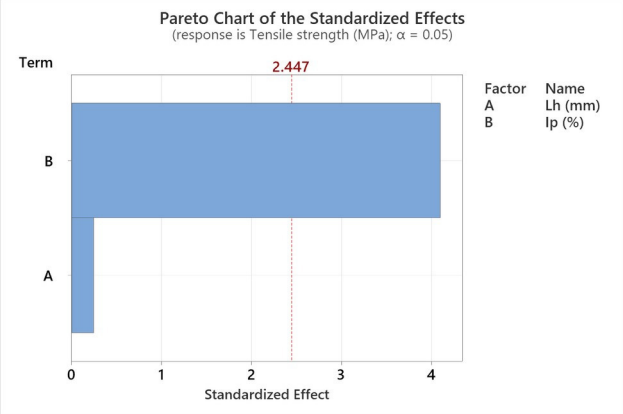

Fig. 9 . Pareto chart for influence of A = L_h and B = I_p on breaking strengths.

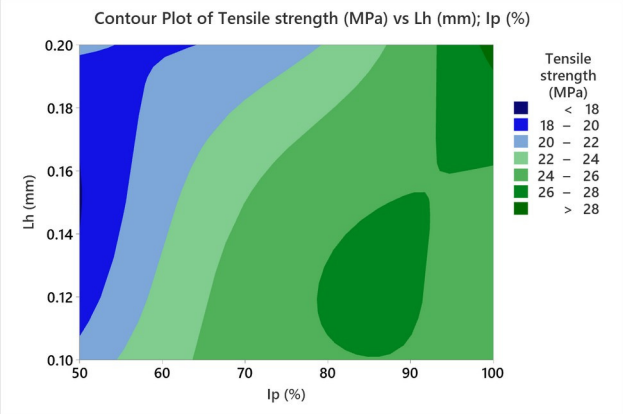

Fig. 10 . Contour plot for influence of A = L_h and B = I_p on breaking strengths.

D. Influence of heat treatment and thermoplastic extrusion parameters on the percentage elongation at break of additively manufactured specimens from PETG filament

Figure 11 graphically represents the average values corresponding to the percentage elongations at break of tensile specimens additively manufactured from PETG filament with L_h = (0.10; 0.15; 0.20) mm and I_p = (50; 75; 100)% and heat treated.

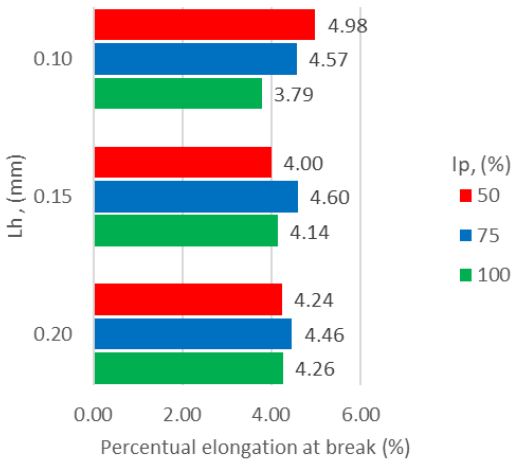

Fig. 11. Average percentual elongation at break of annealed tensile samples made by thermoplastic extrusion of PETG filament.

The highest average value related to the percentage elongation at break of tensile specimens made from PETG filament (4.98)%, was observed for the group of specimens produced with L_h = 0.10 mm and I_p = 50%. For an identical height of the layer applied in one pass, raising I_p from 50% to 75% resulted in a reduction of the percentage elongation at break by 8.32%, while increasing Ip from 75% to 100% led to a decrease in the percentage elongation at break by 16.99%

By utilizing Minitab software, the graphs from figures 12 and 13 was generated, which show the influence of variable parameters of thermoplastic extrusion on the percentage elongations at break for tensile specimens made from PETG and subsequently subjected to heat treatment. The Pareto chart depicted in figure 12 illustrates the impact of the variable parameters of thermoplastic extrusion (A = L_h and B = I_p) on the percentage elongations at break of tensile specimens that were additively manufactured from PETG and then subjected to heat treatment. Based on the graph in figure 12, factor B = I_p shows a much stronger effect than factor A = L_h, yet statistically, both factors do not affect the percentage elongations at break values.

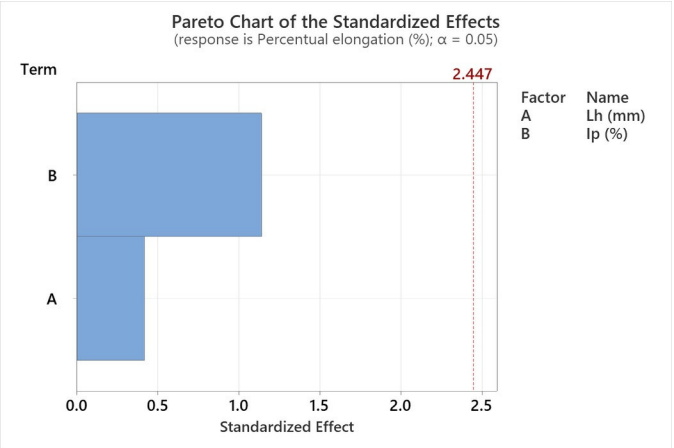

Fig. 12 Pareto chart for influence of A = L_h and B = I_p on percentual elongations at break.

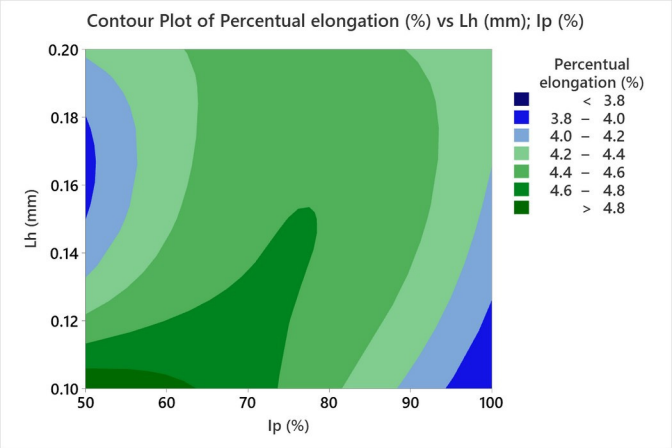

Fig. 13. Contour plot for influence of A = L_h and B = I_p on percentual elongations at break.

The contour plot in Figure 13 expresses the influence of thermoplastic extrusion parameters on the percentage elongations at break of tensile specimens additively manufactured from PETG filament and subsequently heat treated.

E. Influence of heat treatment and thermoplastic extrusion parameters on the elastic modulus of additively manufactured PETG filament specimens

Figure 14 graphically represents the average values of the elastic modulus corresponding to tensile specimens additively manufactured from PETG filament with L_h = (0.10; 0.15; 0.20) mm and I_p = (50; 75; 100)% and subsequently heat treated.

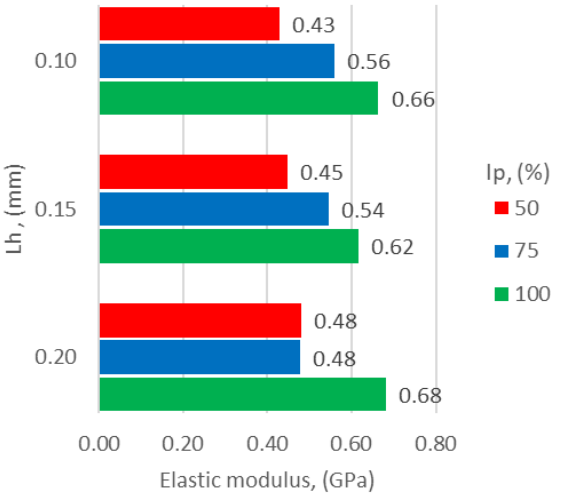

Fig. 14. Average elastic modulus of annealed tensile samples made by thermoplastic extrusion of PETG filament.

The maximum average values of the elastic modulus were recorded for the specimens manufactured with Ip = 100%, (0.62 – 0.68) GPa. The decrease of I_p from 100% to 75% generated a decrease of the elastic modulus by (13.14 – 42.83)%, and the reduction of I_p from 75% to 50% caused the decrease of the elastic modulus by up to 30.50%.

With the elastic modulus values and process parameters, the Pareto chart in Figure 15 was created in Minitab. This outlines the effect of extrusion parameters on the mechanical characteristics of PETG specimens produced through additive manufacturing and subsequently heat treated.

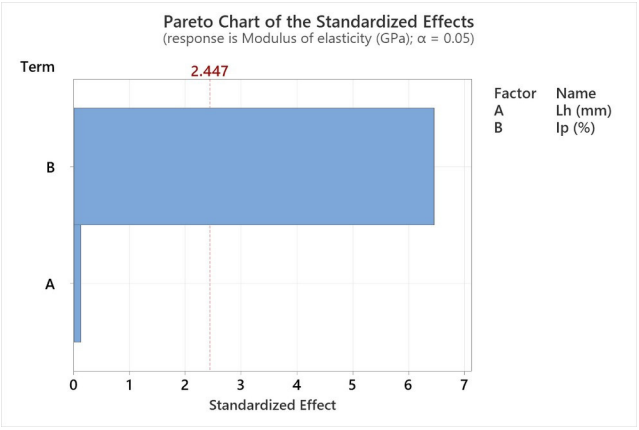

Fig. 15. Pareto chart for influence of A = L_h and B = I_p on modulus of elasticity.

Analyzing the Pareto chart in figure 15, we can see that the parameter B = I_p has an overwhelming influence on the elastic modulus of the samples additively manufactured from PETG filament and heat treated, the same being demonstrated by the contour chart in figure 16.

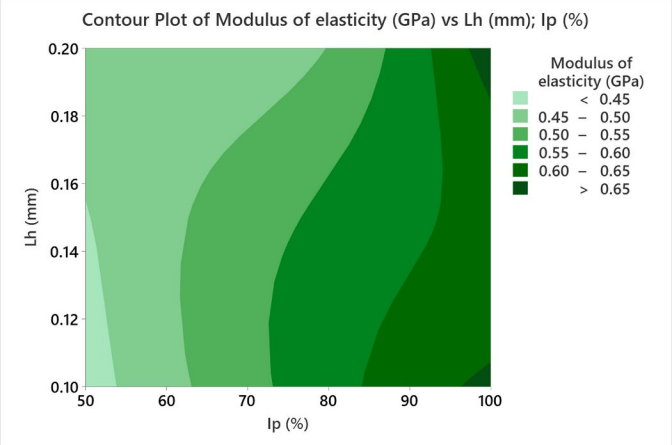

Fig. 16. Contour plot for influence of A = L_h and B = I_p on modulus of elasticity.

To maximize the tensile strength of annealed 3D printed specimens from PETG, was determined the optimal thermoplastic extrusion parameters. The resulting optimization graphs are shown in Figure 17.

Analyzing the optimization graphs in Figure 17, we observe that the optimal thermoplastic extrusion parameters for additive manufacturing of PETG tensile specimens are L_h = 0.10 mm and I_p = 100%.

III. CONCLUSIONS

This paper show the research on the effects of annealing heat treatment on the tensile mechanical properties of sam-

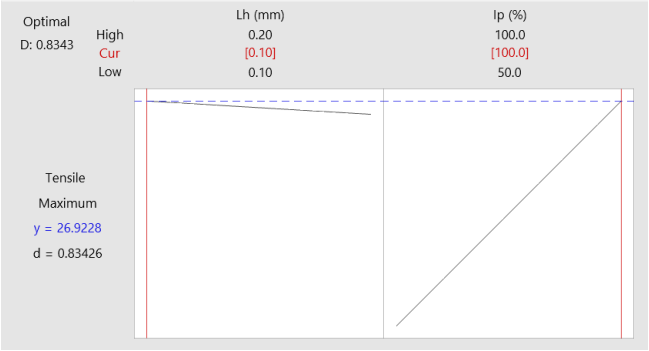

Fig. 17. Optimization plots of thermoplastic extrusion parameters (L_h and I_p) for maximizing of breaking strenghts of PETG tensile samples.

ples produced through thermoplastic extrusion of PETG filament. To realize the study, employing the thermoplastic extrusion settings, the layer height , L_h = (0.10; 0.15; 0.20) mm and the infill percentage, I_p = (50; 75; 100) %, 27 tensile samples were additively produced through thermoplastic extrusion of PETG filament on the Anycubic 4 Max Pro 2.0 3D printer. The 27 tensile specimens underwent an annealing heat treatment that involved placing them in the ATS FAAR S110 FTE/D electric oven preheated to 75 ºC, holding the specimens in the oven at 75 ºC for 180 minutes, and then gradually cooling the parts. All 27 heat-treated samples underwent tensile testing on the Barrus White 20 kN machine, where the next tensile properties were determinated: tensile strength, elongation percentage at failure, and modulus of elasticity

The lowest average tensile strength values of the additively manufactured samples from PETG filament and heat-treated were recorded for the specimens made with L_h = 0.15 mm and I_p = 50%, while the highest average tensile strength values were recorded for the specimens made with L_h = 0.20 mm and I_p = 100%

The lowest average percentage elongation at break of the additively produced PETG filament and heat-treated samples was noted for those produced with L_h = 0.10 mm and I_p = 100%, whereas the highest average percentage elongation at break was noted for the samples made with L_h = 0.10 mm and I_p = 50%.

The lowest average value of the elastic modulus for the tensile specimens made from PETG filament and heat treated was recorded for the specimens produced with L_h = 0.20 mm and the = 100%, while the highest average value of the elastic modulus was recorded for the specimens created with L_h = 0.10 mm and the = 50%

The average breaking strength of the 27 tensile specimens additively manufactured from PETG and heat treated is 23.33 MPa, which is 10.50% higher than the average breaking strength of the tensile specimens manufactured from PETG, but not heat treated, in the study [32]. The annealing heat treatment has beneficial effects on the additively manufactured parts, through which the defects generated by the poor adhesion between the layers are remedied.

The results of this study demonstrate that heat treatment of additively manufactured parts made of PETG filament represents a solution for increasing mechanical tensile performance, which is (5.90 – 17.88)% higher compared to those of specimens manufactured from the same material, using identical parameters, but not heat treated.

The authors aim to study the effect of heat treatment on other mechanical characteristics (compression, 3-point bending, impact), but also on other types of materials.

References

[1] K. A. Bello and R. W. Maladzhi, “Innovative and best practices in sustainable strategies for waste reduction in additive manufacturing,” Hybrid Advances, vol. 11, p. 100527, Dec. 2025, https://doi.org/10.1016/j.hybadv.2025.100527.

[2] R. M. Shiferaw, K. L. Debela, and C. A. Kero, “Effect of green leadership on sustainable performance of large manufacturing firms using leader innovation behaviour as a mediating role: Evidence from large manufacturing firm in Ethiopia,” Sustainable Futures, vol. 10, p. 101005, Dec. 2025, https://doi.org/10.1016/j.sftr.2025.101005.

[3] W. Shi, L. Ying, G. Ma, Y. Niu, Y. Lv, and X. Xu, “Intelligent manufacturing, media attention, and sustainable development performance,” International Review of Financial Analysis, vol. 106, p. 104481, Oct. 2025, https://doi.org/10.1016/j.irfa.2025.104481.

[4] R. Gul, X. Cao, R. A. Mohammad, A. Rauf, and S. Ullah khan, “Sustainable Entrepreneurial Dynamics in Manufacturing: Innovative Business Models and Social Value Creation in Chinese Enterprises,” Sustainable Futures, p. 101022, Jul. 2025, https://doi.org/10.1016/j.sftr.2025.101022.

[5] A. D. Jayal, F. Badurdeen, O. W. Dillon, and I. S. Jawahir, “Sustainable manufacturing: Modeling and optimization challenges at the product, process and system levels,” CIRP Journal of Manufacturing Science and Technology, vol. 2, no. 3, pp. 144–152, Jan. 2010, https://doi.org/10.1016/j.cirpj.2010.03.006.

[6] M. A. Rosen and H. A. Kishawy, “Sustainable Manufacturing and Design: Concepts, Practices and Needs,” Sustainability, vol. 4, no. 2, pp. 154–174, Feb. 2012, https://doi.org/10.3390/su4020154.

[7] Y. H. Dang et al., “Conversion of an FDM printer to direct ink write 3D bioprinter utilizing an efficient and cost-effective extrusion system,” Annals of 3D Printed Medicine, vol. 19, p. 100212, Aug. 2025, https://doi.org/10.1016/j.stlm.2025.100212.

[8] R. Kumaresan, K. Kadirgama, M. Samykano, W. S. W. Harun, A. Thirugnanasambandam, and K. Kanny, “In-depth study and optimization of process parameters to enhance tensile and compressive strengths of PETG in FDM technology,” Journal of Materials Research and Technology, vol. 37, pp. 397–416, Jul. 2025, https://doi.org/10.1016/j.jmrt.2025.06.013.

[9] L. Changhui et al., “Balanced Optimization of Dimensional Accuracy and Printing Efficiency in FDM Based on Data-Driven Modeling,” Additive Manufacturing Frontiers, vol. 4, no. 2, p. 200220, Jun. 2025, https://doi.org/10.1016/j.amf.2025.200220.

[10] I. J. Solomon, P. Sevvel, and J. Gunasekaran, “A review on the various processing parameters in FDM,” Materials Today: Proceedings, vol. 37, pp. 509–514, Jan. 2021, https://doi.org/10.1016/j.matpr.2020.05.484.

[11] J. Torres, J. Cotelo, J. Karl, and A. P. Gordon, “Mechanical Property Optimization of FDM PLA in Shear with Multiple Objectives,” JOM, vol. 67, no. 5, pp. 1183–1193, May 2015, https://doi.org/10.1007/s11837-015-1367-y.

[12] S. Hartomacıoğlu, M. Oksuz, A. Ekinci, and M. Ates, “Optimization of Produced Parameters for PA6/PA6GF30 Composite Produced by 3D Printing with Novel Knitting Method,” Polymers, vol. 17, no. 12, p. 1590, Jan. 2025, https://doi.org/10.3390/polym17121590.

[13] V.-L. Trinh, T.-D. Hoang, and Q.-T. Ngo, “The Influence of Processing Parameters on the Tensile Strength of 3D Printed Products”, Eng. Technol. Appl. Sci. Res., vol. 15, no. 3, pp. 22663–22668, Jun. 2025.

[14] O. A. Mohamed, S. H. Masood, J. L. Bhowmik, M. Nikzad, and J. Azadmanjiri, “Effect of Process Parameters on Dynamic Mechanical Performance of FDM PC/ABS Printed Parts Through Design of Experiment,” Journal of Materials Engineering and Performance, vol. 25,

no. 7, pp. 2922–2935, Jul. 2016, https://doi.org/10.1007/s11665-016-2157-6.

[15] D. Popescu, A. Zapciu, C. Amza, F. Baciu, and R. Marinescu, "FDM process parameters influence over the mechanical properties of polymer specimens: A review," Polymer Testing, vol. 69, pp. 157–166, Aug. 2018, https://doi.org/10.1016/j.polymertesting.2018.05.020.

[16] R. Patel, C. Desai, S. Kushwah, and M. H. Mangrola, "A review article on FDM process parameters in 3D printing for composite materials," Materials Today: Proceedings, vol. 60, pp. 2162–2166, Jan. 2022, https://doi.org/10.1016/j.matpr.2022.02.385.

[17] B. Mallikarjuna, P. Bhargav, S. Hiremath, K. G. Jayachristiyan, and N. Jayanth, "A review on the melt extrusion-based fused deposition modeling (FDM): background, materials, process parameters and military applications," International Journal on Interactive Design and Manufacturing (IJIDeM), vol. 19, no. 2, pp. 651–665, Feb. 2025, https://doi.org/10.1007/s12008-023-01354-0.

[18] I. Plamadiala, C. Croitoru, M. A. Pop, and I. C. Roata, "Enhancing Polylactic Acid (PLA) Performance: A Review of Additives in Fused Deposition Modelling (FDM) Filaments," Polymers, vol. 17, no. 2, p. 191, Jan. 2025, https://doi.org/10.3390/polym17020191.

[19] X. Zhai, T. Corre, and V. Lazarus, "A FDM-based experimental benchmark for evaluating quasistatic crack propagation in anisotropic linear elastic materials," Engineering Fracture Mechanics, vol. 324, p. 111175, Jul. 2025, https://doi.org/10.1016/j.engfracmech.2025.111175.

[20] R. Kumaresan, M. Samykano, K. Kadirgama, Dr. A. Pandey, and Prof. Dr. Md. M. Rahman, "Effects of printing parameters on the mechanical characteristics and mathematical modeling of FDM-printed PETG," The International Journal of Advanced Manufacturing Technology, vol. 128, pp. 1–19, Aug. 2023, https://doi.org/10.1007/s00170-023-12155-w.

[21] A. Özen, B. E. Abali, C. Völlmecke, J. Gerstel, and D. Auhl, "Exploring the Role of Manufacturing Parameters on Microstructure and Mechanical Properties in Fused Deposition Modeling (FDM) Using PETG," Applied Composite Materials, vol. 28, no. 6, pp. 1799–1828, Dec. 2021, https://doi.org/10.1007/s10443-021-09940-9.

[22] A. Szust and G. Adamski, "Using thermal annealing and salt remelting to increase tensile properties of 3D FDM prints," Engineering Failure Analysis, vol. 132, p. 105932, Feb. 2022, https://doi.org/10.1016/j.engfailanal.2021.105932.

[23] Y. He, M. Shen, Q. Wang, T. Wang, and X. Pei, "Effects of FDM parameters and annealing on the mechanical and tribological properties of PEEK," Composite Structures, vol. 313, p. 116901, Jun. 2023, https://doi.org/10.1016/j.compstruct.2023.116901.

[24] S. Valvez, A. P. Silva, P. N. B. Reis, and F. Berto, "Annealing effect on mechanical properties of 3D printed composites," Procedia Structural Integrity, vol. 37, pp. 738–745, Jan. 2022, https://doi.org/10.1016/j.prostr.2022.02.004.

[25] E. Kösemen, M. Bakkal, and A. T. Kuzu, "Enhancing Mechanical Performance of FDM-Printed ABS Parts Through Annealing Optimization," Polymer Engineering & Science, vol. n/a, no. n/a, https://doi.org/10.1002/pen.70008.

[26] R. A. Wach, P. Wolszczak, and A. Adamus-Wlodarczyk, "Enhancement of Mechanical Properties of FDM-PLA Parts via Thermal Annealing," Macromolecular Materials and Engineering, vol. 303, no. 9, p. 1800169, 2018, https://doi.org/10.1002/mame.201800169.

[27] J. R. Stojković et al., "An Experimental Study on the Impact of Layer Height and Annealing Parameters on the Tensile Strength and Dimensional Accuracy of FDM 3D Printed Parts," Materials, vol. 16, no. 13, p. 4574, Jan. 2023, https://doi.org/10.3390/ma16134574.

[28] D. G. Zisopol, A. I. Portoaca, and M. Tanase, "Improving the Impact Resistance through Annealing in PLA 3D Printed Parts", Eng. Technol. Appl. Sci. Res., vol. 13, no. 5, pp. 11768–11772, Oct. 2023.

[29] D. G. Zisopol, "The Place and Role of Value Analysis in the Restructuring of Production (Case Study)," Economic Insights - Trends and Challenges, vol. I, no. 4/2012, pp. 27–35, 2012.

[30] Available online: ISO 527-1:2019, Plastics — Determination of tensile properties, https://www.iso.org/standard/527-1, (accesed January 24, 2025).

[31] Availabe online: https://www.minitab.com/en-us/, (accessed June. 5, 2025).

[32] D. G. Zisopol, M. Minescu, and D. V. Iacob, "A Study on the Influence of FDM Parameters on the Tensile Behavior of Samples made of PET-G", Eng. Technol. Appl. Sci. Res., vol. 14, no. 2, pp. 13487–13492, Apr. 2024.

Author Index